SAE Aerospace
An SAE International Group

AEROSPACE INFORMATION REPORT

SAE AIR1168/12 | REV. A

Issued 2004-09
Stabilized 2011-07

Superseding AIR1168/12

Spacecraft Thermal Balance

RATIONALE

This document has been determined to contain basic and stable technology which is not dynamic in nature.

STABILIZED NOTICE

This document has been declared “Stabilized” by the AC-9 Technical Committee and will no longer be subjected to periodic reviews for currency. Users are responsible for verifying references and continued suitability of technical requirements. Newer technology may exist.

PREFACE

This document is one of 14 Aerospace Information Reports (AIR) of the Third Edition of the SAE Aerospace Applied Thermodynamics Manual. The manual provides a reference source for thermodynamics, aerodynamics, fluid dynamics, heat transfer, and properties of materials for the aerospace industry. Procedures and equations commonly used for aerospace applications of these technologies are included.

In the Third Edition, no attempt was made to update material from the Second Edition nor were SI units added. However, all identified errata were corrected and incorporated and original figure numbering was retained, insofar as possible.

The SAE AC-9B Subcommittee originally created the SAE Aerospace Applied Thermodynamics Manual, and, for the Third Edition, used a new format consisting of AIR1168/1 through AIR1168/10. AIR1168/11 through AIR1168/14 were created by the SAE SC-9 Committee.

The AIRs comprising the Third Edition are shown below. Applicable sections of the Second Edition are shown parenthetically in the third column.

AIR1168/1	Thermodynamics of Incompressible and Compressible Fluid Flow	(1A,1B)
AIR1168/2	Heat and Mass Transfer and Air-Water Mixtures	(1C,1D,1E)
AIR1168/3	Aerothermodynamic Systems Engineering and Design	(3A,3B,3C,3D)
AIR1168/4	Ice, Rain, Fog, and Frost Protection	(3F)

TO PLACE A DOCUMENT ORDER: **Tel: 877-606-7323 (inside USA and Canada)**
Tel: +1 724-776-4970 (outside USA)
Fax: 724-776-0790
Email: CustomerService@sae.org
SAE WEB ADDRESS: **http://www.sae.org**

SAE values your input. To provide feedback on this Technical Report, please visit
http://www.sae.org/technical/standards/AIR1168/12A

PREFACE (Continued)

AIR1168/5	Aerothermodynamic Test Instrumentation and Measurement	(3G)
AIR1168/6	Characteristics of Equipment Components, Equipment Cooling System Design, and Temperature Control System Design	(3H,3J,3K)
AIR1168/7	Aerospace Pressurization System Design	(3E)
AIR1168/8	Aircraft Fuel Weight Penalty Due to Air Conditioning	(3I)
AIR1168/9	Thermophysical Properties of the Natural Environment, Gases, Liquids, and Solids	(2A,2B,2C,2D)
AIR1168/10	Thermophysical Characteristics of Working Fluids and Heat Transfer Fluids	(2E,2F)
AIR1168/11	Spacecraft Boost and Entry Heat Transfer	(4A,4B)
AIR1168/12	Spacecraft Thermal Balance	(4C)
AIR1168/13	Spacecraft Equipment Environmental Control	(4D)
AIR1168/14	Spacecraft Life Support Systems	(4E)

F.R. Weiner, formerly of Rockwell International and past chairman of the SAE AC-9B Subcommittee, is commended for his dedication and effort in preparing the errata lists that were used in creating the Third Edition.

TABLE OF CONTENTS

LIST OF FIGURES

LIST OF FIGURES (Continued)

LIST OF FIGURES (Continued)

LIST OF FIGURES (Continued)

LIST OF FIGURES (Continued)

LIST OF FIGURES (Continued)

LIST OF TABLES

LIST OF TABLES (Continued)

1. INTRODUCTION:

1.1 Scope:

In the design of spacecraft, heat transfer becomes a criterion of operation to maintain structural and equipment integrity over long periods of time.

The spacecraft thermal balance between cold space and solar, planetary, and equipment heat sources is the means by which the desired range of equipment and structural temperatures are obtained. With the total spacecraft balance set, subsystem and component temperatures can be analyzed for their corresponding thermal requirements.

This section provides the means by which first-cut approximations of spacecraft surface, structure, and equipment temperatures may be made, using the curves of planetary and solar heat flux in conjunction with the desired coating radiative properties. Once the coating properties have been determined, the material to provide these requirements may be selected from the extensive thermal radiative properties tables and curves.

These can then be cross checked to determine the degradation effects of space that may cause extensive temperature changes over long periods of time. The paragraphs reviewing previous spacecraft thermal designs, test facilities, and methods of testing should be used as a guide in the development of a design. This section assumes that the reader is familiar with the methods of thermal analyzer techniques and has available, through SHARE or other agencies, multinodal programs to solve the detailed temperature distributions required to complete a design.

1.2 Nomenclature:

a	=	Albedo, dimensionless
A	=	Cross-sectional area, ft^2
C_p	=	Specific heat capacity at constant pressure, Btu/lb
D	=	Diameter, ft
e^-	=	Electron
e	=	Base of Naperian logarithms
E	=	Energy, MeV, keV
E	=	Exposure, sun-hours
E_{cr}	=	Cratering energy density, $ergs/cm^3$
f_1	=	Friction factor, dimensionless
F_a	=	Geometric albedo factor, dimensionless
F_A	=	Geometric shape factor, dimensionless
F_p	=	Geometric planetary factor, dimensionless
F_e	=	Effective emittance, dimensionless
g	=	Gravitational constant 32.174 ft/s^2
h	=	Altitude, sm (statute miles), nm (nautical miles)
h_e	=	Effective altitude, sm or nm
h_{ev}	=	Boiling heat transfer coefficient, Btu/h-ft^2-°F
H_λ	=	Extraterrestrial solar spectral intensity at wavelength λ (Johnson curve), Btu/h-ft^2-μ
H	=	Total radiant intensity, Btu/h-ft^2

1.2 (Continued):

i	=	Inclination; angle from equator, deg
I	=	Current, A
I	=	Sun intensity, dimensionless
k	=	Thermal conductivity, Btu-ft/h-ft^2-°F
L	=	Body length, ft
m	=	Mass, lb
m_p	=	Mass of impacting particles, g
n	=	Integer
N_{Re}	=	Reynolds No. ($VD(\rho g)/\mu$)
N_{Pr}	=	Prandtl No. ($\mu C_p/k$)
N_{Nu}	=	Nusselt No. (LD/k)
N_{St}	=	**Stanton No. ($N_{St} = N_{Nu}/(N_{Re})(N_{Pr}) = h/(\rho g V C_p \times 3600)$)**
N_P	=	Pressure term G $(\rho g)/P^2$
P	=	Pressure, lb/ft^2
P	=	Proton
q	=	Heat flow, Btu/h
Q	=	Heat flux, Btu/h-ft^2
Q'	=	Instantaneous heat flux, Btu/h-ft^2
r	=	Body radius, ft
r	=	Ionization dose, roentgens
r_c	=	Meniscus radius, ft
R	=	Radius of planet, statute miles (sm)
R	=	Resistance, Ω
R	=	Radiancy, W/cm^2, Btu/h-ft^2
R_{b_λ} (T)	=	Planck's blackbody function for temperature, T, or $(dR_b/d\lambda)_{\lambda T}$, Btu/h-ft^2-μ
R_p	=	Planetary flux, Btu/h-ft^2
S	=	Solar constant, 442 Btu/h-ft^2
t	=	Time, h
t	=	Temperature, °F
T	=	Temperature, °R, K
ΔT	=	Temperature drop, °R
T_p	=	Planet blackbody temperature, °R
V	=	Velocity along flow path, ft/s
v_p	=	Particle velocity, cm/s
w	=	Heat pipe groove width, ft
x	=	Thermal path length, ft
α	=	Angle from surface normal to horizon of planet, deg
α	=	Absorptance (see Par. 1.4.1), dimensionless
α_s	=	Solar absorptance, dimensionless
β	=	Angle between orbital plane and sun-planet plane, deg
γ	=	Angle between the surface normal and the planet radius vector to the surface zenith (γ=0 deg for a surface facing the planet and 180 deg when facing space), deg
∈	=	Emittance (see Par. 1.4.1)

1.2 (Continued):

$$\varepsilon = \text{Exposure} = \frac{1}{10^7}\sum_{i=1}^{n}\frac{1}{2}m_{pi}v_{pi}^2, \text{ joules}$$

ε = Total kinetic energy, joules
Δ = Difference or change in the term that follows it
θ = Heat pipe wetting angle, deg
θ = Angle between the surface normal and sun line, deg
θ_s = Angle between the planet-sun line and planet radius vector to the body zenith, deg
λ = Discrete wavelength, μ
λ = Heat of vaporization, Btu/lb
μ = Unit of wavelength, micron, 1 micron = 10^{-6} m
μ = Absolute viscosity lb/ft-h, lb/ft-s
ν = Orbit angle about the planet (ν = 0 deg at "noon" position), deg
ν = Kinematic viscosity ft^2/h
ρ = Reflectance, dimensionless (see Par. 1.4.1)
π = 3.141 radians
ρ = Mass density $lb\text{-}s^2/ft^4$
(ρg) = Specific weight (density), lb/ft^3
σ = Stefan-Boltzmann constant
0.1714×10^{-8} Btu/h-ft^2-°R^4 or 5.673×10^{-12} W/cm^2-K^4
σ = Surface tension, lb/ft
τ = Time, h, year
τ = Transmittance, dimensionless
Ω = Ohms
φ_c = One of the attitude parameters. The angle of rotation about the planet radius vector to the surface normal (φ_c = 0 deg when the normal lies in the plane containing the planet-surface vector and the planet-Sun vector), deg.
ψ = Angle between planet-Sun line and the orbital plane (ψ = 0 deg for a "noon" orbit). Note: $\cos\theta_s = \cos\psi\cos\nu$, deg.

Subscripts:

a = Albedo
a = After exposure to particles, nondimensional
abs = Absorbed
Al = Aluminum
b,0 = Blackbody
B = Equipment side of skin
c = Sample or condenser
c = Chamber
cap = Capillary head
eq = Equipment
eq = Equilibrium
eff = Effective

1.2 (Continued):

EV	=	Evaporator
ev	=	Evaporative
ev	=	Electron volts
H	=	Hemispherical
H	=	Heat sink
HB	=	Between heat sink and skin
i	=	Initial
L	=	Liquid
My	=	Mylar
N	=	Normal
p	=	Particle
p	=	Planetary
pc	=	Projected area of sample as viewed in direction of illumination
s	=	Solar
sf	=	Surface
sp	=	Space
SN	=	Solar normal
SK	=	Skin
ss	=	Solar simulator
TH	=	Total hemispherical
TN	=	Total normal
T	=	Total radiancy (see Par. 1.4.1.1)
V	=	Vapor
W	=	Wall
1	=	Surface 1
2	=	Surface 2
12	=	From surface 1 to surface 2
∞	=	Infinite exposure
θ	=	Angle of incidence from surface normal, deg
θ	=	Directional emittance (see Par. 1.4.1.1)
λ	=	Spectral wavelength, μ
λH	=	Spectral hemispherical emittance (see Par. 1.4.1.1)
λN	=	Spectral normal emittance (see Par. 1.4.1.1)
τ	=	Time
φ	=	Azimuthal surface angle, deg

1.3 Common Abbreviations:

A	=	Amperes
Å	=	Angstroms
Ag	=	Silver
Al	=	Aluminum
alt	=	Altitude
approx.	=	Approximately
ARS J	=	American Rocket Society Journal

1.3 (Continued):

Au	=	Gold
Btu (BTU)	=	British thermal units
cm (CM)	=	Centimeter(s)
conc.	=	Concentration
Cu	=	Copper
deg	=	Degree(s)
degrad.	=	Degradation
dia	=	Diameter
eV	=	Electron-volts
°F	=	Degrees Fahrenheit
ft (FT)	=	Feet
GE	=	General Electric
GSFC	=	Goddard Space Flight Center
h (H)	=	Hour(s)
Hg	=	Mercury
in (IN)	=	Inch(es)
J.	=	Journal
JPL	=	Jet Propulsion Laboratory
K	=	Degrees Kelvin
kW	=	Kilowatts
LM	=	Lunar Module
LMSC	=	Lockheed Missiles and Space Co.
LN_2	=	Liquid nitrogen
Mg	=	Magnesium
mil	=	1/1000 of an inch
MKS system	=	Metric system of units; meters, kilograms, seconds, etc.
MSD	=	Missiles and Space Division
N_2	=	Nitrogen
NASA	=	National Aeronautics and Space Administration
Ni	=	Nickel
nm	=	Nautical miles
NRL	=	Naval Research Laboratory
NS	=	Not specified
OD	=	Outside diameter
ONR	=	Office of Naval Research
OSO	=	Orbiting solar observatory
oxid.	=	Oxidized
oz	=	Ounces
Pb	=	Lead
pol.	=	Polished
psi	=	Pounds per square inch
°R	=	Degrees Rankine
rec.	=	Received
ref	=	Reference
rms	=	Root-mean-square

1.3 (Continued):

s	=	second(s)
sec	=	second(s)
sm	=	Statute miles
sol.	=	Solution
SS	=	Stainless steel
Ti	=	Titanium
torr	=	Millimeters of mercury
UV	=	Ultraviolet
V	=	Volts
VHF	=	Very high frequency
W	=	Watts
Xe	=	Xenon
μ	=	Microns (10^{-6} meter)
μ	=	One-millionth (where used as an adjective, e.g., μin)

1.4 Definitions and Terminology:

The first group of definitions, Par. 1.4.1, follows the notation of Worthing (Reference 1). This notation and the applied concepts have appeared in recent reports by WADC (Reference 2) and the Battelle Memorial Institute (Reference 3), and have been adopted throughout the aerospace industry.

1.4.1 Thermal Radiation Terms: When the term is expressed in units, such unit is given in the definition.

Radiancy, R: The rate of radiant energy emission from a unit area of a source in all the radial directions of the overspreading hemisphere. The subscript b or 0 indicates a blackbody value. Given in units of Btu/h-ft^2.

Steradiancy, $R_{\theta\phi}$: The rate of radiant energy emission per unit of solid angle per unit of projected area of a source, in a stated angular direction from the surface. Given in units of Btu/h-ft^2.

Blackbody: An ideal emitter that radiates energy at the maximum possible rate per unit area at each wavelength for any given temperature. A blackbody also absorbs all radiant energy incident upon it.

Gray Body: A nonblackbody whose emittance may be considered as being independent of wavelength and temperature.

Diffuse Body: A body from which emitted radiant energy has the same flux density in all directions in the overspreading hemisphere.

Specular Reflector: A mirror-like surface for which the reflected steradian angle equals the incident steradian angle.

1.4.1 (Continued):

Emittance, ϵ: The ratio of the rate of radiant energy emission from a body, as a consequence of its temperature only, to the corresponding rate of emission from a blackbody at the same temperature.

Absorptance, α: The ratio of radiant energy absorbed by a body to that incident upon it.

Reflectance, ρ: The ratio of radiant energy reflected by a body to that incident upon it.

Emissivity, Absorptivity, Reflectivity (ϵ, α, ρ): Special cases of emittance, absorptance, and reflectance, which are fundamental properties of a material that has an optically smooth surface and is sufficiently thick to be opaque.

Transmittance, τ: The ratio of radiant energy transmitted through a body to that incident upon it.

1.4.1.1 Additional Qualification of Terms: Each property defined beyond ϵ, α, ρ and τ requires additional qualifications to arrive at a precise definition. The terms total and spectral, and the terms hemispherical, normal, and directional are used to subscript the general property. Emittance will be used to define the total, spectral, hemispherical, normal, and directional terms. Each of the following forms of ϵ is a consequence of the surface temperature referenced to a blackbody at the same temperature.

Spectral Emittance, ϵ_λ: Spectral radiancy (or monochromatic radiancy at a given wavelength) from a body to that of a blackbody.

Total Emittance, ϵ_T: Total radiancy (radiation over the entire spectrum of emitted wavelength) from a body to that of a blackbody.

Hemispherical Emittance, ϵ_H: Radiancy from a body to that of a blackbody.

Directional Emittance, ϵ_θ: Steradiancy from a body to that of a blackbody.

Normal Emittance, ϵ_N: The special case of directional emittance when the emittance is in a direction normal to the surface.

Therefore, precise definitions of emittance will take the following nomenclature:

ϵ_{TH} = Total hemispherical emittance, dimensionless
ϵ_{TN} = Total normal emittance, dimensionless
$\epsilon_{\lambda H}$ = Spectral hemispherical emittance, dimensionless
$\epsilon_{\lambda N}$ = Spectral normal emittance, dimensionless

1.4.2 Space Technology Terms: Dimensional units are not included, since these appear elsewhere, when applicable.

Albedo (Reflected Solar Radiation): The ratio of the total solar radiant energy reflected by a body to the total solar radiant energy incident on the body. Albedo is associated with specific bodies; for example, Earth albedo, lunar albedo.

Insolation (Solar Radiation): The irradiation of a body by direct total solar radiant energy.

Earth Shine (Earth Radiation): Refers to the total radiancy from the Earth as a consequence of its apparent temperature.

Celestial Sphere: A sphere of infinite radius whose center is the center of the Earth and upon which appear projected the stars and other astronomical bodies.

Ecliptic: The great circle on the celestial sphere formed by its intersection with the plane of the Earth's orbit.

Ecliptic Plane: The plane defined by the orbit of the Earth about the Sun.

Planet Inclination: The angle defined between the orbit of the planet about the Sun and the ecliptic plane.

Equatorial Inclination: The angle between the planet's equator and the ecliptic.

2. BASIC HEAT TRANSFER THEORY:

2.1 Conduction:

Reference is made to AIR1168/2, Par. 1. The general conduction equation holds in space as in a gravity field, although surface interface conductances may be altered as a result of vacuum effects.

$$q_{12} = \frac{k}{x} A(t_1 - t_2) \qquad \text{(Eq.1)}$$

where:

k/x is the thermal conductance in Btu/h-ft^2-°F and other terms are defined in Par. 1.2

Thermal joint conduction in a vacuum has been analyzed by Fried and Costello (References 4 and 5) and some typical examples are presented in Figures 1 through 3.

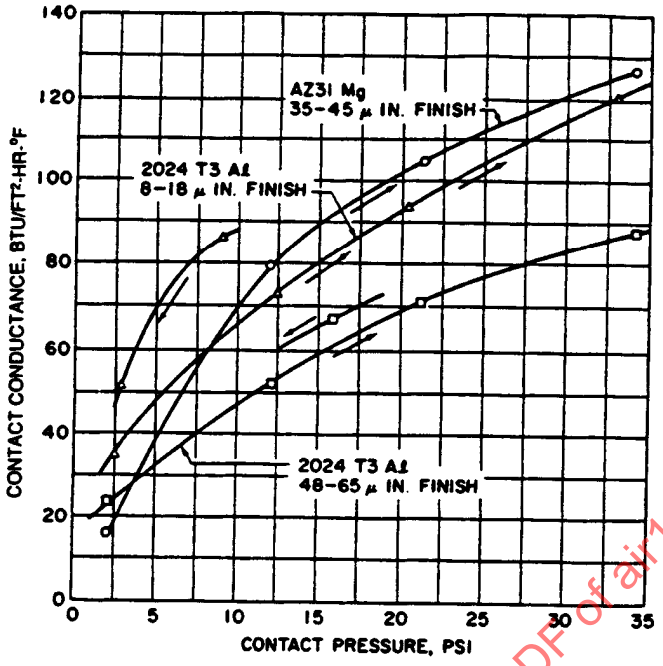

FIGURE 1 - Thermal Contact Conductance for Aluminum and Magnesium Joints in Vacuum (References 4 and 5)

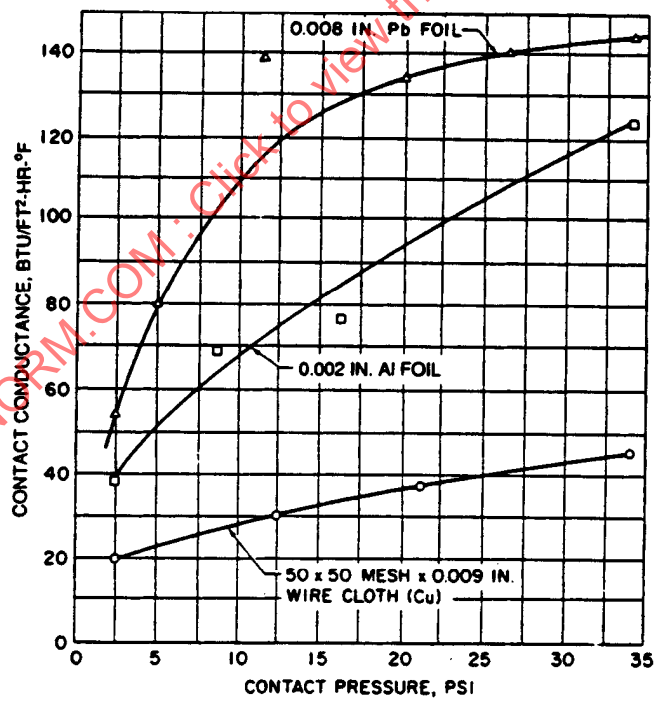

FIGURE 2 - Thermal Contact Conductance for Aluminum Joint with Metallic Shims in Vacuum (References 4 and 5)

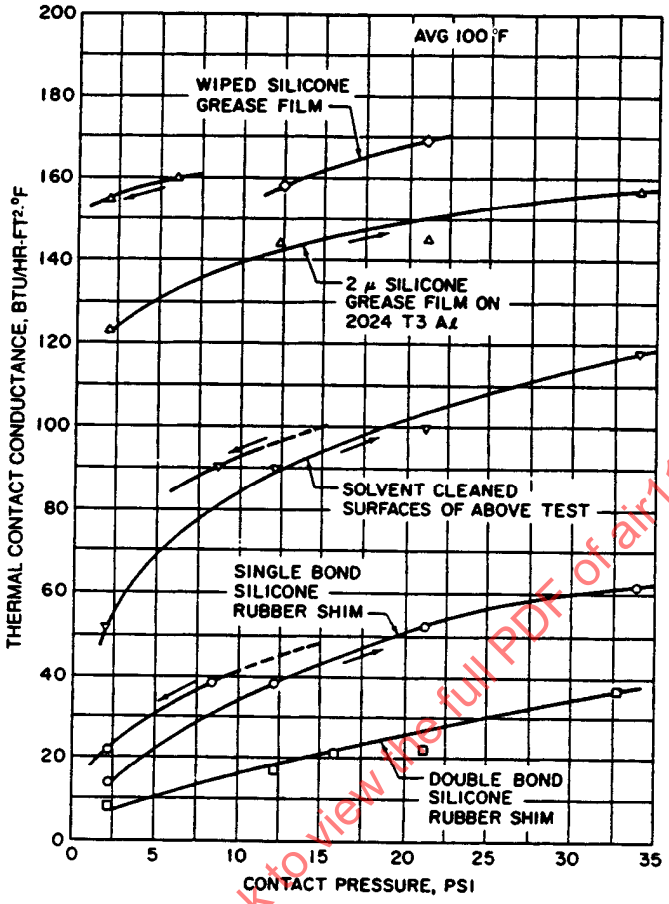

FIGURE 3 - Thermal Contact Conductance for Nonmetallic Shims in Vacuum (References 4 and 5)

2.2 Radiation (Reference 3):

2.2.1 Lambert's Cosine Law: This law states that the intensity of radiation streaming from a plane source varies as the cosine of the angle between the direction of emission and the surface normal. A diffusely radiating body has the same apparent brightness regardless of the angle from which it is viewed. Actually, the emittance of all true surfaces exhibits a certain degree of dependence on the angle of emission.

2.2.2 Stefan-Boltzmann's Fourth Power Law: Heat radiating from a body is proportional to the fourth power of its absolute temperature. For nonblackbodies, the emittance is the ratio of the nonblackbody radiancy to blackbody radiancy; therefore, the nonblackbody radiancy equals the blackbody radiancy multiplied by the emittance:

$$R_b = \sigma T^4; \quad R = \epsilon \sigma T^4 \qquad \text{(Eq.2)}$$

2.2.3 Kirchhoff's Law: As derived from the original law, the total emittance of a nonblackbody at any given temperature is equal to its total absorptance of radiation from a blackbody at the same temperature, or $\epsilon = \alpha$. This applies equally well to spectral radiation and becomes

$$\epsilon_\lambda = \alpha_\lambda \qquad \text{(Eq.3)}$$

2.2.4 Wien's Displacement Law: The product of the absolute temperature of a blackbody and the wavelength at which the maximum intensity of radiation is emitted for that temperature is a constant:

$$\lambda_{max} = \frac{2897.9}{T}\ \mu\text{-K (MKS system)} \qquad \text{(Eq.4)}$$

$$= \frac{5216}{T}\ \mu\text{-}^\circ\text{R} \quad \text{(British system)} \qquad \text{(Eq.5)}$$

2.2.5 Planck's Distribution Law: Spectral radiancy distribution is a function of temperature as shown by Planck's formula:

$$R_{b,\lambda} = \frac{C_1 \lambda^{-5}}{e^{C_2/\lambda T} - 1} \qquad \text{(Eq.6)}$$

where:

for temperature in the MKS system (using K), C_1 = 37,436 W-μ^4/cm^2 and C_2 = 1.4388 cm-K = 14,388 μ-K

2.2.5 (Continued):

In the British system (using °R), C_1 = 1.187 x 10^8 Btu-μ^4/ h-ft^2 and C_2 = 25896 μ-°R. This law holds for all wavelengths and over the entire spectrum.

$$R_b = \int_0^\infty R_{b,\lambda} d\lambda = \sigma T^4 \quad \text{(Eq.7)}$$

2.2.6 General Relationships: As a general case, any radiant energy incident on a body must be reflected, absorbed, or transmitted by the body. If the fraction of the incident radiation absorbed is α, the fraction transmitted τ, and the fraction reflected ρ, then by the law of conservation of energy:

$$\alpha + \rho + \tau = 1 \quad \text{(Eq.8)}$$

and for an opaque surface (τ = 0):

$$\alpha + \rho = 1 \quad \text{(Eq.9)}$$

2.2.7 Radiation Heat Transfer Between Two Surfaces: The applicable equation for heat transfer is

$$q_{12} = A_1 F_{A,12} F_{e,12} \sigma (T_1^4 - T_2^4) \quad \text{(Eq.10)}$$

where:

F_A and F_e are defined for some common surfaces as follows:

(1) Surface A_1 small compared with the totally enclosing surface A_2: F_A = 1, $F_e = \epsilon_1$.

(2) Surfaces A_1 and A_2 of parallel discs, squares, 2:1 rectangles, long rectangles: For F_A, see Figure 4; $F_e = \epsilon_1 \epsilon_2$.

In Figure 4, curves are presented for the following geometries:

(a) Curves 1-2-3-4: Direct radiation between planes.
(b) Curves 5-6-7-8: Planes connected by nonconducting but reradiating walls.
(c) Curves 1,5: Discs.
(d) Curves 2,6: Squares.
(e) Curves 3,7: Rectangle, 2:1.
(f) Curves 4,8: Long, narrow rectangles.

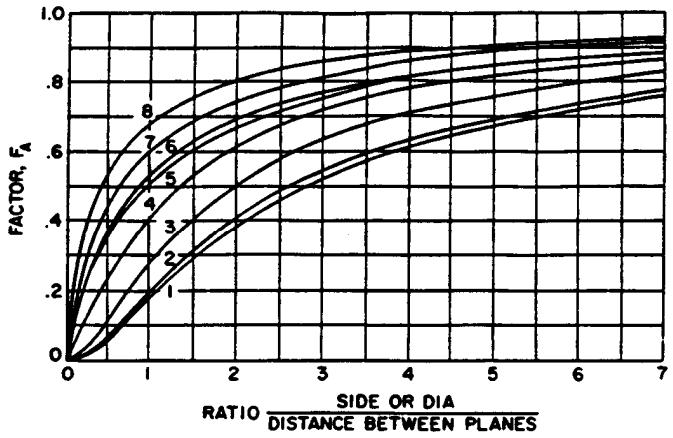

FIGURE 4 - Radiation Between Parallel Plates Directly Opposed
(Hottel, Reference 6)

2.2.7 (Continued):

(3) Surface dA_1 and parallel rectangular surface A_2 with one corner of rectangle above dA_1: For F_A, see Figure 5; $F_e = \epsilon_1 \epsilon_2$.

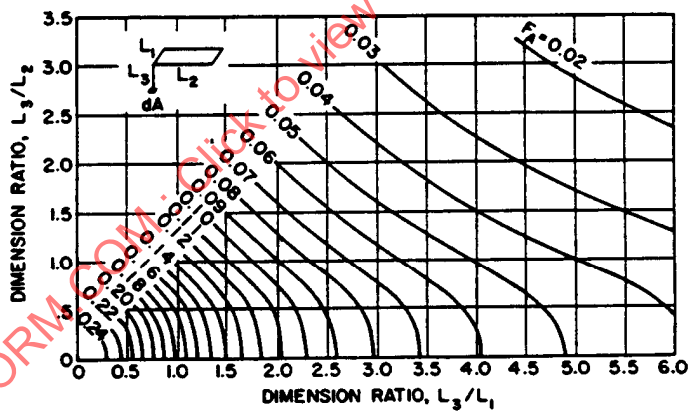

FIGURE 5 - Radiation Between Surface Element dA and Rectangle Above and Parallel to it with One Corner of Rectangle Contained in Normal to dA; L_1, L_2 = Sides of Rectangle, L_3 = Distance from dA to Rectangle, and F_A = Fraction of Direct Radiation from dA Intercepted by Rectangle (Reference 6)

(4) Surfaces A_1 or A_2 of perpendicular rectangles having a common side: For F_A, see Figure 6; $F_e = \epsilon_1 \epsilon_2$. Referring to the sketch in Figure 6, R_1 = y/x, which is the length of the unique side of a rectangle on whose area the heat transfer equation is based in ratio to the length of the common side. Also, R_2 = z/x, which is the length of the unique side of the other rectangle in ratio to the length of the common side.

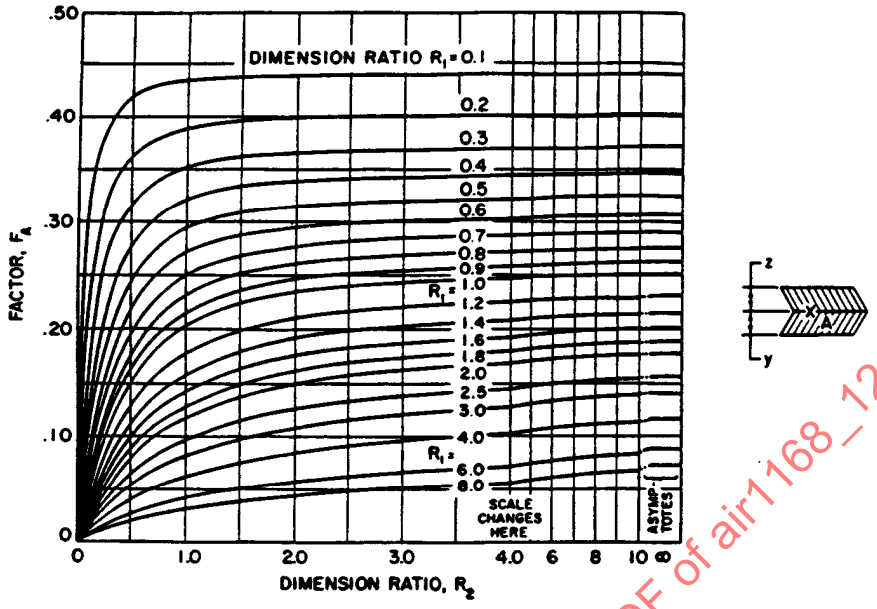

FIGURE 6 - Radiation Between Adjacent Rectangles in Perpendicular Planes (Hottel, Reference 6)

2.2.7 (Continued):

(5) Surfaces A_1 and A_2 of infinite parallel planes or surface A_1 of a completely enclosed body is small compared with A_2: $F_A = 1$ and

$$F_e = \frac{1}{[1/\epsilon_1 + 1/\epsilon_2] - 1} \qquad \text{(Eq.11)}$$

(6) Concentric spheres or infinite concentric cylinders with surfaces A_1 and A_2: $F_A = 1$ and

$$F_e = \frac{1}{(1/\epsilon_1) + (A_1/A_2)[(1/\epsilon_2) - 1]} \qquad \text{(Eq.12)}$$

For further information on form factor relationships, see Reference 7 and AIR1168/2, Par. 4.7.5.

2.2.8 Shape Factors Using String Technique (Reference 52): The AF product for interchange between two surfaces of an enclosure, per unit depth normal to that shown in Figure 7, is the sum of the lengths of straight crossed strings stretched between the ends of the lines representing the two surfaces, less the sum of the lengths of uncrossed strings similarly stretched between the surfaces, all divided by 2. Referring to Figure 7, for an enclosure (a) formed by three surfaces A_1, A_2, A_3.

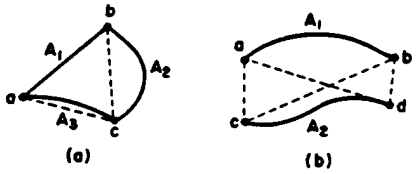

FIGURE 7 - String Technique to Obtain Shape Factors

$$A_1F_{12} \equiv A_2F_{21} = \frac{ab + bc - ac}{2} \text{ x unit depth} \qquad \text{(Eq.13)}$$

and for opposing surfaces (b),

$$A_1F_{12} \equiv A_2F_{21} = \frac{(ad + bc) - (ac + bd)}{2} \text{ x unit depth} \qquad \text{(Eq.14)}$$

3. SOLAR SYSTEM CONSTANTS:

Table 1 contains the planetary constants that are useful in determining the heat flux to spacecraft. The spectral data of solar, albedo, and Earth radiation, Figures 8, 9, and 10, can be used in the determination of the thermal properties of materials in the vicinity of the Earth.

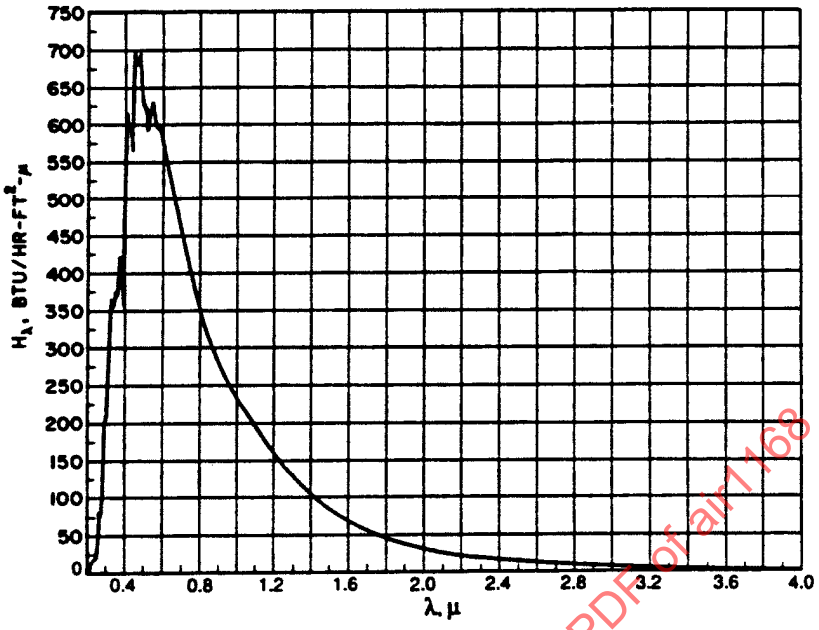

FIGURE 8 - Spectral Solar Irradiance (Reference 14)

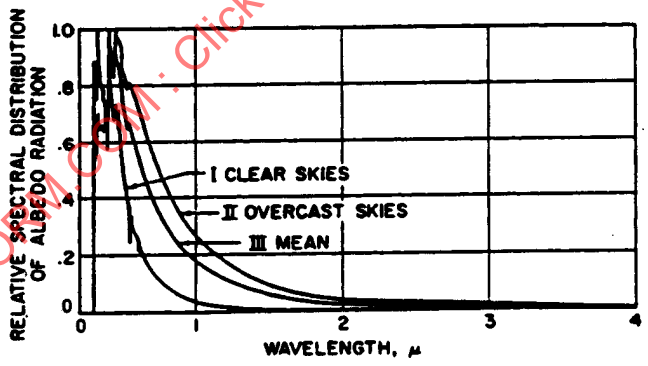

FIGURE 9 - Relative Spectral Distributions of Albedo Radiation Under Various Sky Conditions (Reference 11)

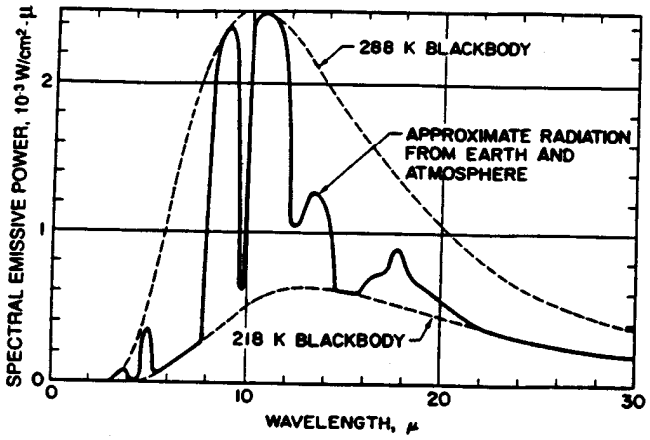

FIGURE 10 - Typical Spectral Emission Curve for the Thermal Radiation Leaving the Earth. The 288 K Blackbody Curve Approximates the Radiation from the Earth's Surface and the 218 K Blackbody Curve Approximates the Radiation from the Atmosphere in Those Spectral Regions Where the Atmosphere is Opaque (Reference 11)

TABLE 1 - Planetary Constants for Thermal Design

Constant	Sun	Mercury	Venus	Earth	Mars	Jupiter	Saturn	Uranus	Neptune	Pluto	Moon
Major Semi-axis, A.U.[1], Reference 13	.....	0.3871	0.7233	1.000	1.524	5.203	9.539	19.18	30.06	39.52	384,400 km
Perihelion, A.U.[1], Reference 13	.....	0.3075	0.7184	0.9833	1.381	4.951	9.008	18.28	29.80	29.69	
Aphelion, A.U.[1], Reference 13	.....	0.4667	0.7282	1.0167	1.666	5.455	10.070	20.09	30.32	49.34	
Radius, km, Reference 13	696,000	2,500	6,200	6,378.39	3310	69,880	57,500	25,500	25,000	.....	1738
Inclination, Reference 13											
Orbital to Ecliptic	.....	7°0'14"	3°23'39"	.....	1°50'51"	1°18'20"	2°29'42"	46°23'	1°46'27"	17°8'38"	
Equatorial to Ecliptic	.....	.....	.....	23°26'59"	25°12'	3°7'7"	26°45'	97°59'	29°		
Solar Heat Flux Q_s, Btu/h-ft^2, Reference 10	.....	2953.9	846.3	442.4	190.5	16.4	4.9	1.2	0.5	0.3	442.2
Albedo a, Reference 10	.....	0.07	0.76	0.35[3]	0.15	0.51	0.50	0.66	0.62	0.16	0.124
Blackbody Planet Temperature T_p											
K, Reference 13[2]	5,800[4,5] 6,000[4,6]	450	700[7]	250[3]	225	122	90	64	51	45	243[8]
°R	10,440 10,800	810	1260	450	405	220	162	115	92	81	430[9]
Planet Heat Flux, R_p, Btu/h-ft^2	.....	745	4360	70.9	46	4	1.2	0.3	0.1		

[1] A.U. = Astronomical unit = 149.4 x 10^6 km.
[2] Temperature of space assumed to be 4 K.
[3] Grumman design for OAO.
[4] Reference 11.
[5] Total emitted radiation.
[6] Visible and infrared radiation; UV not included;
[7] Reference 9.
[8] Hot side = 374 K; cold side = 120 K.
[9] Hot side = 673 °R; cold side = 216 °R. Reference 8.

4. SPACECRAFT THERMAL COATINGS:

In the thermal balance of passive spacecraft, the temperature of the internal electronic equipment and structure is governed by the exterior surface properties, that is, by the absorptance of solar, albedo, and planetary radiation, and the thermal emittance.

4.1 Ideal Versus Available Materials:

Figures 11 and 12 (Reference 11) show the ideal thermal radiative properties of materials in comparison with those now available. Reference 45 also describes an availability range of materials.

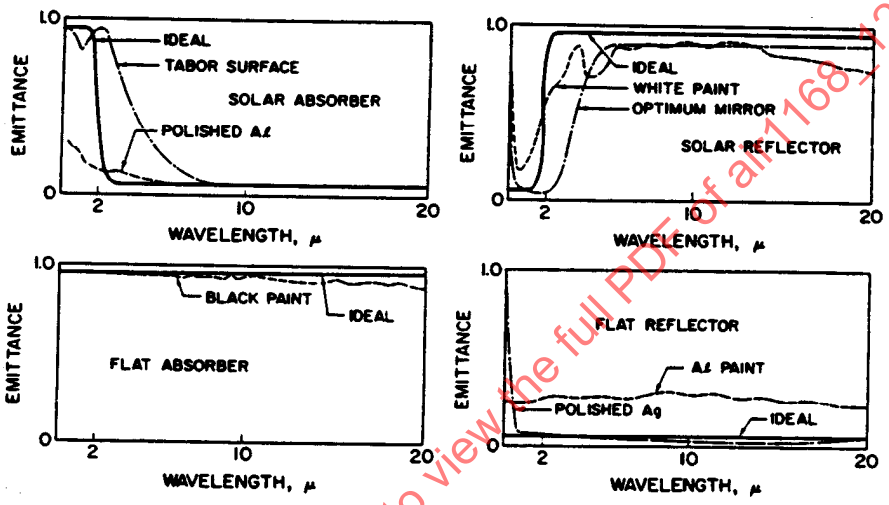

FIGURE 11 - Representative Spectral Emittance Curves for Four Ideal Surfaces (Reference 11)

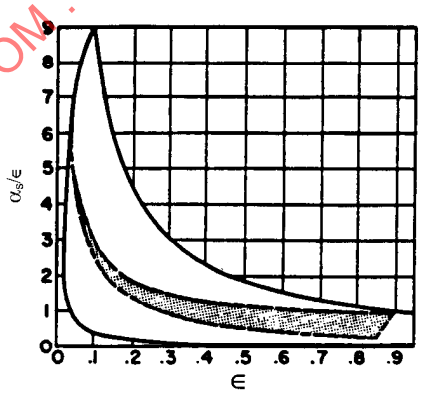

FIGURE 12 - Radiation Characteristics Attainable with Four Optimum Surfaces Compared to Those Attainable with Currently Available Materials. The Solid Lines Show Limits of Characteristics with Known Surfaces and the Dashed Lines Show Limits of Characteristics with Available Surfaces (Reference 11)

4.2 Solar Absorptance:

According to Johnson's work (Reference 14), 95.3% of the sun's emitted energy falls in the spectral region between 0.3 and 2.5 μ, 1.2% falls below 0.3 μ, and 3.4% falls above 2.5 μ. The maximum spectral intensity lies in the 0.5 μ region. Therefore, the solar absorptance α_s of a coating is approximated by the thermal radiation properties of the coating in the 0.3 to 2.5 μ range of the spectrum.

The solar absorptance α_s would then be further defined by the angle of incidence of solar energy to the coating surface shown in the following equations (Reference 15). For the case of azimuthal symmetry, the solar reflectance is:

$$\rho_{s,\theta} = \frac{\int_{0.3\mu}^{2.5\mu} \rho_{\lambda,\theta} H_\lambda d\lambda}{\int_{0.3\mu}^{2.5\mu} H_\lambda d\lambda} \quad \text{(Eq.15)}$$

and for opaque surfaces:

$$\alpha_{s,\theta} = 1 - \rho_{s,\theta} \quad \text{(Eq.16)}$$

where:

θ = constant angle of incidence, deg

4.3 Surface Emittance:

4.3.1 Temperature Dependence: The spectral range in which a surface emits energy is determined by the temperature of the surface. In accordance with Equation 5, the wavelength of peak radiancy can be computed for any given temperature. Dividing Equation 6 by T^5, the radiancy term becomes a function of λT and can be plotted as shown in Figure 13. The blackbody radiancy for any λT combination can be obtained from this curve.

In Figure 14 the percentage of total energy emitted from a blackbody surface is shown as a function of surface temperature and wavelength. For a 100 °F body, 92% of the total emitted energy falls below 40 μ and 0.5% of the energy falls below 4.5 μ; thus between these limits, 92% of the blackbody energy is contained.

An approximate spectral definition of emittance at 100 °F would be

$$\epsilon_{100°F} = \frac{\int_{4.5\mu}^{40\mu} \epsilon_\lambda R_{b,\lambda}(t) d\lambda}{\int_{4.5\mu}^{40\mu} R_{b,\lambda}(t) d\lambda} \quad \text{(Eq.17)}$$

At colder temperatures the emittance of surfaces are influenced by their thermal radiation properties in the far infrared region.

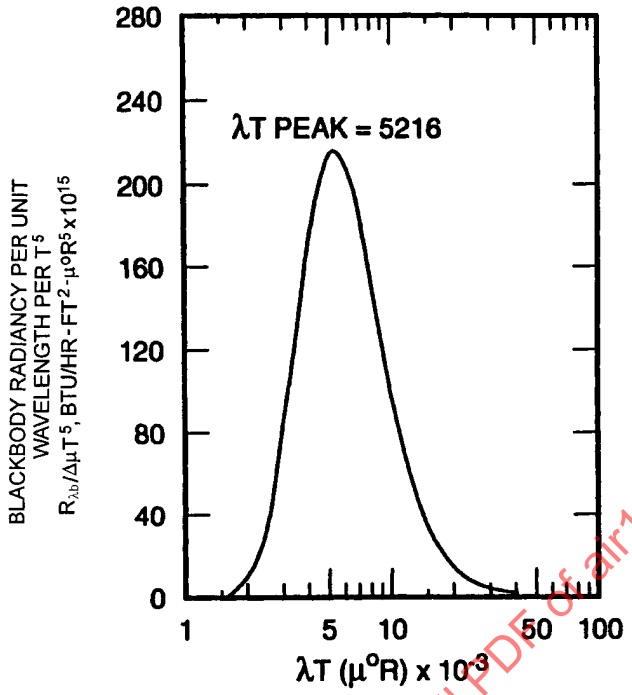

FIGURE 13 - Blackbody Radiance ($R_{b_\lambda}/\Delta\mu T^5$) as a Function of Temperature and Wavelength

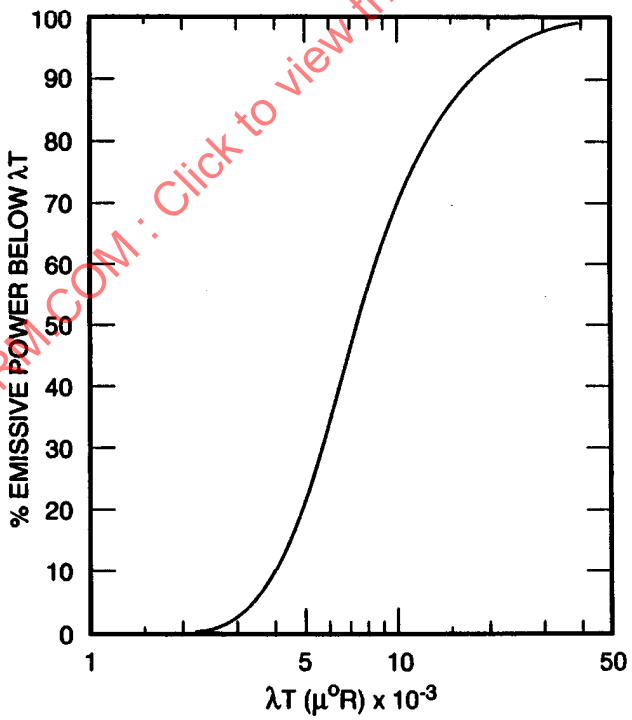

FIGURE 14 - Percent of Total Blackbody Energy Below λT as a Function of Temperature and Wavelength

4.3.2 Angular Dependence: Total hemispherical emittance and total normal emittance for opaque surfaces depend upon how total directional reflectance varies with the angle of incidence. The following set of equations (azimuthal symmetry case) describe the relationship of total hemispherical emittance to the spectral directional reflectance of a coating (Reference 15).

$$\rho_{TH}(t) = \frac{\int_{\lambda_1}^{\lambda_2}\int_{\theta=0}^{\theta=\pi/2} \rho_{\lambda,\theta}\, 2\pi \sin\theta \times \cos\theta\, d\theta\, R_{b\lambda}(t)\, d\lambda}{\int_{\lambda_1}^{\lambda_2}\int_{\theta=0}^{\theta=\pi/2} 2\pi \sin\theta \times \cos\theta\, d\theta\, R_{b\lambda}(t)\, d\lambda} \quad \text{(Eq.18)}$$

$$\epsilon_{TH}(t) = 1 - \rho_{TH}(t) \text{ (opaque surface)} \quad \text{(Eq.19)}$$

$$\epsilon_{TH}(t) = \alpha_{TH}(t) \text{ (Kirchhoff's law at thermal equilibrium)} \quad \text{(Eq.20)}$$

where:

λ_1 and λ_2 are the end wavelength limits to cover 92% of $\int R_{b\lambda}(t)\, d\lambda$

The equations for total normal emittance, which is readily measured in the laboratory, would be

$$\rho_{TN}(t) = \frac{\int_{\lambda_1}^{\lambda_2} \rho_{\lambda\theta}\, R_{b\lambda}(t)\, d\lambda}{\int_{\lambda_1}^{\lambda_2} R_{b\lambda}(t)\, d\lambda} \quad \text{(Eq.21)}$$

where:

θ = 0 deg, and

$$\epsilon_{TN}(t) = 1 - \rho_{TN}(t) \text{ (opaque surface)} \quad \text{(Eq.22)}$$

$$\epsilon_{TN}(t) = \alpha_{TN}(t) \text{ (Kirchhoff's law)} \quad \text{(Eq.23)}$$

For metal surfaces, the ratio $\epsilon_{TH}/\epsilon_{TN}$ is greater than 1, and for dielectric surfaces, the ratio $\epsilon_{TH}/\epsilon_{TN}$ may vary from 0.92 to slightly above 1.0.

The relation is plotted as a function of the measurable normal emittance in Figure 15 (Reference 16). For an ideal diffuse emitter (emits according to Lambert's law), $\epsilon_{TH}/\epsilon_{TN}$ = 1.

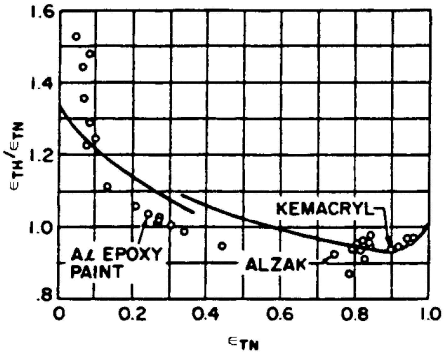

FIGURE 15 - Ratio of Total Hemispherical Emittance to Normal Emittance

4.4 Measurement of Absorptance and Emittance:

There are two distinct measurement techniques employed for obtaining α_s and ϵ: the spectral reflectance technique and calorimetric techniques.

4.4.1 Spectral Measurements: The reflectance method is based on the definition of reflectance, which requires that the reflected energy be measured over the entire overspreading hemisphere. In determining α_s, the definition is complied with in the 0.25 to 2.5 μ range, using an integrating sphere-spectrophotometric apparatus (Reference 18). The resultant property measured is the directional spectral reflectance. Integration of the spectral reflectance data over the Johnson curve (by IBM program or equal energy increment summation techniques) yields total normal solar reflectance as shown in Equation 15. When subtracted from 1, α_s is realized.

Based upon the reflectance reciprocity relation, the normal or directional spectral reflectance in the 2.5 to 50 μ range may be measured with a heated cavity reflectometer-spectrophotometer type of apparatus (Reference 19). In this case the sample is irradiated hemispherically and viewed at a specific angle by the spectrophotometer's optical system.

Integration of the spectral reflectance data over the appropriate spacecraft temperature blackbody curve yields the total normal emittance properties of the material. The total normal emittance must be converted to total hemispherical emittance, using Figure 15. For detailed thermal control design where total hemispherical properties are required, the normal spectral reflectance data should be supplemented with directional reflectance information and an integration (or discrete summation) be performed in accordance with Equation 18.

The spectral normal reflectance data for several materials (Reference 23) appear in Figures 16 to 22.

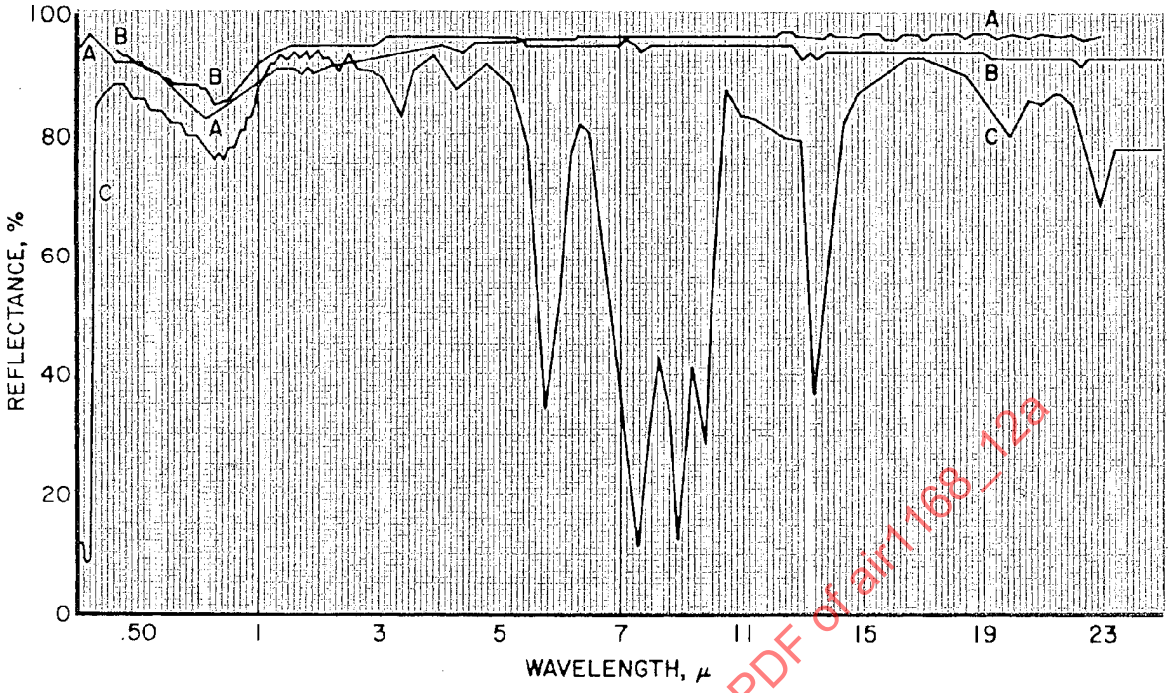

FIGURE 16 - Compiled Spectral Reflectances; A, Evaporated Al, 25 μin on Polished Al 6061-T6; B, Evaporated Al (0.2 μ) on 1/4 mil Mylar Crumpled and Stretched (Looking at Al); C, Evaporated Al (0.2 μ) on 1/4 mil Mylar Crumpled and Stretched (Looking at Mylar) (Reference 23)

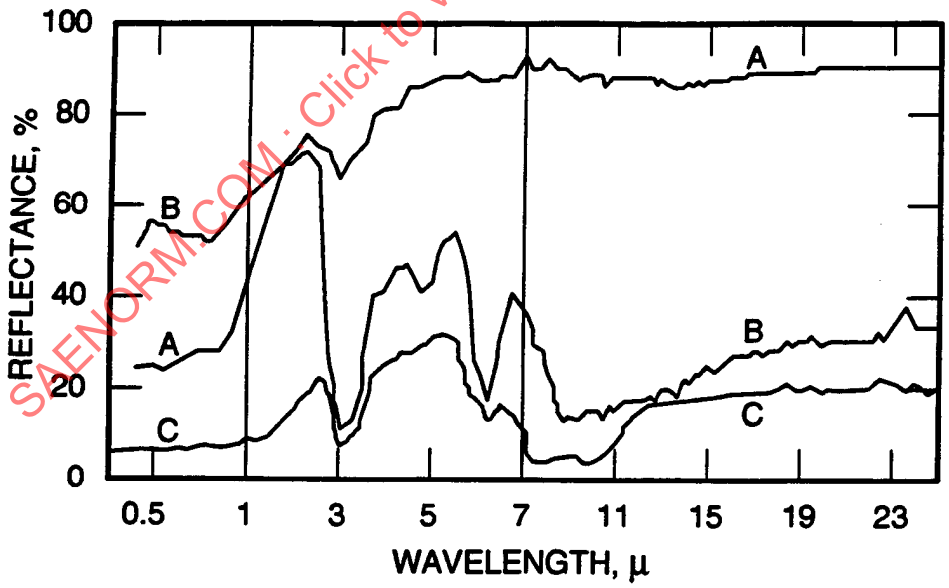

FIGURE 17 - Compiled Spectral Reflectances: A, Chromic Acid Anodize on Al 24S-T81; B, Sulfuric Acid Anodize on Extruded Al 24S-T81; C, Hard Anodize (1 mil) on Al 6061-T6 (35 A/ft^2 at 45 V, 20 °F) (Reference 23)

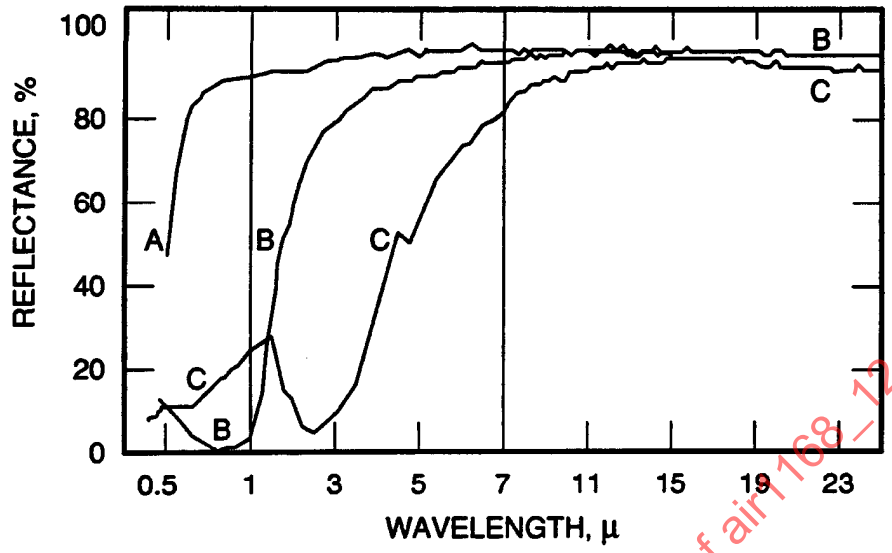

FIGURE 18 - Compiled Spectral Reflectances: A, Polished Cu, 17 mils Thick; B, Tabor Solar Collector Chemical Treatment (110-30) on Ni-plated Cu; Tabor Solar Collector Chemical Treatment (125-30) on Ni-plated Cu (Reference 23)

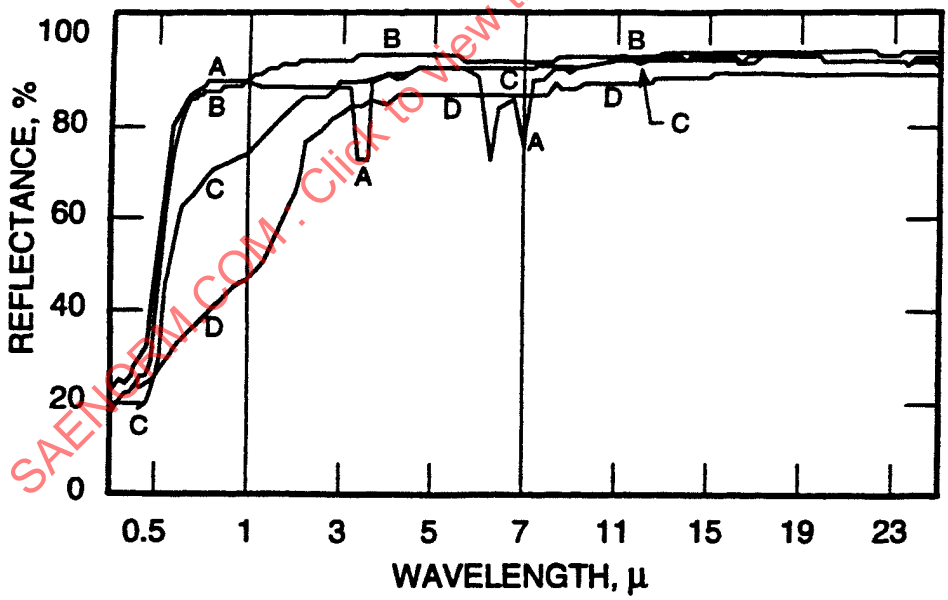

FIGURE 19 - Compiled Spectral Reflectances; A, Immersion Au Approximately 0.03 mil on Ni-plated Cu Plate on Polished Al 6061-T6, Aged 6 months in Air Unpolished; B, Vacuum Evaporated Au on Fiberglas Laminate; C, Au Ash (80 μ) on 0.4 mil Ag on Epon Glass; D, White Au on Polished MIL-S-5059 Steel (Reference 23)

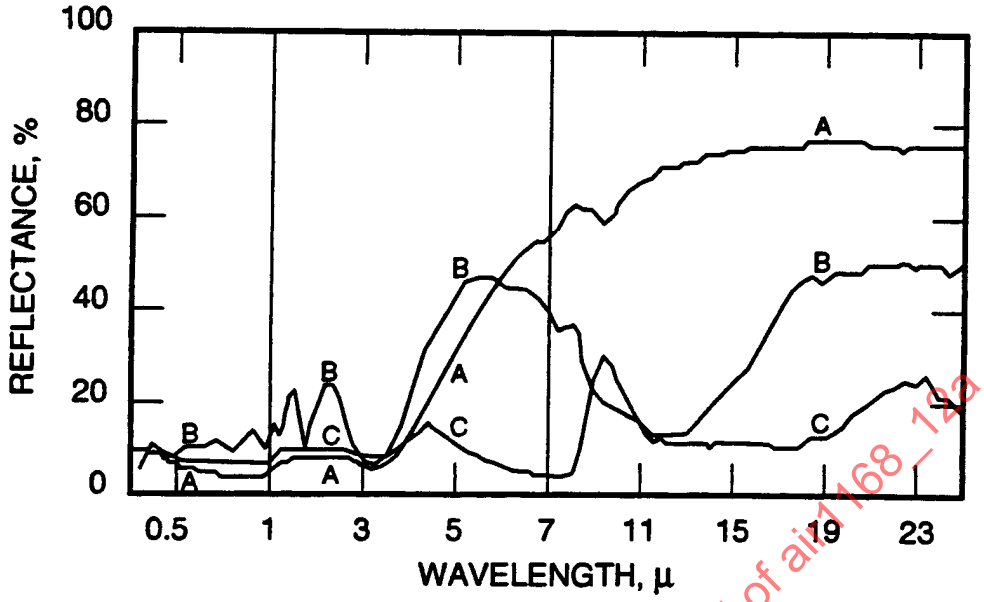

FIGURE 20 - Compiled Spectral Reflectances: A, Silicon Solar Cell (Intl. Rectifier Corp.); B, Silicon Solar Cell (Intl. Rectifier Corp.), 1.11 μ Vaporized Coating SiO, Fast Deposition Rate; C, Silicon Solar Cell (Hoffman Corp.) type 120-C, 3 mil Glass Cover (Reference 23)

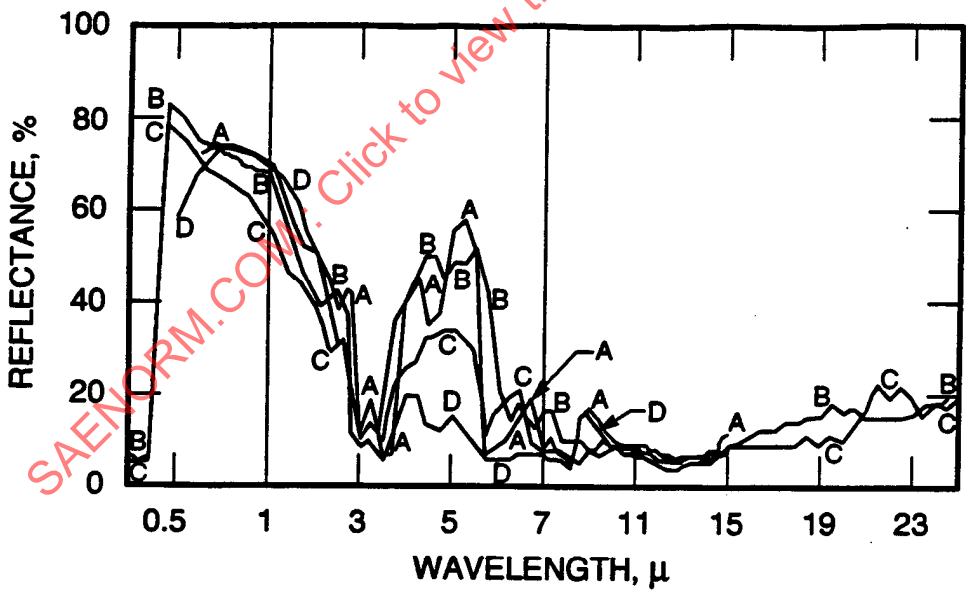

FIGURE 21 - Compiled Spectral Reflectances: A, Flat White Paint, Fuller No. 2882 on 2 mil Polished Al; B, White Epoxy Resin Paint, Mg; C, Flat White Acrylic Resin, Sherwin-Williams M49WC8-CA-10144, MIL-C-15328A Pretreatment Wash Coating on 22 mil SS 301, Half-Hard; D, White Paint Mixed With Powdered Glass, 7 mil on Polished Al (Reference 23)

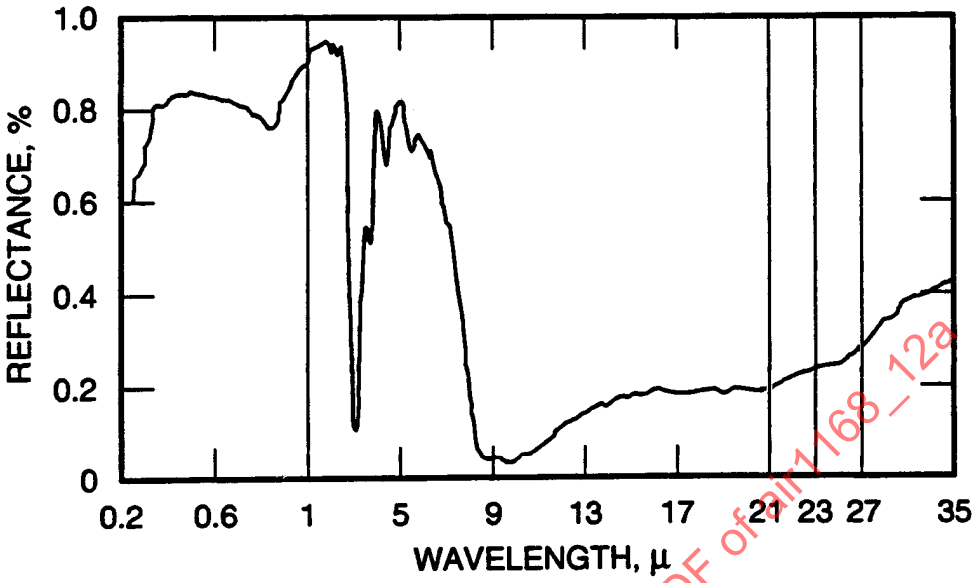

FIGURE 22 - Spectral Reflectance of Alzak (Typical); (Reference 20);
α_s = 0.145 and $\epsilon_{TH,100\,^\circ F}$ = 0.773

4.4.2 Calorimetric Measurements: Calorimetric measurements of α_s and ϵ will yield ϵ_{TH} directly, but the α_s measurement validity depends on matching the solar simulator to the spectral distribution of Figure 8. Relative spectral curves of solar, carbon arc, and a bare xenon lamp are shown in Figures 78 and 79. The carbon arc simulates the solar spectrum more closely than do other light sources.

Calorimetric measurements are made in a vacuum chamber having black liquid N_2, cold walls, and preferably a cooled reflecting mirror similar to the design of the GE chamber of Figure 75. Thus, direct emission of the hot port window is eliminated. Other secondary effects are radiation from the chamber and mirror walls plus internal reflection off the walls.

For measurements made at sample equilibrium temperatures the following can be used, neglecting wall reflectance:

1. Electrical heating of the sample, property ϵ_{TH}:

$$\epsilon_{TH} = \frac{I^2 R_c}{A_c \sigma (T_c^4 - T_w^4)} \qquad \text{(Eq.24)}$$

4.4.2 (Continued):

2. Solar simulator as heater, property α_s/ϵ_{TH}:

$$\frac{\alpha_s}{\epsilon_{TH}} = \frac{\sigma A_c}{H_{ss} A_{pc}} (T_c^4 - T_w^4) \quad \text{(Eq.25)}$$

Dynamic measurements may also be made using a solar simulator as a heater (References 15 and 20). Measure the slope of the cooldown curve and solve for ϵ_{TH}. Neglecting wall radiation and reflections,

$$\epsilon_{TH} = \frac{-mC_p(dT_c/d\tau)}{A_c \sigma T_c^4} \quad \text{(Eq.26)}$$

Measuring the heat-up portion,

$$mC_p \frac{dT_c}{d\tau} = A_{pc} \alpha_s H_{ss} - A_c \epsilon_{TH} \sigma T_c^4 (\alpha_s) \quad \text{(Eq.27)}$$

where:

$$\alpha_s = \frac{mC_p(dT_c/d\tau) + A_c \epsilon_{TH} \sigma T_c^4}{A_{pc} H_{ss}} \quad \text{(Eq.28)}$$

Since the thermal radiation properties are dependent not only on the material but also on the coatings, thickness, and surface condition, published numerical values for α_s and ϵ_{TH} must be used cautiously. Data on the values of α_s and ϵ should include a complete statement as to coating surface roughness, coating thickness, cleanliness, precise coating chemical composition, and a complete substrate definition (Reference 22). Current published data seldom supply sufficient coating descriptions, may even fail to distinguish between ϵ_{TN} and ϵ_{TH}, or may not associate a temperature with a given emittance figure.

4.4.3 Thermal Radiation Data: The thermal radiation properties data of Table 2, and Figures 23 through 41 with their corresponding tables (Tables 3 through 19) are meant only as a guide in materials selection. After a coating has been selected and its method of formulation, application, and handling have been fixed, the α_s and ϵ_{TH} properties should be measured.

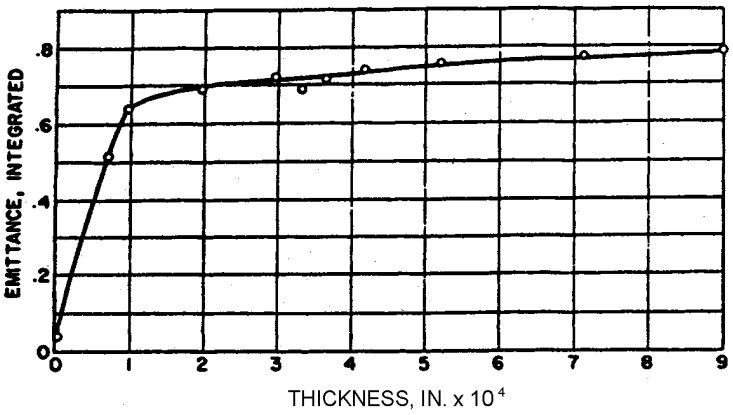

FIGURE 23 - Effect of Film Thickness on Emittance of Anodized Coating (Reference 26)

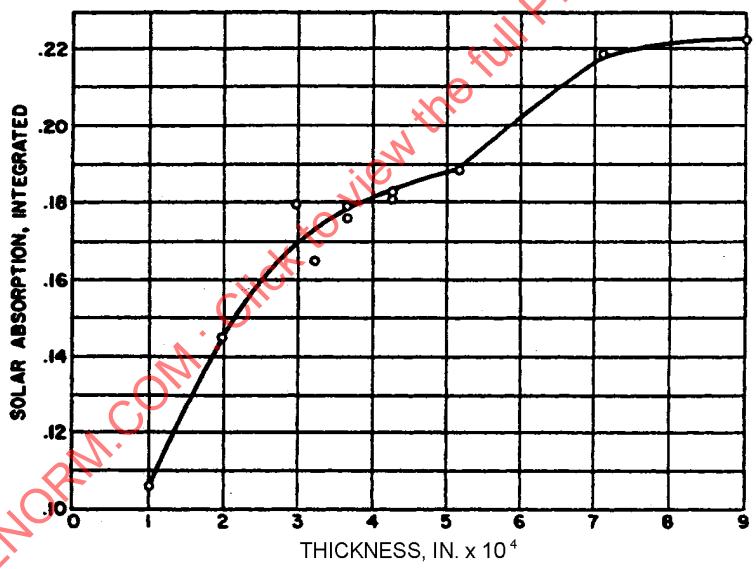

FIGURE 24 - Solar Absorption Versus Coating Thickness of Anodized Al (Reference 26)

TABLE 2 - Thermal Radiation Properties of Materials

Material	α_s	Temp., °R	ϵ_{TN}	ϵ_{TH}	α_s/ϵ_T	Ref.
ALUMINUM (Al)						
Commercial plate		671	0.09	...	...	24
Commercial plate, pol.		671	0.05	...	...	24
Commercial plate dipped in HNO_3		671	0.05	...	...	24
Commercial plate dipped in hot hydroxide		671	0.04	...	...	24
2024 Al alloy, as rec.	0.27	400	...	0.02	13.5	21
		500	...	0.02	13.5	
		600	...	0.02	13.5	
2024 Al alloy, cleaned	0.34	400	...	0.06	5.66	21
		500	...	0.06	5.66	
		600	...	0.07	4.85	
2024 Al alloy, mechanically pol. and degreased	0.31	400	...	0.05	6.20	21
		500	...	0.06	6.20	
		600	...	0.06	5.16	
2024 Al alloy, sand blasted	0.67	400	...	0.25	2.68	21
		500	...	0.27	2.48	
		600	...	0.30	2.23	
6061 Al alloy, as rec.	0.41	400	...	0.05	8.2	21
		560	...	0.04	10.25	
6061 Al alloy, chemically cleaned	0.18-0.44	400	...	0.03-0.11	...	21
		500	...	0.03-0.12	...	
		600	...	0.04-0.12	...	
6061 Al alloy, pol. and degreased	0.35	400	...	0.04	8.75	21
		500	...	0.04	8.75	
		560	...	0.05	7.00	
6061 Al alloy, 120 size grit blasted	0.60	400	...	0.40	1.5	21
		500	...	0.41	1.46	
		600	...	0.41	1.46	
Alzak on Al, 190 µin thick	0.15	410	0.79	0.74	0.20	20
		530	0.77	0.72	0.21	
		580	0.75	0.70	0.21	
Reynolds wrap Al foil, shiny side, as rec.	0.19	400	...	0.03	6.33	21
		500	...	0.04	4.75	
		550	...	0.025	...	20
Fasson adhesive backed Al foil	0.17	400	...	0.03	5.66	21
		500	...	0.03	5.66	

TABLE 2 (Continued)

Material	α_s	Temp., °R	ϵ_{TN}	ϵ_{TH}	α_s/ϵ_T	Ref.
Mylar, metallized with vacuum deposited Al	0.20	400	...	0.05	4.0	21
		500	...	0.05	4.0	
Al vacuum deposited on Mg with standard silicone undercoat	0.13	400	...	0.04	3.25	21
		500	...	0.04	3.25	
		600	...	0.04	3.25	
Anodized Al (see Figures 23 and 24)	...	...	...	...	...	26
Al 6061 T-6, hard anodize 1 mil thick	0.92	450	...	0.841	1.10	23
		410	0.830	...	...	20
		460	0.842	...	...	
		560	0.863	...	...	
ANTIMONY (Sb)						
Polished	...	671	0.03	...	...	24
Rolled plate		540	0.06	...	...	24
Shim stock		531	...	0.03	...	24
Oxidized		900	0.60	...	...	24
		671	0.60			
QMV Be alloy, 64 rms finish	0.70	400	...	0.16	4.37	21
		600	...	0.17	4.11	
CADMIUM (Cd)						
Electroplate (mossy)	...	540	0.02	...	...	24
		531	...	0.03	...	24
CHROMIUM (Cr)	...	540	0.08	...	...	24,25
Cr plate 0.1 mil thick on 0.5 mil Ni plate on 321 SS steel exposed to JP-4 combustion products 50 h at 1100 °F	0.78	555	...	0.15	5.18	23
COBALT (Co)	...	531	0.03	...	...	24
COLUMBIUM (Cb), 0.5 mil foil	0.41	560	0.04	...	10.0	20,25
Cb alloy (Cb-10Ti-10Mo)	...	...	...	...	...	25

TABLE 2 (Continued)

Material	α_s	Temp., °R	ϵ_{TN}	ϵ_{TH}	α_s/ϵ_T	Ref.
COPPER (Cu)						
Black oxidized	...	540	0.78	...	...	24
Scraped	...	540	0.07	...	...	24
Commercial pol.	...	540	0.03	...	...	24
Electrolytic, careful pol.	...	635	0.018	...	...	24
		531	...	0.015	...	
Chromic acid dip	...	531	...	0.017	...	24
Pol.	...	531	...	0.019	...	24
Liquid honed	...	531	...	0.088	...	24
Electrolytic polish	...	531	0.006	...	...	24
Mechanical polish	...	531	0.015	...	...	24
Carefully prepared surface of pure Cu	...	531	0.008	...	...	24
Cu-Be alloy	...	...	0.036	...	...	20
EBANOL						
Ebanol C on Cu treated 5 min at 196 °F in 219 °F boiling point, sol.	0.91	555	...	0.11	8.25	23
Ebanol S on steel treated 15 min in a 286 °F boiling sol.	0.85	555	...	0.10	8.49	23
GLASS, 3 mils thick on silicone solar cell	0.93	450	...	0.84	1.10	23
GOLD (Au)						
Au (99.95% fine)	0.21	850	...	0.04	5.2	24
0.000010 in leaf (on glass or Lucite)	...	531	...	0.063	...	24
0.000040 in foil (on glass or Lucite)	...	531	...	0.023	...	24
0.0005 in foil (on glass or Lucite)	...	531	...	0.016	...	24
0.0015 in foil (on glass or Lucite)	...	531	...	0.01	...	24
Au plate 0.00005 in on SS (1% Ag in Au)	...	531	...	0.027	...	24
Au plate 0.0001 in on SS (1% Ag in Au)	...	531	...	0.027	...	24
Au plate 0.0002 in on SS (1% Ag in Au)	...	531	...	0.025	...	24
Au plate 0.0002 in on Cu (1% Ag in Au)	...	531	...	0.025	...	24
Au vaporized onto 2 sides of 0.0005 in Mylar	...	531	...	0.02	...	24
Deep electroplated Au on Al	...	410	0.02	...	...	20
		460	0.02	...	...	
		560	0.02	...	...	

TABLE 2 (Continued)

Material	α_s	Temp., °R	ϵ_{TN}	ϵ_{TH}	α_s/ϵ_T	Ref.
Au plate on Al 7075	0.30	400	...	0.03	10.0	21
		500	...	0.03	10.0	
Vacuum deposited Au on buffed Ti	0.33	400	...	0.05	6.6	21
		500	...	0.05	6.6	
		600	...	0.05	6.6	
Vacuum deposited Au on Al with resin undercoat	0.24	400	...	0.04	6.0	21
		500	...	0.04	6.0	
		600	...	0.04	6.0	
GRAPHITE (crushed carbon electrodes) 16 mils thick on Na silicate on pol. Al	0.96	450	...	0.91	1.06	23
INCONEL						25
Inconel foil (0.005) as rec.	0.55	400	...	0.21	2.62	21
		500	...	0.23	2.39	
Inconel X (see Figures 25 and 26)	...	...	...	...	...	25
Inconel X oxidized 4 h at 1825 °F in air followed by 10 h at 1300 °F in air	0.90	450	...	0.71	1.26	23
IRIDIUM (Ir)	...	531	0.04	...	...	24
IRON (Fe)	...	...	...	...	...	25
Electrolytic	...	959	0.07	...	...	24
		671	0.05			
		531	0.05			
Cast Fe, pol.	...	560	0.21	...	...	24
Cast Fe, oxidized		560	0.63	...	...	24
		959	0.66			
		1460	0.76			
Fe sheet, rusted red	...	531	0.69	...	...	24
Fe, oxidized	...	2700	0.89	...	...	24
		671	0.74			
Fe-Ni alloys	...	...	...	...	...	25
Tinned Fe sheet	...	535	0.064	...	...	24
Galvanized Fe	...	657	0.07	...	...	24
Polished Armco	0.36	850	0.12	...	3.0	34

TABLE 2 (Continued)

Material	α_s	Temp., °R	ϵ_{TN}	ϵ_{TH}	α_s/ϵ_T	Ref.
KAPTON Aluminized Polyamide Film (H Film-Kapton)						
1/4 mil Film side	0.31	560	0.36	0.39	0.80	20
1/2 mil Film side	0.36	560	0.38	0.42	0.86	20
1/2 mil Aluminized side	0.10	560	0.02	0.025	4.0	20
1 mil Film side	0.45	560	0.59	0.56	0.80	20
2 mil Film side	0.45	560	0.69	0.68	0.66	20
5 mil Film side	0.49	560	0.83	0.80	0.61	20
LEAD (Pb)						
Unoxidized, pol.	...	671	0.05	...	...	24
Gray oxidized	...	531	0.28	...	...	24
Oxidized 473 K	...	851	0.63	...	...	24
Red Pb	...	671	0.93	...	...	24
Pb 0.004 in foil	...	531	...	0.036	...	24
MAGNESIUM (Mg)	...	531	0.07	...	...	24
		959	0.13			
		1460	0.18			
MANGANIN, bright rolled	...	704	0.048	...	...	24
		531	0.076			
MOLYBDENUM (Mo) See Figures 27, 28	...	4140	0.24	...	...	24,25
		3240	0.19			
		2341	0.13			
		671	0.07			
		531	0.05			
Mo, as rec.	0.48	500	0.12	...	4.0	21
Mo, pol.	0.40	850	0.08	...	5.0	34
K MONEL 5700 (See Figures 29, 30)	...	...	...	...	...	25
MYLAR						
1/4 mil aluminized Mylar						
Al side	0.11	540	0.025	...	...	20
Aged and crinkled alum. side	...	540	0.04	...	...	20
Mylar side	0.15	540	0.30	...	...	20
1 mil aluminized Mylar						
Al side	...	540	0.03	...	...	20
Mylar side	...	540	0.63	...		

TABLE 2 (Continued)

Material	α_s	Temp., °R	ϵ_{TN}	ϵ_{TH}	α_s/ϵ_T	Ref.
NICKEL (Ni)	...	...	...	...	...	25
Pol.	...	711	0.045	...	...	24
Bright matte	...	711	0.041	...	...	24
0.004 in foil	...	531	...	0.022	...	24
Electrolytic Ni	...	1460	0.10	...	...	24
		959	0.07			
		560	0.06			
		531	0.04			
Electroplated Ni						
On Fe and unpol.	...	531	0.11	...	...	24
On Fe and pol.	...	531	0.045	...	...	24
On Cu	...	540	...	0.03	...	24
Electroless Ni (Dow Chemical Co.)	0.45	400	...	0.16	2.81	21
		500	...	0.17	2.65	
Oxidized Ni	...	2700	0.85	...	...	24
		900	0.37			
Pol. Ni	0.37	850	...	0.10	3.7	34
Nichrome						
"Driver Harris" Nichrome heater strip	...	460	0.11	...	...	20
		560	0.12			
		660	0.13			
Nichrome V	...	...	...	...	...	25
Nimonic 75	...	...	...	...	...	25
PAINTS						
Ditzler mixing white lacquer, 4 coats, 2 coats zinc chromate primer, thickness total 0.006 in	0.21	400	...	0.85	0.25	21
		500	...	0.85	0.25	
		600	...	0.86	0.24	
Sherwin-Williams Kemacryl white paint No. M49WC12, 4 mils over one wash primer coat on alodined Al 2024-T6	...	410	0.90	...	...	20
		460	0.91			
		560	0.91			
Kemacryl lacquer white No. M49WC17, 4 wet coats, 1 coat pretreat primer P40GC1 (Sherwin-Williams)	0.26	400	...	0.73	0.36	21
		500	...	0.75	0.35	
		600	...	0.77	0.34	

TABLE 2 (Continued)

Material	α_s	Temp., °R	ϵ_{TN}	ϵ_{TH}	α_s/ϵ_T	Ref.
Zinc sulfide pigment, acryloid A-10 binder, pigment to volume conc. 30%, 5.5 mils over one wash primer coat on alodined Al 2024-T6	...	410 460 560	0.90 0.90 0.90	...	...	20
Grumman thermal control paint. Zinc oxide in RTV-602 silicone, 6 mils thick on 2024 Al	0.21	560	0.91	0.88	0.24	20
Lithofrax 72662, 11 mils on vapor honed Al 2014-T6 substrate	0.15	410 460 560	0.92 0.92 0.93	...	0.16	20
Z-93 white paint, zinc oxide in potassium silicate binder, 5 mils thick on 2024 Al	0.19	410 460 560	0.94 0.94 0.95	0.91	0.21	20
Z-93S white paint, zinc oxide in potassium silicate binder, 6 mils thick on Al	0.18	410 460 560	0.92 0.92 0.92	0.88	0.20	20
S-13G white paint, zinc oxide pigment coated with potassium silicate in silicone binder, 5 mils thick on Al	0.25	560	0.92	0.90	0.28	20
White epoxy resin paint, "Cat-a-lac," Finch Paint and Chemical Co., No. 463-1-8 on Al	0.25	450	...	0.88	0.28	23
Skyspar A-423 color SA8818 (white), 4 wet coats over one coat epoxy primer P-323 (Andrew Paint Co.)	0.22	400 500 600	... ...	0.82 0.83 0.84	0.27 0.27 0.26	21
Fuller 517-B-2 white gloss silicone (W.P. Fuller Co.), 3 wet coats	0.30	400 500 600	... ...	0.82 0.81 0.80	0.36 0.37 0.37	21

TABLE 2 (Continued)

Material	α_s	Temp., °R	ϵ_{TN}	ϵ_{TH}	α_s/ϵ_T	Ref.
Pemco No. R46H60 porcelain enamel on steel	0.22	400	...	0.76	0.29	21
		500	...	0.78	0.28	
		600	...	0.79	0.28	
Ditzler strong black lacquer, 4 coats, 2 coats zinc chromate primer, thickness 0.002 in	0.92	400	...	0.71	1.30	21
		500	...	0.74	1.24	
		600	...	0.75	1.23	
Kemacryl lacquer black No. M49BC12, 4 wet coats, 1 coat pretreat. P40GC1 (Sherwin-Williams)	0.94	400	...	0.81	1.16	21
		500	...	0.83	1.13	
		600	...	0.84	1.12	
Pyromark white paint (Tempel Co.), UV degrad. 320 sun days (8 days 40 suns)	0.20	...	...	0.85	0.24	
	0.35	...	...	0.85	0.41	
Grumman black epoxy paint 1019, 2 wet coats over 1 coat 1012 primer on alodined Al 2014-T6	...	410	0.90	...	...	20
		460	0.90			
		560	0.91			
Flat black epoxy resin paint "Cat-a-lac," Finch Paint and Chemical Co., No. 463-1-8 on Al	0.95	450	...	0.89	1.07	23
"Cat-a-lac," black epoxy paint, 2 coats on 300 series SS	...	410	0.89	...	...	20
		460	0.89			
		560	0.90			
Warnow black epoxy paint applied on alodined Al 2014-T6	...	410	0.91	...	...	20
		460	0.92			
		560	0.92			
Fuller 517-B-2 flat black silicone 4 mils wet film	0.89	400	...	0.80	1.11	21
		500	...	0.81	1.10	
		600	...	0.82	1.09	
3M black velvet paint over zinc chromate primer on alodined Al	0.97	410	0.92	...	1.05	20
		460	0.92			
		560	0.93			

TABLE 2 (Continued)

Material	α_s	Temp., °R	ϵ_{TN}	ϵ_{TH}	α_s/ϵ_T	Ref.
Krylon 1602 black paint over Al		410	0.86	...	...	20
		460	0.86			
		560	0.88			
Al leafing pigment in clear epoxy binder, in oz pigment/gal	...	...	...	...	...	20
20	...	560	0.66			
40	...	560	0.34			
60	...	560	0.22			
80	...	560	0.24			
PALLADIUM (Pd)	...	531	0.03	...	...	24
PLATINUM (Pt)	...	2461	0.18	...	...	24
		1460	0.10			
		959	0.06			
		671	0.05			
		531	0.03			
		522	0.016			
QUARTZ (fused)	...	531	0.93	...	...	24
RHODIUM (Rh), plated on SS	...	531	0.05	...	...	24
ROKIDE, flame sprayed alumina on 410 SS heated to 1300 °F in air in 60 s and held 30 additional seconds	0.28	450	...	0.80	0.34	23
SILICON solar cell, International Rectifier Corp., approx. 1 mm thick on electroless Ni plate substrate, boron doped surface	0.94	555	...	0.32	2.93	23
SILVER (Ag)	...	1460	0.03	...	...	24
		671	0.025			
		531	0.022			
		492	0.02			
Silver (999+ fine)	0.13	850	...	0.03	4.3	34
SOLDER, 50-50 on Cu	...	531	...	0.03	...	24

TABLE 2 (Continued)

Material	α_s	Temp., °R	ϵ_{TN}	ϵ_{TH}	α_s/ϵ_T	Ref.
STAINLESS STEEL						
Pol.	...	671	0.08	...	...	24
301 (See Figures 31, 32)	...	...	...	...	...	25
302	...	760	...	0.05	...	24
302 mech. pol.	0.38	400	...	0.17	2.24	21
		500	...	0.19	2.0	
		600	...	0.20	1.90	
303	...	...	...	...	...	25
316 (See Figures 33, 34)	...	...	...	...	...	25
321, pol.	...	...	0.09	0.12	...	20,25
347 (See Figures 35, 36)	...	...	...	...	...	25
410 heated to 1300 °F in air	0.76	555	...	0.130	5.88	23
446	...	...	...	...	...	25
PH 15-7 Mo	...	...	...	...	...	25
17-7 PH	...	...	...	...	...	25
18-8 (See Figure 37)	...	...	...	...	...	25
AM-350	...	...	...	...	...	25
Vickers F.D.P.	...	...	...	...	...	25
Armco black oxide on type 301	0.89	450	...	0.75	1.19	23
René 41 alloy mech. pol.	0.38	400	...	0.17	2.24	21
		500	...	0.19	2.0	
		600	...	0.20	1.90	
Haynes alloy B	...	...	...	...	...	25
Haynes alloy X	...	...	...	...	...	25
Haynes alloy 25, pol. and oxid.	...	560	0.16	...	...	20,25
TABOR						
Solar collector chemical treatment of galvanized Fe	0.89	555	...	0.12	7.25	23
Solar collector chemical treatment 110-30 on Ni plated Cu	0.85	555	...	0.05	17.4	23
TAPES						
3M Al foil 425	...	550	0.09	...	...	20
3M foil cleaned with MEK	...	550	0.03	...	...	20
3M Al foil Y-9040	...	550	0.02	...	...	20
Permacel Al foil EE 6600	0.12	550	0.03	...	4.0	20
Johns Manville Al Foil 330	...	550	0.03	...	...	20
3M chrome colored Scotchcal 630	0.18	460	0.63	...	0.28	35
3M gold colored Scotchcal 633	0.33	460	0.74	...	0.45	35
3M silver Scotchlite reflective sheet 3270	0.45	460	0.90	...	0.50	35
3M Mylar tape 850	0.34	460	0.58	...	0.59	20
3M Aluminized Mylar 852	0.147	460	0.58	...	0.25	20

TABLE 2 (Continued)

Material	α_s	Temp., °R	ϵ_{TN}	ϵ_{TH}	α_s/ϵ_T	Ref.
TANTALUM (Ta; see Figures 38, 39, 40)	...	...	...	...	...	25
		4140	0.26			24
		3240	0.21			
		531	0.05			
Polished	0.45	850	0.10	...	4.5	34
TELLURIUM (Te)	...	531	0.22	...	...	24
TITANIUM (Ti)						
Alloy Ti-6 Al-4 Va	...	...	...	...	...	25
Alloy Ti-6 Al-4 Va, as rec.	0.66	400	...	0.19	3.47	21
		500	...	0.20	3.3	
		600	...	0.22	3.0	
Alloy Ti-5 Al-2.5 Sn	...	...	...	...	...	25
Ti vapor coated on bright side of Reynolds wrap Al foil, 80 to 100 μ thick heated 3 h at 750 °F in air	0.75	555	...	0.14	5.40	23
Ti C-110M (AMS 4908) heated 300 h at 850 °F in air	0.77	555	...	0.20	3.88	23
Ti C-110M (AMS 4908) heated 100 h at 800 °F in air	0.52	555	...	0.16	3.24	23
Ti 75A (AMS 4901) heated 300 h at 850 °F in air	0.80	555	...	0.21	3.78	23
Anodized Ti	0.51	450	...	0.87	0.59	23
TITANOX-RA 2 miles thick on black paint	0.15	450	...	0.89	0.17	23
TIN (Sn)						
1% indium	...	531	0.012	...	...	24
5% indium	...	531	0.017	...	...	24
Sn foil, 0.001 in	...	531	0.012	...	...	24
TUNGSTEN (W). See Figure 41	...	...	...	...	...	25
Filament	...	4140	0.28	...	...	24
		3240	0.23			
		2340	0.15			
		1440	0.09			
		900	0.05			
		540	0.03			
ZINC (Zn)	...	531	0.05	...	...	24

TABLE 3 - Normal Total Emittance of Inconel X (Reference Information for Figure 25)

Investigator	Symbol	Composition and Surface Condition	Test Method	Remarks
1.	o Δ X	Oxidized As received or wiped clean Polished	Normal total emittance Resistance heated specimens Thermistor-bolometer detector Comparison blackbody Temperatures measured with thermocouples	Measured in vacuum Data taken from curves
2.	●	Stably oxidized at 2000 °F	Normal total emittance Thermopile detector Comparison blackbody Temperatures measured with thermocouples	Measured in air Data taken from curves
3.	■	Polished After prolonged heating and cycling above 2000 °F (some oxide indicated)	Normal total emittance Total radiation detector Comparison blackbody Temperatures measured with thermocouples	Measured in a 10 μ pressure of helium

SOURCE: Reference 25.

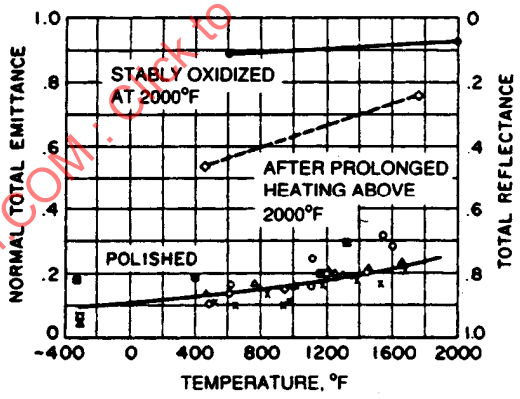

FIGURE 25 - Normal Total Emittance and Total Reflectance of Inconel X; see Table 3 (Reference 25)

TABLE 4 - Total Solar Absorptance of Inconel X (Reference Information for Figure 26)

Investigator	Symbol	Composition and Surface Condition	Test Method	Remarks
1.	o	As received	Total solar absorptance	Measured in air at
	Δ	Clean and smooth	Comparison standards	100 °F
	□	Polished	Comparison pyro-heliometer	Temperatures are those to which samples had been heated previously
			Output measured with thermocouples	

SOURCE: Reference 25.

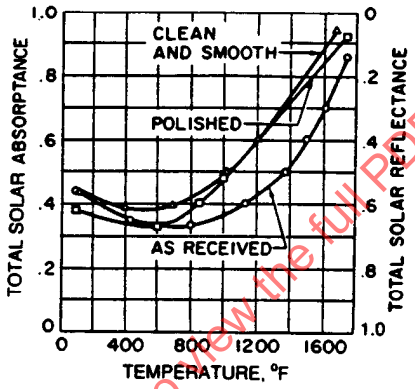

FIGURE 26 - Total Solar Absorptance and Reflectance of Inconel X at 100 °F; see Table 4 (Reference 25)

TABLE 5 - Hemispherical Total Emittance of Molybdenum (Reference Information for Figure 27)

Investigator	Symbol	Composition and Surface Condition	Test Method	Remarks
1.		As received and chemically cleaned. Purity not given. As-received specimen Hole-in-tube measurements	Hemispherical total emittance Hole-in-tube and resistance-heated strip-specimen methods	Measured in vacuum Data taken from curves Numerous temperature cycles were made on each specimen
	o	Temperature measured with pyrometer	Temperatures measured with optical pyrometer or thermocouple	All specimens were from the same stock of material
	X	Temperature measured with thermocouples heated strip measurements Heated strip measurements		
	□	Run No. 1		
	Δ	Vapor blasted First heating Fourth heating		
2.		Blasted with No. 90 (PMC3043A) Al oxide	Hemispherical total emittance Resistance-heated strip specimen Temperatures measured with thermocouples	
	■	Held at temperature 17 h at 892 °F and again at 1475 °F		
3.	●	Polished with 0000 abrasive paper	Hemispherical total emittance Power dissipated from electrically heated rod specimen Test Method Remarks Brightness temperatures measured with optical pyrometer converted to true temperatures using values obtained at the melting point	Measured in flow of argon gas Data taken from curves

TABLE 5 (Continued)

Investigator	Symbol	Composition and Surface Condition	Test Method	Remarks
4.	+	10 mil dia. wire. Surface changes noted after heating	Hemispherical total emittance Power dissipated per unit length of electrically heated wire Temperatures measured with a two-color photo-electric pyrometer, an optical pyrometer and known resistivity versus temperature data	Measured in vacuum Data taken from curves
5.		Highly polished. Vacuum arc cast, machined, extruded, recrystallized, and rolled	Hemispherical total emittance Disc specimen Temperatures measured with thermocouples Emittance calculated from the mass, specific heat, and rate of change of temperature of the specimen	Measured in vacuum Data taken from curves

SOURCE: Reference 25

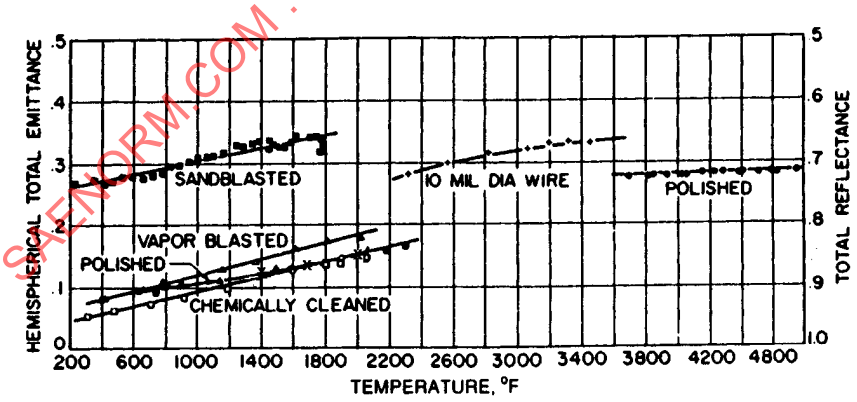

FIGURE 27 - Hemispherical Total Emittance and Reflectance of Mo; see Table 5 (Reference 25)

TABLE 6 - Total Solar Absorptance of Molybdenum
(Reference Information for Figure 28)

Investigator	Symbol	Composition and Surface Condition	Test Method	Remarks
1.	o	Highly polished Vacuum arc cast, machined, extruded, recrystallized, and rolled	Total solar absorptance Carbon arc image furnace Disc specimen Temperatures measured with thermocouples Absorptance calculated from mass, specific heat, rate of change of temperature, and known irradiance of the surface (Solar spectrum simulated by carbon arc)	Measured in vacuum

SOURCE: Reference 25

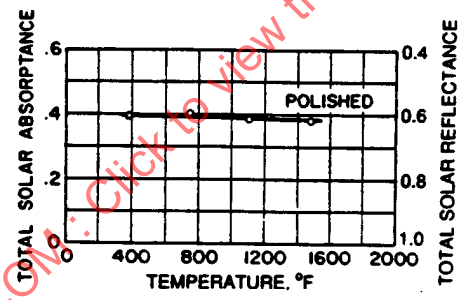

FIGURE 28 - Total Solar Absorptance and Reflectance of Mo;
see Table 6 (Reference 25)

TABLE 7 - Normal Total Emittance of K-Monel 5700
(Reference Information for Figure 29)

Investigator	Symbol	Composition and Surface Condition	Test Method	Remarks
1.	X	Polished	Normal total emittance	Measured in a 10 μ pressure of helium
	Δ	Clean and smooth	Total radiation detector	
	□	As received	Comparison blackbody	
	●	After prolonged heating and cycling above 2000 °F (some oxide indicated)	Temperatures measured with thermocouples	

SOURCE: Reference 25

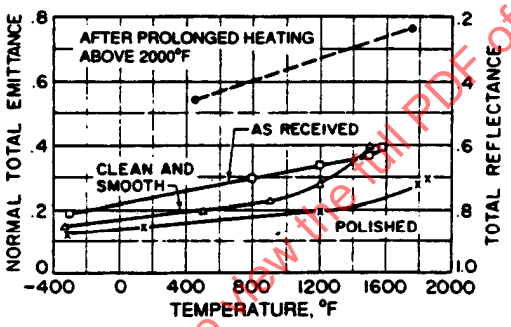

FIGURE 29 - Normal Total Emittance and Reflectance of K-Monel 5700; see Table 7 (Reference 25)

TABLE 8 - Total Solar Absorptance of K-Monel 5700
(Reference Information for Figure 30)

Investigator	Symbol	Composition and Surface Condition	Test Method	Remarks
1.	□	Polished	Total solar absorptance	Measured in air
	Δ	Clean and smooth	Comparison standards	at 100 °F
	o	As received	Comparison pyro-heliometer	Temperatures are those to which samples had been heated previously
			Output measured with thermocouples	

SOURCE: Reference 25

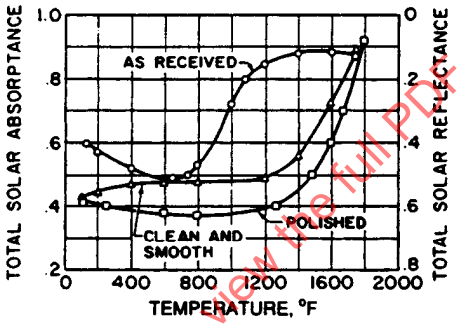

FIGURE 30 - Total Solar Absorptance and Reflectance of K-Monel 5700 at 100 °F; see Table 8 (Reference 25)

TABLE 9 - Normal Total Emittance of Stainless Steel Type 301
(Reference Information for Figure 31)

Investigator	Symbol	Composition and Surface Condition	Test Method	Remarks
1.		First heating	Normal total emittance	Measured in 10 μ pressure of helium
	o	As received	Total radiation detector	
	Δ	Clean and smooth	Comparison blackbody	
	□	Polished	Temperature measured with thermocouples	
		After repeated heating and cooling		
	●	As received		
		Clean and smooth		
	■	Polished		
2.	X	As received (surface oxidation indicated after test)	Normal total emittance Calibrated thermopile detector Comparison blackbody Temperatures measured with thermocouples	Measured in flow of helium gas

SOURCE: Reference 25

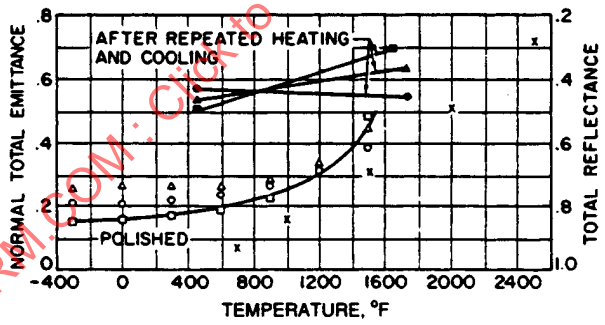

FIGURE 31 - Normal Total Emittance and Total Reflectance of SS 301;
see Table 9 (Reference 25)

TABLE 10 - Total Solar Absorptance of Stainless Steel Type 301 at 100 °F
(Reference Information for Figure 32)

Investigator	Symbol	Composition and Surface Condition	Test Method	Remarks
1.	□	Polished	Total solar absorptance	Measured in air
	Δ	Clean and smooth	Comparison standards	at 100 °F
	o	As received	Comparison pyro-heliometer	Temperatures shown are those to which samples had been heated previous to tests
			Output measured with thermocouples	

SOURCE: Reference 25

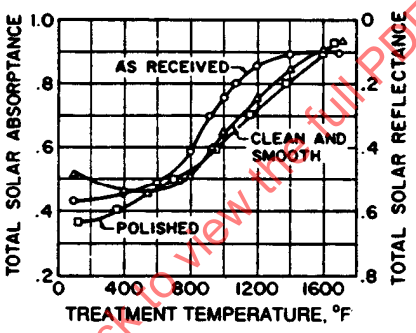

FIGURE 32 - Total Solar Absorptance and Reflectance of SS 301 at 100 °F; see Table 10 (Reference 25)

TABLE 11 - Normal Total Emittance of Stainless Steel Type 316
(Reference Information for Figure 33)

Investigator	Symbol	Composition and Surface Condition	Test Method	Remarks
1.		First heating	Normal total emittance	Measured in 10 μ pressure of helium
	o	As received	Total radiation detector	
	Δ	Clean and smooth	Comparison blackbody	
	□	Polished	Temperatures measured with thermocouples	
		After repeated heating and cooling		
	●	As received		
		Clean and smooth		
	■	Polished		
2.	∇	Rms finish of approximately 15 μ-in	Normal total emittance Thermistor-bolometer detector	Measured in vacuum
	+	Rms finish of approximately 2 μ-in	Resistance heated strip specimens	

SOURCE: Reference 25

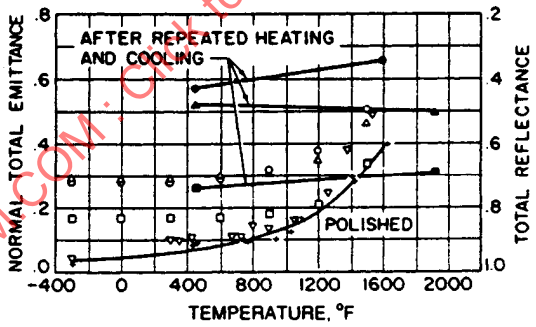

FIGURE 33 - Normal Total Emittance and Total Reflectance of SS 316;
see Table 11 (Reference 25)

TABLE 12 - Total Solar Absorptance of Stainless Steel Type 316 at 100 °F
(Reference Information for Figure 34)

Investigator	Symbol	Composition and Surface Condition	Test Method	Remarks
1.	□	Polished	Total solar absorptance	Measured in air
	Δ	Clean and smooth	Comparison standards	at 100 °F
	o	As received	Comparison pyro-heliometer	Temperatures shown are those to which samples had been heated previous to tests
			Output measured with thermocouples	

SOURCE: Reference 25

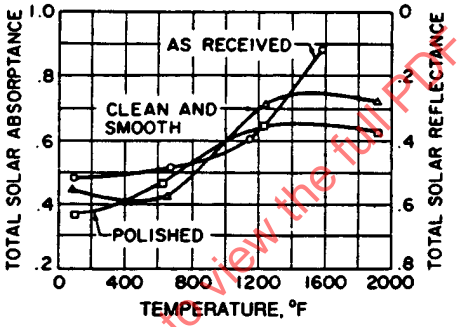

FIGURE 34 - Total Solar Absorptance and Reflectance of SS 316 at 100 °F; see Table 12; All Measurements Made at 100 °F and Temperatures are Those to Which Samples had Been Heated Previous to Tests (Reference 25)

TABLE 13 - Normal Total Emittance of Stainless Steel Type 347
(Reference Information for Figure 35)

Investigator	Symbol	Composition and Surface Condition	Test Method	Remarks
1.		First heating	Normal total emittance	Measured in 10 μ pressure of helium
	o	As received	Total radiation detector	
	Δ	Clean and smooth	Comparison blackbody	
	□	Polished	Temperatures measured with thermocouples	
		After repeated heating and cooling		
	●	As received		
		Clean and smooth		
	■	Polished		
2.	X	Stably oxidized at 2000 °F	Normal total emittance Thermopile detector Comparison blackbody Temperatures measured with thermocouples	Measured in air Measurements were taken normally and at various angles with the normal Normal total equals hemispherical total emittance for this specimen
3.		Bare (polished)	Normal total emittance	Measured in air
	♦	Oxidized blue (100 h at 1200 °F)	Calibrated thermopile detector	

SOURCE: Reference 25

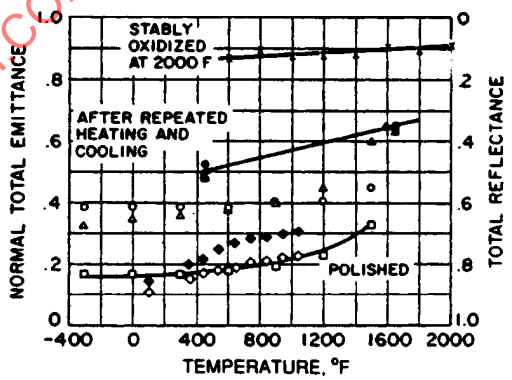

FIGURE 35 - Normal Total Emittance and Total Reflectance of SS 347;
see Table 13 (Reference 25)

TABLE 14 - Total Solar Absorptance of Stainless Steel Type 347 at 100 °F
(Reference Information for Figure 36)

Investigator	Symbol	Composition and Surface Condition	Test Method	Remarks
1.	o	As received	Total solar absorptance	Measured in air
	Δ	Clean and smooth	Comparison standards	at 100 °F
	☐	Polished	Comparison pyro-heliometer Output measured with thermocouples	Temperatures shown are those to which samples had been heated previous to tests

SOURCE: Reference 25

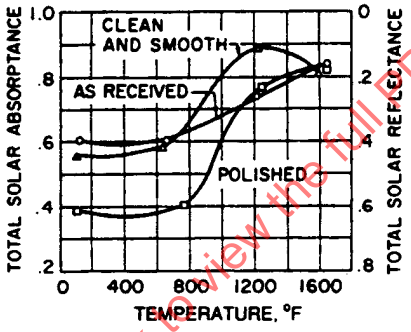

FIGURE 36 - Total Solar Absorptance and Reflectance of SS 347 at 100 °F; see Table 14; All Measurements at 100 °F and Temperatures are Those to Which Samples had Been heated Previous to Tests (Reference 25)

TABLE 15 - Normal Total Emittance of Stainless Steel Type 18-8
(Reference Information for Figure 37)

Investigator	Symbol	Composition and Surface Condition	Test Method	Remarks
1.	o	Nominal composition Oxidized at 500 °F and weathered	Normal total emittance Thermopile detector Temperatures measured with thermocouples	Measured in air
	Δ	Sandblasted and weathered		
	□	Chromic and sulfuric acid treated		
	∇	Unpolished		
	X	Polished		

SOURCE: Reference 25

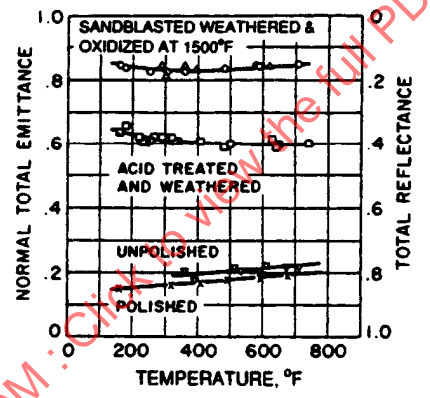

FIGURE 37 - Normal Total Emittance and Total Reflectance of SS 18-8;
see Table 15 (Reference 25)

TABLE 16 - Hemispherical Total Emittance of Tantalum
(Reference Information for Figure 38)

Investigator	Symbol	Composition and Surface Condition	Test Method	Remarks
1.		Polished with 0000 abrasive paper	Hemispherical total emittance	Measured in flow of argon gas
	o	Fansteel material	Power dissipated from electrically heated rod specimen	
	□	National Research material	Brightness temperatures measured with optical pyrometer; converted to true temperatures using values obtained at the melting point	
2.	X	Highly polished Commercially pure, arc cast, or sintered	Hemispherical total emittance Carbon arc image furnace Disc specimen Temperatures measured with thermocouples Emittance calculated from mass, specific heat, and rate of change of temperature of specimen	Measured in vacuum

SOURCE: Reference 25

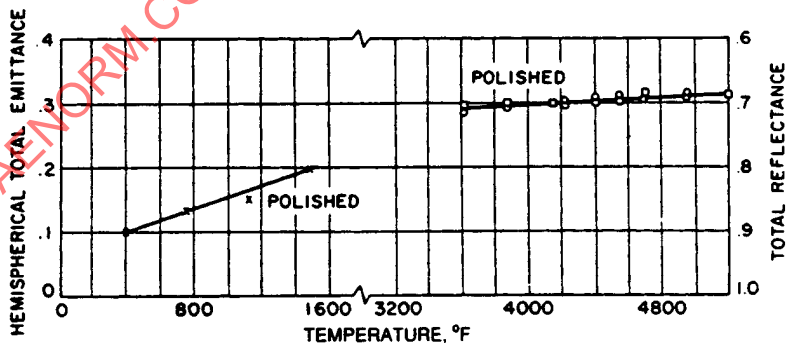

FIGURE 38 - Hemispherical Total Emittance and Total Reflectance of Ta;
see Table 16 (Reference 25)

TABLE 17 - Normal Total Emittance of Tantalum
(Reference Information for Figure 39)

Investigator	Symbol	Composition and Surface Condition	Test Method	Remarks
1.		Composition "pure"	Normal total emittance	Measured in vacuum
	o	Cleaned	Resistance heated specimen	
	Δ	Polished	Thermistor-bolometer detector	
	X	Oxidized 30 min at "red heat"	Comparison blackbody	
			Temperatures measured with thermocouples	
2.		Composition not given	Total normal emittance	Measured in air
		Oxidized 50 min at 1000 °F	Thermopile detector	
	■	Oxidized 60 min at 1000 °F	Comparison blackbody	
	●	Oxidized 80 min at 1000 °F	Temperatures measured with thermocouples	
	◓	Oxidized 110 min at 1000 °F		
		Note: The oxide formed was flakey, porous, and unstable		
3.	¤	Highly polished	Normal total emittance	Measured in positive pressure of argon
		Composition not given	Induction-heated specimen	
			Comparison blackbody hole in specimen	
			Total detector	
			Temperatures measured with optical pyrometer	

SOURCE: Reference 25

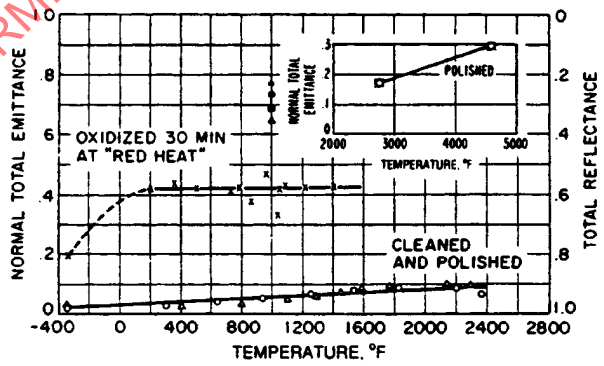

FIGURE 39 - Normal Total Emittance and Total Reflectance of Ta; see Table 17 (Reference 25)

TABLE 18 - Total Solar Absorptance of Tantalum
(Reference Information for Figure 40)

Investigator	Symbol	Composition and Surface Condition	Test Method	Remarks
1.	o	Highly polished Commercially pure, arc cast or sintered	Total solar absorptance Carbon arc image furnace Disc specimen Temperatures measured with thermocouples Absorptance calculated from mass, specific heat, rate of change of temperature, and known irradiance of surface (Solar spectral distribution simulated by carbon arc)	Measured in vacuum

SOURCE: Reference 25

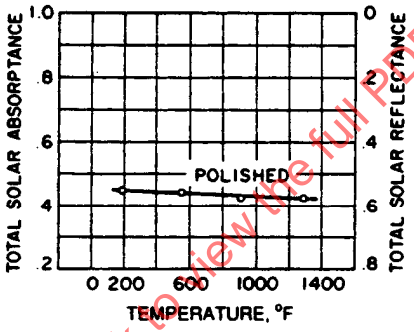

FIGURE 40 - Total Solar Absorptance and Reflectance of Ta;
see Table 18 (Reference 25)

TABLE 19 - Hemispherical Total Emittance of Tungsten
(Reference Information for Figure 41)

Investigator	Symbol	Composition and Surface Condition	Test Method	Remarks
1.	● ■	Polished with 0000 abrasive papers Fansteel material Wah Chang material	Hemispherical total emittance Power dissipated from electrically heated rod specimen Brightness temperatures measured with optical pyrometer; converted to true temperature using values obtained at melting point	Measured in flow of argon gas
2.	Δ	Spectrographically pure straight wire (0.010 in dia)	Hemispherical total emittance Electrically heated wire Measured power input to constant temperature zone Temperatures measured with two-color photoelectric pyrometer	Measured in vacuum Data taken from curve Investigators estimated accuracy ±10%

TABLE 19 - Hemispherical Total Emittance of Tungsten
(Reference Information for Figure 41) (Continued)

Investigator	Symbol	Composition and Surface Condition	Test Method	Remarks
3.		Purity and surface condition not given	Hemispherical total emittance	Measured in vacuum of 10^{-5} to 10^{-9} mm of Hg
	o	Total emittance equipment	Power dissipated from resistance-heated strip specimen	
	□	Spectral emittance equipment	Temperatures measured with thermocouples (Optical pyrometer in spectral-hole-in-tube method)	
4.		Porous tungsten	Hemispherical total emittance	Measured in positive pressure of argon
		% of theoretical density:	Heat radiated from solid rod of resistance-heated material to cold walls	
	X	90	Temperature calculated from brightness temperature and spectral emittance data	
	■	90		
	▽	70		
	●	70		
	☆	70		

SOURCE: Reference 25

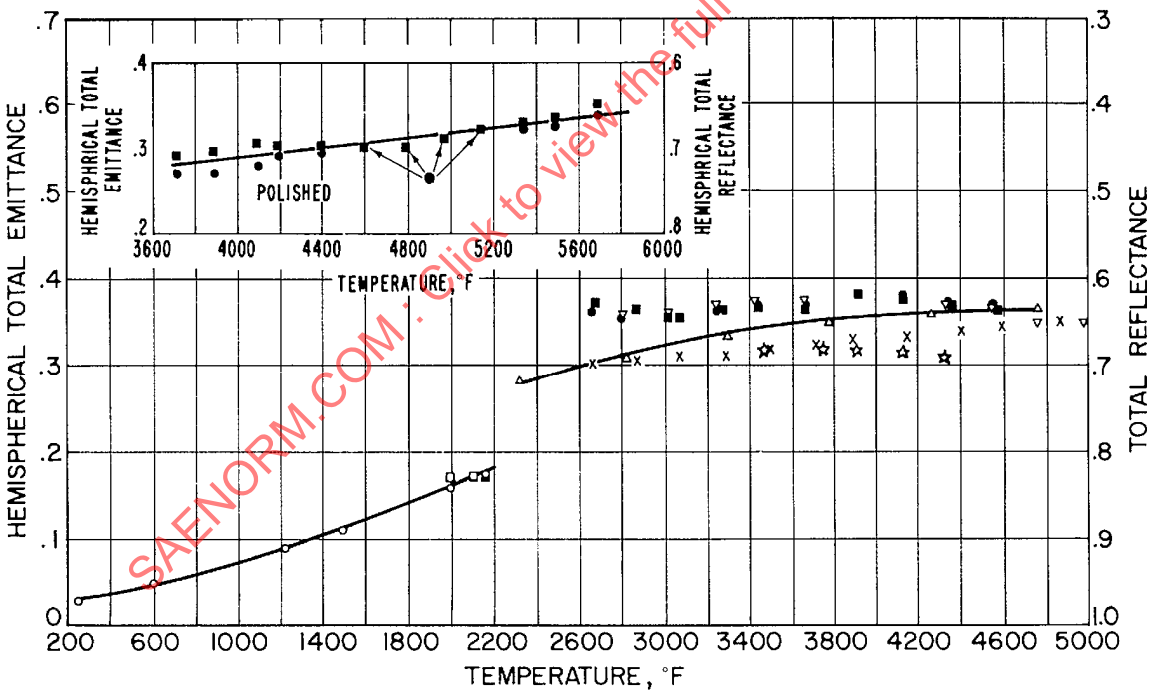

FIGURE 41 - Hemispherical Total Emitttance and Total Reflectance of W;
see Table 19 (Reference 25)

4.4.3 (Continued):

The concept of passive thermal control is foreign to many engineering personnel and to almost all manufacturing and assembly people unless they have received special training. The exterior thermal control surfaces of a spacecraft constitute the crux of that vehicle's passive control system; these control surfaces often have the appearance of ordinary paints, metals, or foils. This fact, combined with the ignorance of shop personnel regarding the special nature of these surfaces, will generally result in contamination and hence degradation (often permanent) of the thermal radiation characteristics unless special precautions are taken to prevent such contamination.

If the surface thermal radiation properties as specified by the designer are to be preserved during launching of the vehicle, special protection, handling, and inspection procedures are mandatory.

5. SPACECRAFT THERMAL BALANCE:

5.1 Deep Space Probes:

All spacecraft traveling between planets are thermally influenced by the solar heat flux. In Figure 42 the solar heat flux associated with the planet distance from the sun is plotted as the ordinate (Reference 10). The parameter of surface temperatures of a flat plate normal to the sun is plotted as a function of the surface α_s/ϵ ratio and its coordinate within the solar system.

The heat flux to any incremental surface area at an arbitrary position in space is computed by multiplying the solar heat flux at the particular distance from the sun times the cosine between the surface normal and the sun line. For an average value over the spacecraft surface this is the projected surface area to the sun (Figure 43).

Thus, the incident radiation is

$$Q_s = S \cos \theta \qquad \text{(Eq.29)}$$

the absorbed radiation is

$$Q_{abs} = Q_s \alpha_s \qquad \text{(Eq.30)}$$

and for a perfectly insulated surface, the temperature T_{sf} is obtained from:

$$\epsilon_{sf}\, \sigma \left(T_{sf}^4 - T_{sp}^4 \right) = Q_s \alpha_s \qquad \text{(Eq.31)}$$

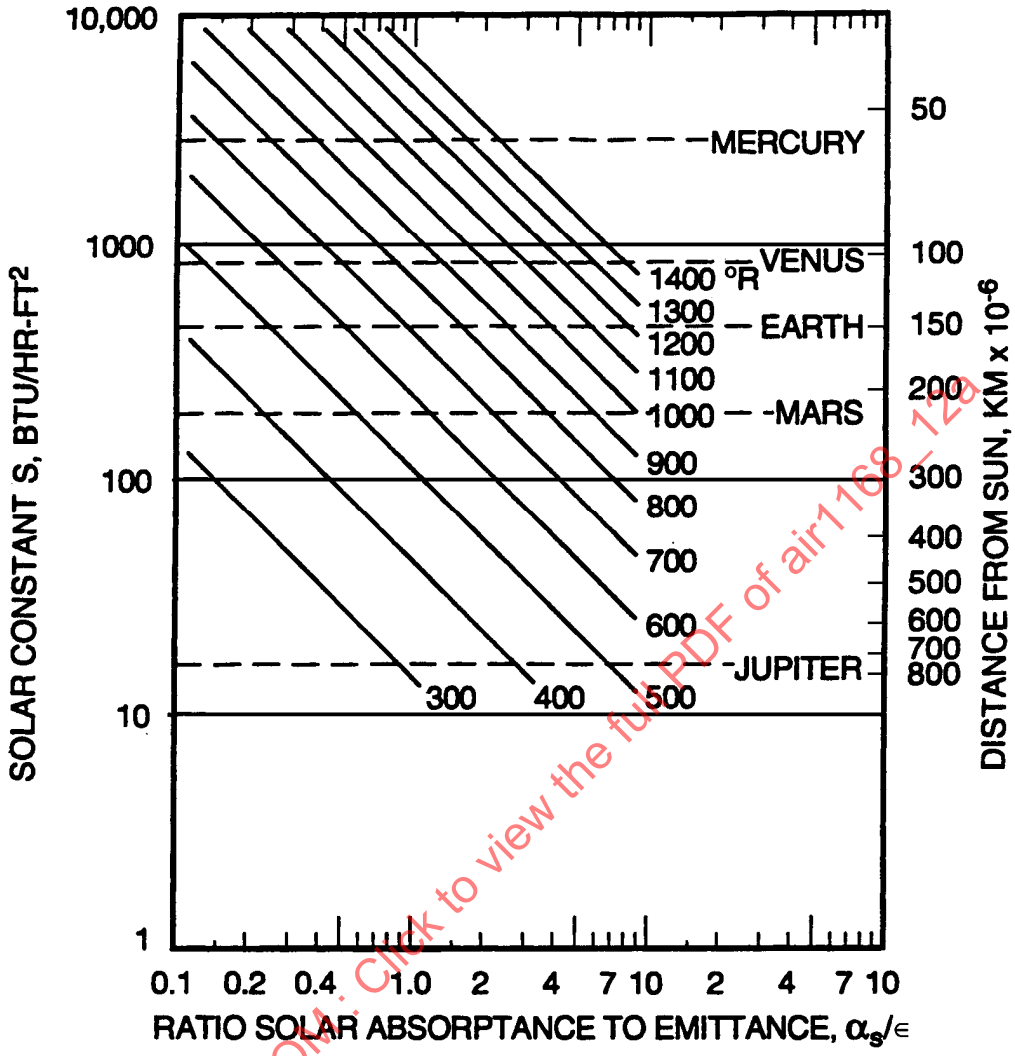

FIGURE 42 - Equilibrium Temperature of a Surface Normal to the Sun Versus Distance from Sun and α_s/ϵ (Reference 10)

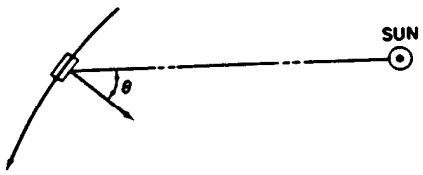

FIGURE 43 - Incident Solar Radiation to a Surface

5.1 (Continued):

or

$$\sigma T_{sf}^4 = Q_s \frac{\alpha_s}{\epsilon_{sf}} \qquad \text{(Eq.32)}$$

where the temperature of space T_{sp} = 4 °R and is assumed negligible for ordinary spacecraft surface temperatures.

5.2 Satellites:

A satellite (a spacecraft orbiting a planet) receives heat flux from three external sources:

1. Solar radiation.
2. Albedo radiation: sunlight reflected off the planet.
3. Planet radiation: radiation from the planet surface acting as a heat source.

5.2.1 Incident Solar Radiation: The solar radiation flux in the orbit of a planet may be obtained from Table 1. Instantaneous solar fluxes are computed as shown in Par. 5.1.

In orbit, a satellite is obscured from the sun when it is in the shadow of the planet. This shadowing and time in the sunlight varies according to the angle β between the orbital plane of the satellite and the plane of the sun-planet (the ecliptic, when considering the Earth). The angle β is determined by the incident launch angle i. For the case of an Earth satellite, the satellite orbit precesses; that is, the normal to the orbital plane will generate a cone about the Earth's axis at a constant half-angle of i. A 500 mile circular orbit at i = 32 deg precesses approximately 6 deg per day.

Because of the precession of the orbit and rotation of the Earth about the Sun, the angle β varies continuously from a maximum (equatorial inclination +i) to a minimum (equatorial inclination -i). The maximum and minimum average solar heat load over the orbit is determined when β is a maximum and when β = 0 deg, respectively.

Figure 44 gives the percentage of time a satellite will be in sunlight as a function of altitude and angle β. Consequently, the average orbital solar flux incident at any point on the surface of a spatially oriented satellite is

$$Q_s = S \cos\theta \text{ (\% time in sun)} \qquad \text{(Eq.33)}$$

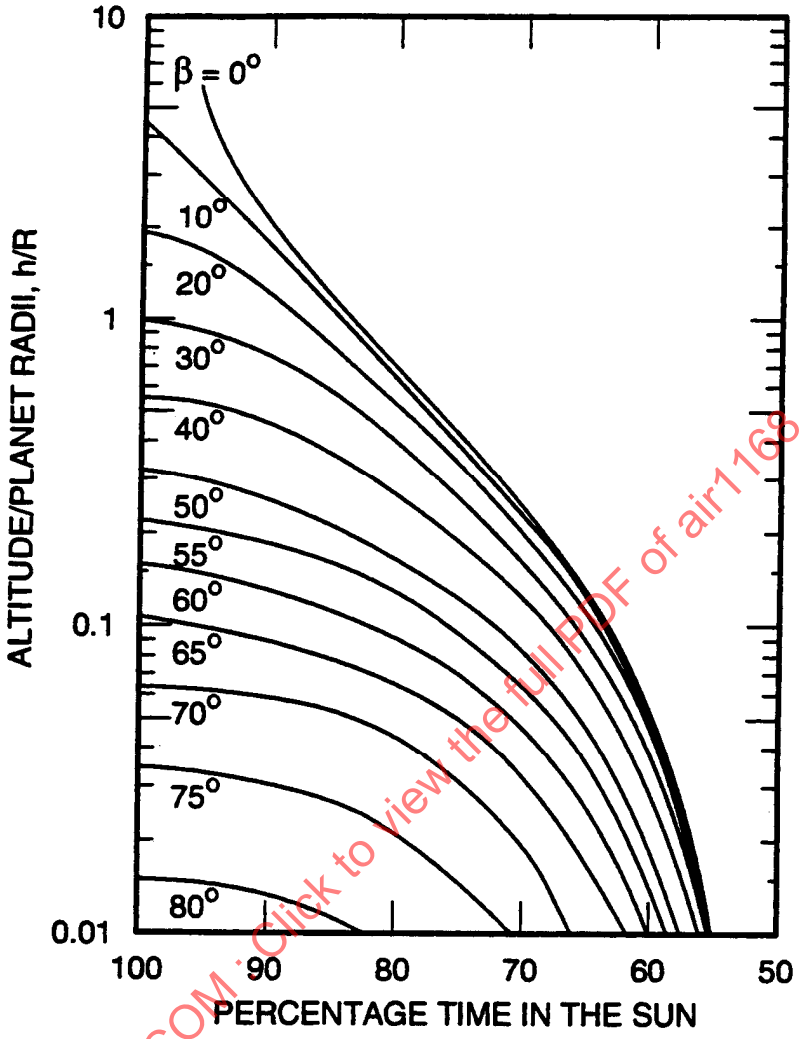

FIGURE 44 - Percentage of Time in Sun Versus Altitude With Orbital Inclination β as Parameter for Vehicle in Circular Orbit

5.2.2 Incident Albedo Radiation: Albedo radiation (having spectral characteristics similar to sunlight) is solar radiation reflected from the gas layer or surface of a planet and is assumed to be diffuse (that is, it follows Lambert's law). A comprehensive study of albedo and planetary configuration factors is found in Reference 53.

The orbit geometry used in defining the incident albedo flux is given in Figure 45, and θ_s, γ, ν, φ_c, and ψ are as defined in Par. 1.2. ψ is to be used only with Figure 57.

Parameters h, γ, θ_s, or ψ and φ_c may vary as the satellite traverses its orbit. Therefore, to obtain average albedo heat fluxes, computations of geometric factors must be made at intervals of orbit angle ν and integrated over the orbit.

Figures 46 through 52 can be used to determine the geometric factor F_a for albedo radiation incident on a sphere, cylinder, and flat plate (Reference 10). In using these curves, approximations must be made for angles of γ between 0 and 90 deg. Variations in φ_c are generally secondary and alter F_a by less than ±0.03.

From these curves, the instantaneous albedo flux is obtained:

$$Q'_{a,\ incident} = SaF_a \qquad \text{(Eq.34)}$$

where a is the planetary solar reflected energy (albedo) and the prime denotes the instantaneous flux. The average heat flux per orbit is obtained from:

$$Q_{a,incident} = Sa\frac{1}{n}\sum_{i=1}^{i=n} F_{a,vi} \qquad \text{(Eq.35)}$$

where vi = 10, 20, . . . 360 deg and i = 1,2,3...n; or

$$Q_{a,incident} = Sa\bar{F}_a \qquad \text{(Eq.36)}$$

To obtain the total incident heat (q Btu/h = QA), use the projected area for A in Figures 46 through 50 and 53 to 55. For the flat plate heat flux the cosine relation is incorporated in the curves, so that the full flat plate area can be used.

5.2.3 Incident Planetary Radiation: Similar geometric factors (Reference 10) are shown in Figures 53 through 56 for planetary radiation to a sphere, hemisphere, cylinder, and flat plate, using the previously described geometry. The angle γ generally varies with orbit angle ν. To obtain the orbital planet heat flux, the geometric factor must be averaged over the orbit.

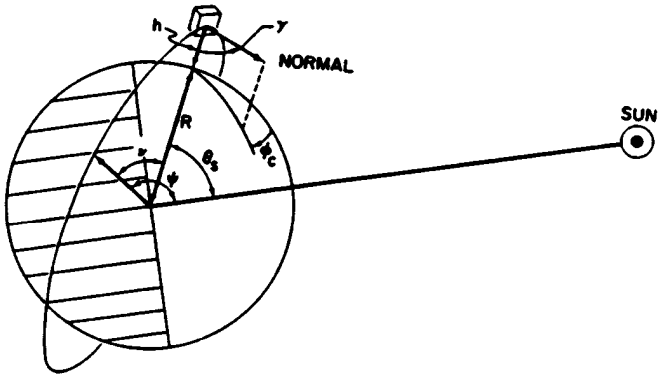

FIGURE 45 - Orbit Geometry

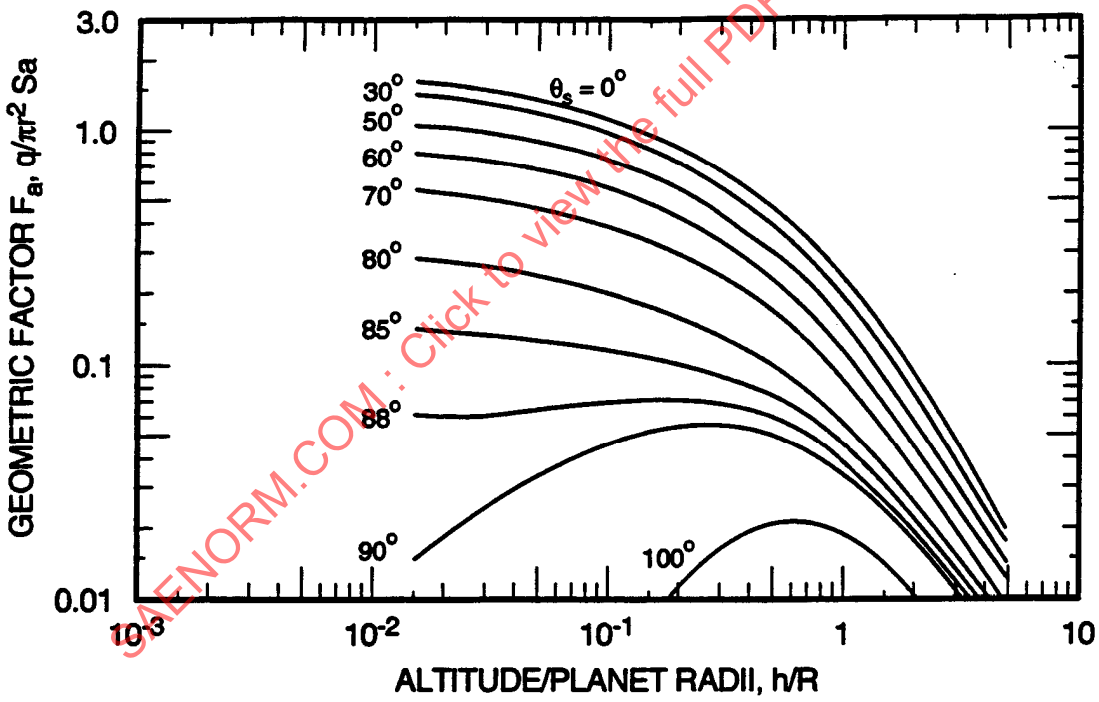

FIGURE 46 - Geometric Factor for Planetary Albedo Radiation Incident to Sphere Versus Altitude, With Angle of Sun as a Parameter (Reference 10)

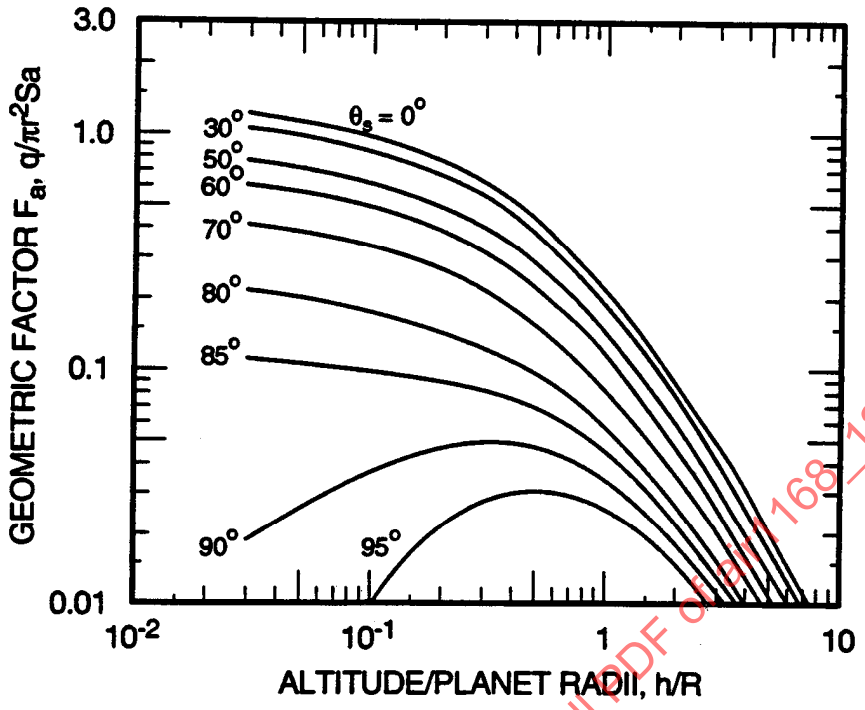

FIGURE 47 - Geometric Factor for Albedo to Hemisphere Versus Altitude With Angle of Sun as Parameter (γ = 0 deg; ϕ_c = 0 deg) (Reference 10)

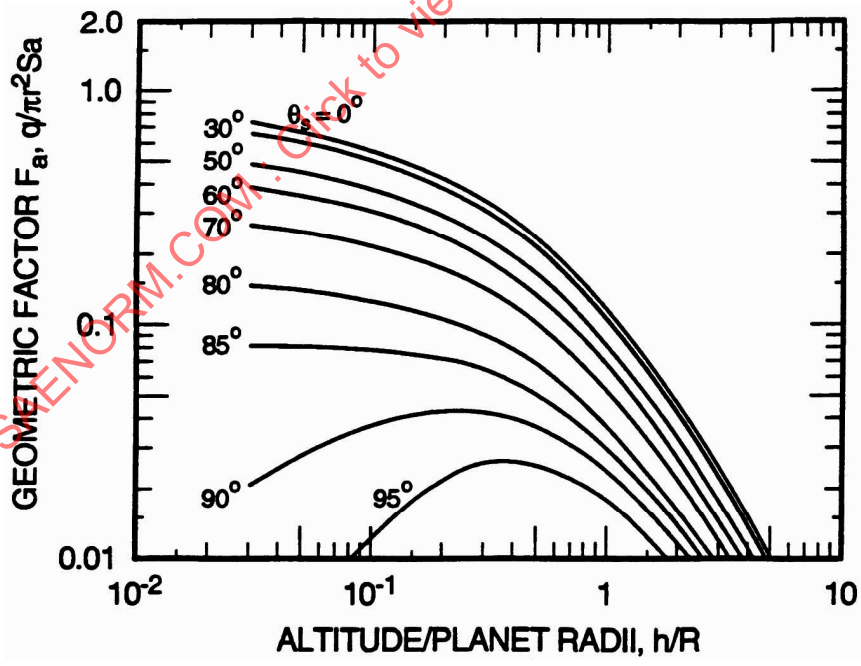

FIGURE 48 - Geometric Factor for Albedo to Hemisphere Versus Altitude With Angle of Sun as Parameter (γ = 90 deg; ϕ_c = 0 deg) (Reference 10)

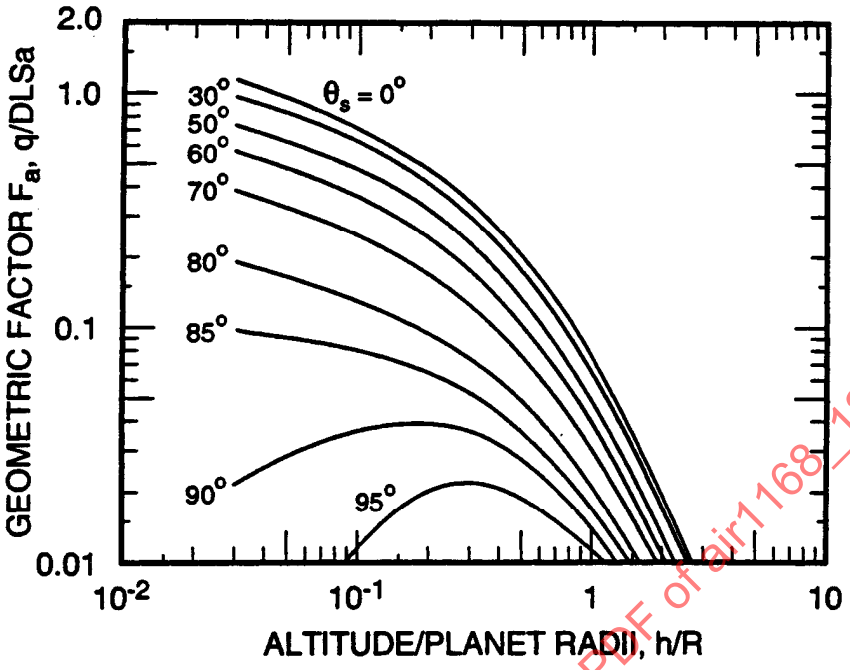

FIGURE 49 - Geometric Factor for Albedo to Cylinder Versus Altitude, With Angle of Sun as Parameter (γ = 0 deg; ϕ_c = 0 deg) (Reference 10)

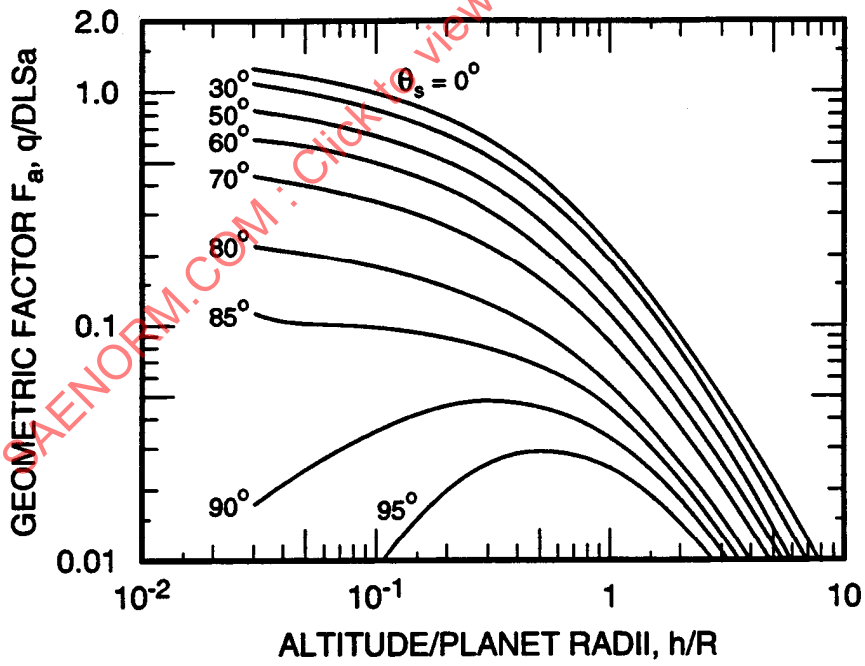

FIGURE 50 - Geometric Factor for Albedo to Cylinder Versus Altitude, With Angle of Sun as Parameter (γ = 90 deg; ϕ_c = 0 deg) (Reference 10)

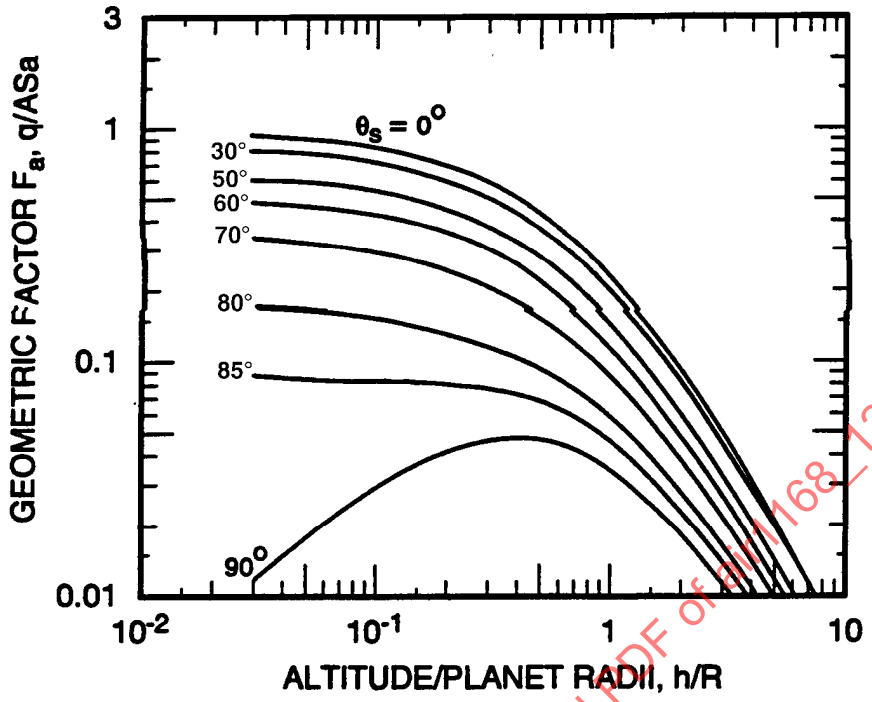

FIGURE 51 - Geometric Factor for Albedo to One Side of Flat Plate Versus Altitude, With Angle of Sun as Parameter (γ = 0 deg; ϕ_c = 0 deg) (Reference 10)

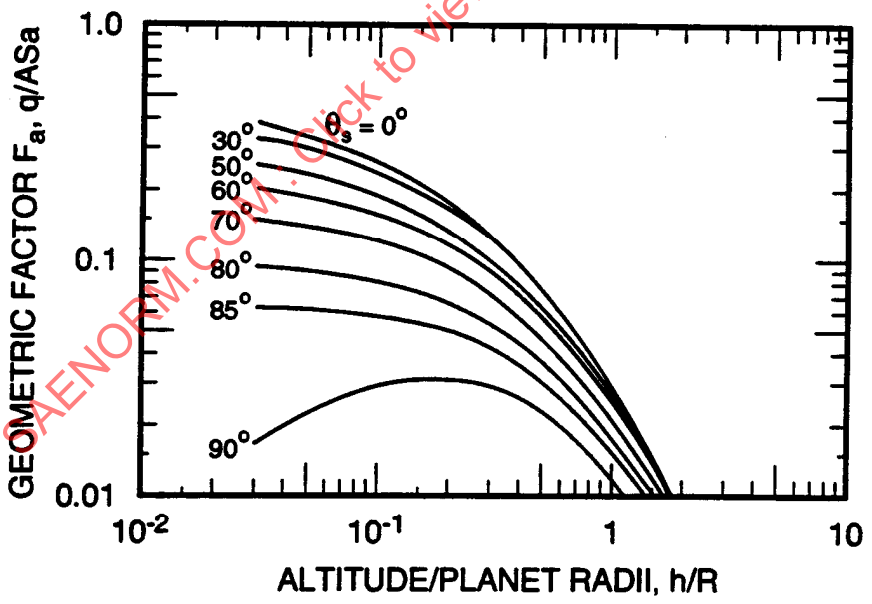

FIGURE 52 - Geometric Factor for Albedo to One Side of Flat Plate Versus Altitude, With Angle of Sun as Parameter (γ = 90 deg; ϕ_c = 0 deg) (Reference 10)

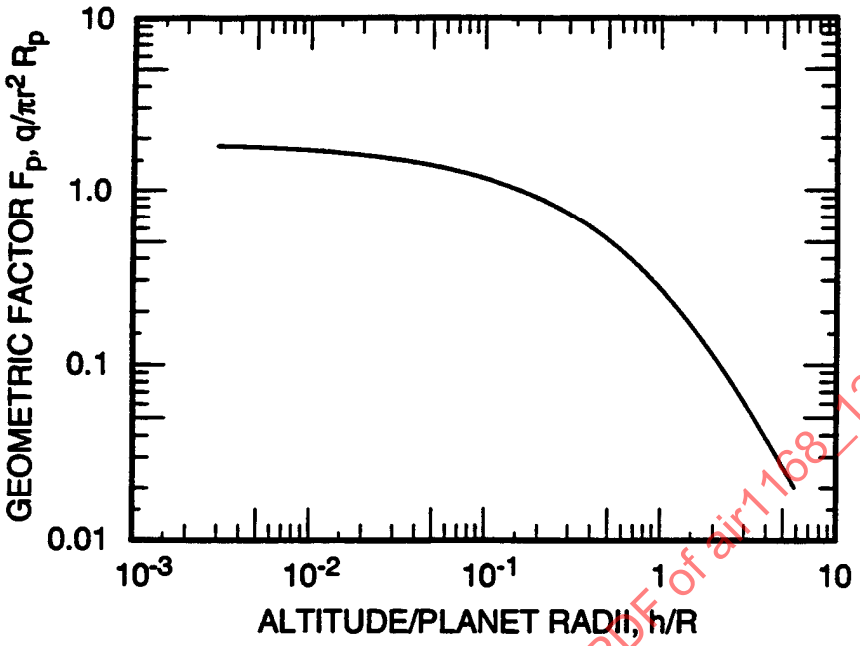

FIGURE 53 - Geometric Factor for Planetary Thermal Radiation Incident to Sphere Versus Altitude (Reference 10)

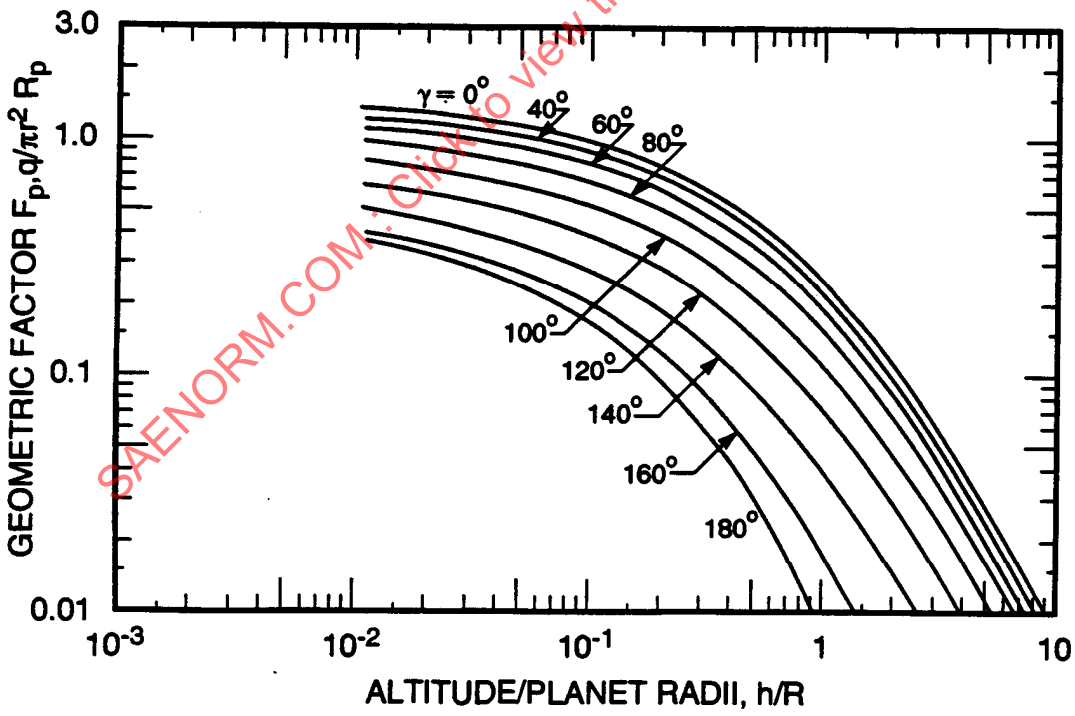

FIGURE 54 - Geometric Factor for Planetary Thermal Radiation Incident to a Hemisphere Versus Altitude, With Attitude Angle as Parameter (Reference 10)

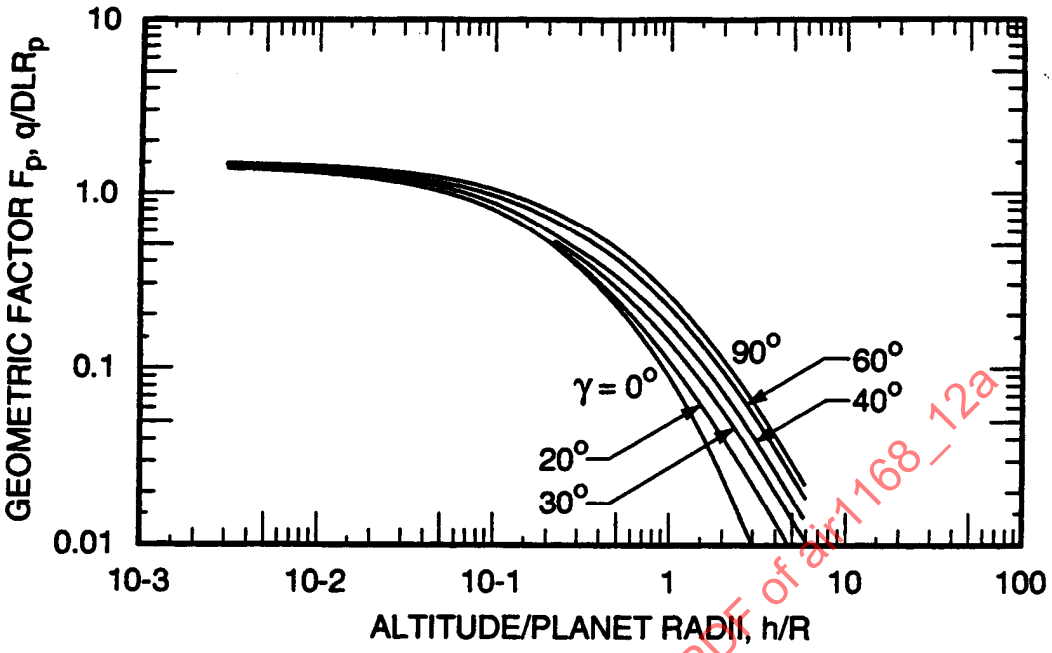

FIGURE 55 - Geometric Factor for Planetary Thermal Radiation to a Cylinder Versus Altitude, With Attitude Angle as Parameter (Reference 10)

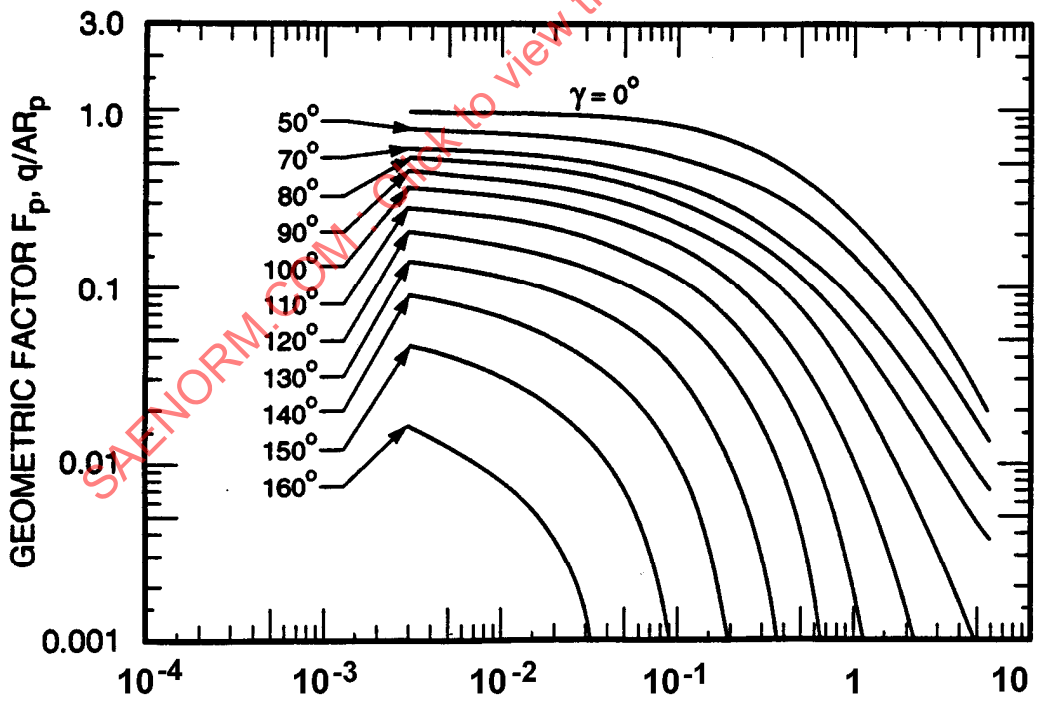

FIGURE 56 - Geometric Factor for Planetary Thermal Radiation Incident to Flat Plate Versus Altitude, with Attitude Angle as Parameter (Reference 10)

5.2.3 (Continued):

The instantaneous planet heat flux is :

$$Q'_p = \epsilon_p \sigma T_p^4 F_p \quad \text{(Eq.37)}$$

Generally the planet emittance ϵ_p is assumed = 1. The planet blackbody temperature is obtained from Table 1 and $\epsilon_p \sigma T_p^4$ becomes the planet radiance R_p. Averaged over the orbit, the planetary heat flux is

$$Q_p = R_p \frac{1}{n} \sum_{i=1}^{i=n} F_{p,vi} \quad \text{(Eq.38)}$$

or

$$Q_p = R_p \bar{F}_p \quad \text{(Eq.39)}$$

5.2.4 Incident Earth Factors: Figure 57 can be used to compute geometric albedo and Earth view factors F_a, F_p, and albedo radiation incident on a flat plate. An approximate technique can be used for surfaces of revolution, using projected flat plate segments. The segments should represent surfaces whose body angle is ≤30 deg. Instructions for use of Figure 57 are as follows:

1. Enter the right-hand scale at the angle between the normal and the zenith, γ.
2. Project a horizontal line intersecting the appropriate altitude line.
3. Find the Earth view factor F_p on the lower scale for ψ.
4. If $\psi = 0$ deg, project a vertical line intersecting the appropriate orbit angle ν. If $\psi \neq 0$ deg, enter the appropriate ψ with the planetary view factor obtained from step 3, where $\psi = 0$ deg, and project a vertical line intersecting the appropriate orbit angle ν.
5. Read the geometric albedo factor F_a and incident albedo radiation on the left-hand scale.

Examples of the procedures in steps 1-5 are:

a. Follow the lines titled 2 in Figure 57 for $\gamma = 20$ deg, $\nu = 20$ deg, and $\psi = 0$ deg at an h = 100 sm: obtain an $F_p = 0.9$, $F_a = 0.83$, and $Q'_a = 134$ Btu/h-ft^2.

b. Follow line 3 for $\gamma = 90$ deg, $\nu = 0$ deg, and $\psi = 0$ deg at an altitude of h = 200 sm, and solve for $F_p = 0.3$, $F_a = 0.30$, and $Q'_a = 47$ Btu/h-ft^2.

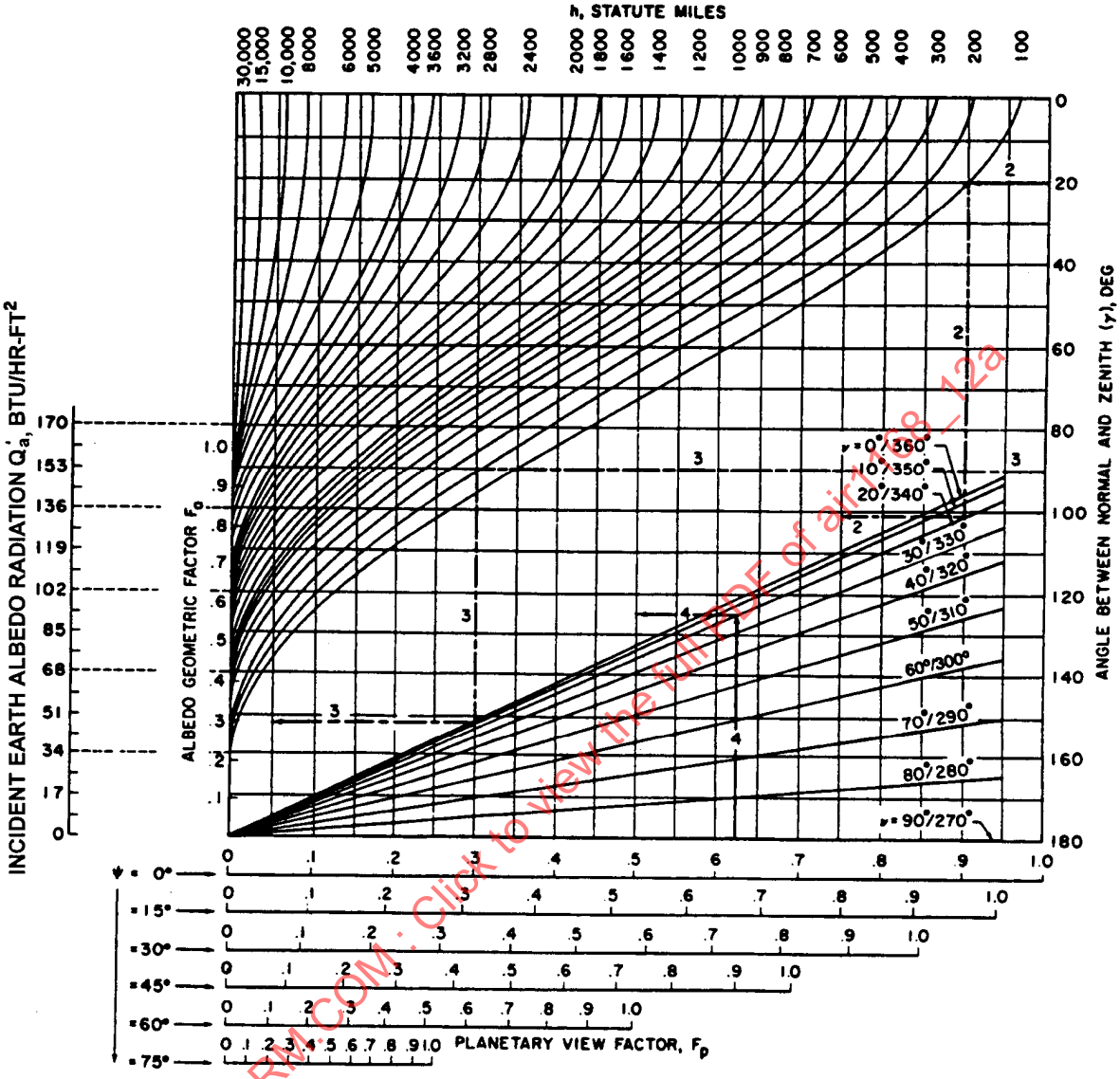

FIGURE 57 - Incident Albedo Radiation, and Albedo and Planetary View Factors F_a, F_p for a Flat Element in Earth Orbit; a = 35% (see Table 1) (Courtesy of Lockheed California Co.)

5.2.4 (Continued):

c. The lines titled 4 are for the same angles and altitudes of example (a) except that ψ = 45 deg. Enter the curve at γ = 20 deg, proceeding to an h = 100 sm, and obtain an Earth view factor F_p = 0.9 at ψ = 0 deg. Now go to the abscissa for ψ = 45 deg at F_p = 0.9 (line 4) and intersect with ν at 20 deg. Read the geometric albedo factor F_a = 0.57 and its equivalent Q'_a of 93 Btu/h-ft^2. The Earth view factor is F_p = 0.9.

The curve in Figure 57 will provide instantaneous values for F_p and F_a which can be averaged over an orbit in similar fashion, as shown in 5.2.3 and in this paragraph. For an Earth oriented satellite in a circular orbit, h, γ and ψ remain constant; therefore the Earth and albedo factors over an orbit can be obtained by varying ν, a relatively simple operation.

To use Figure 57 for planets other than the Earth, an equivalent Earth altitude for the planet must be found. As an example, for a flat plate at 200 sm above the surface of Mars, use the effective altitude h_e in place of h, where

$$h_e = \frac{\text{diaEarth}}{\text{diaMars}} \times 200 \qquad \text{(Eq.40)}$$

The albedo radiation scale cannot be used from Figure 57. However, the planetary diameters and albedo terms can be obtained from Table 1.

The variation of geometric factor with φ_c is very small and cannot be shown in Figure 57. However, should greater accuracy be required, see Reference 53. The effect of omitting φ_c should never exceed F_a values of ±0.03. Figure 57 treats values of ν or ψ close to or beyond 90 deg as a zero geometric factor. Actual values of F_a beyond these points never exceed 0.04. Still greater accuracy can be found in Reference 53.

5.3 Total Incident Space Radiation:

Once the instantaneous geometric factors have been obtained, the sum of solar, albedo, and planetary radiation flux can be calculated from

$$Q'_{\text{incident}} = S \cos\theta + aSF_a + R_pF_p \qquad \text{(Eq.41)}$$

as a function of h, γ, and θ and θ_s, or ψ.

5.3 (Continued):

The orbital average heat flux is

$$\bar{Q}_{incident} = S\cos\theta(\%sun) + aS\bar{F}_a + R_p\bar{F}_p \quad \text{(Eq.42)}$$

$$\bar{Q}_{incident} = Q_s + Q_a + Q_p \quad \text{(Eq.43)}$$

Once the incident heat fluxes of space are known, along with the corresponding spacecraft thermal properties of α_s, α_a, α_p and ϵ_{sf}, the surface temperature T_{sf} of a perfectly insulated material may be computed from

$$\epsilon_{sf}\sigma T_{sf}^4 = Q_s\alpha_s + Q_a\alpha_a + Q_p\alpha_p \quad \text{(Eq.44)}$$

Generally, the absorptance of the material to albedo is equal to its absorptance to the solar spectrum, i.e. $\alpha_s = \alpha_a$, and for the case where planet temperature and skin temperature are similar, the surface absorptance to planet radiation (α_p) is the same as the surface emittance; that is, $\alpha_p = \epsilon_{sf}$. Equation 44 then regroups to the familiar

$$\sigma T_{sf}^4 = (Q_s + Q_a)\frac{\alpha_s}{\epsilon_{sf}} + Q_p \quad \text{(Eq.45)}$$

A chart of σT^4 versus T is helpful in determining surface temperatures and is presented in Figures 58A and B.

5.4 Thermal Design:

In most cases a spacecraft's thermal control system is used for the maintenance of life support, electronic equipment, and structural integrity within specified temperature requirements. A very general range of temperatures required by various spacecraft components is shown in Figure 59.

To satisfy these requirements, the spacecraft thermal coupling to space must be designed to carry the internal power load and yet satisfy the limitations of temperature.

5.4.1 Passive Control: Thermal conditions can be satisfied by a passive system if the orientations and equipment power dissipations are known so that an α_s/ϵ can be chosen for operation within the temperature requirements.

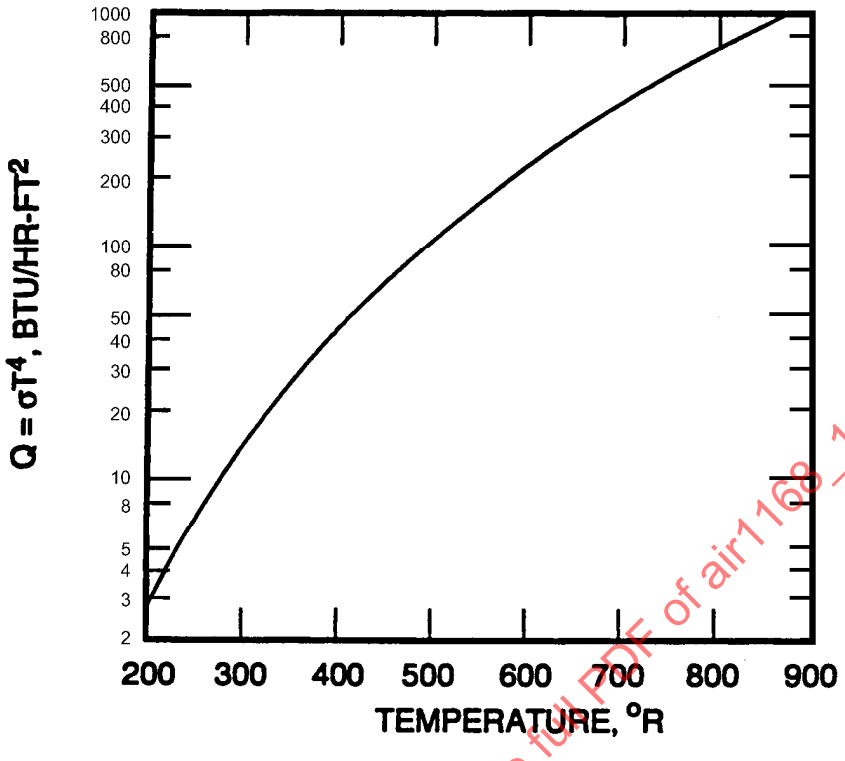

FIGURE 58A - Space Radiation to a Thin Plate, T Versus σT^4;
$\sigma T^4 = (Q_s + Q_a)(\alpha_s/\epsilon) + Q_p$, Where $\sigma = 0.1714 \times 10^{-8}$ Btu/h-ft^2-°R^4

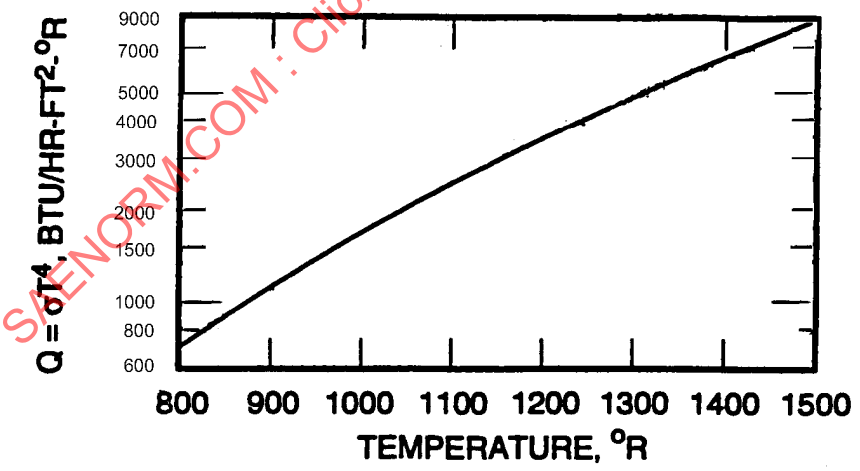

FIGURE 58B - Space Radiation to a Thin Plate, T Versus σT^4

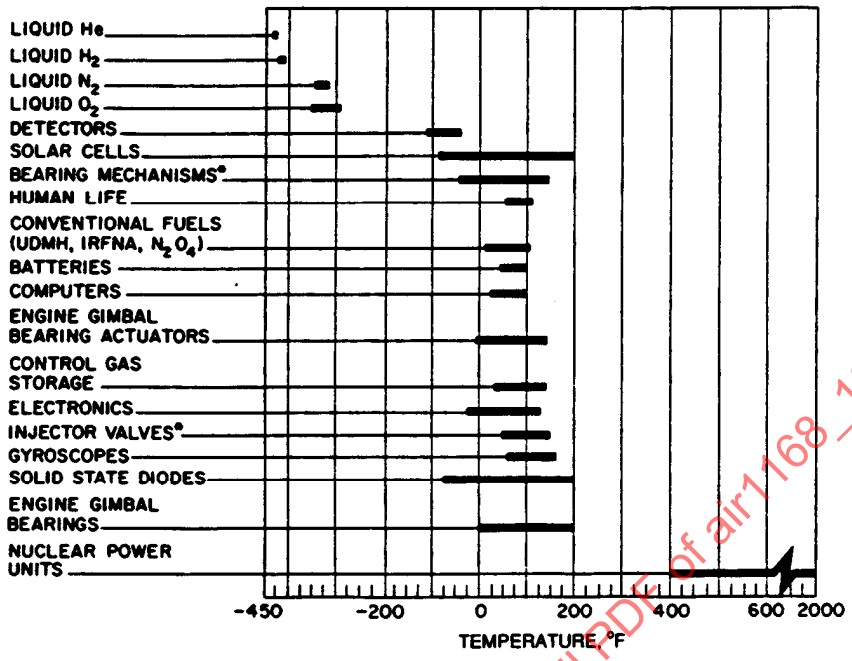

FIGURE 59 - Temperature Tolerances of Typical Spacecraft Components;
Items With Asterisk are Applicable to Storable Propellants
(Courtesy Lockheed California Co.)

5.4.1.1 Equipment Seeing Space: Figure 60 shows the variation in equipment temperature as a function of its power dissipation and thermal coating α_s and ϵ. Figure 60 incorporates solar, Earth albedo, and Earth radiation to a flat plate for a 500 mile circular Earth orbit. All five sides of the equipment box are assumed insulated except for the front surface (heat sink), which faces the space environment. The maximum environment heat input assumes the heat sink normal to the Sun, and the minimum heat input assumes the surface parallel to the rays of the Sun. For α_s/ϵ in the range 0.1 to 2.0 (equipment heat sink normal to Sun, 65% of time in sunlight), the curves are based on incident fluxes of:

Q_s = 286 Btu/h-ft^2
Q_a = 1.3 Btu/h-ft^2
Q_p = 21.3 Btu/h-ft^2

and for α_s/ϵ in the range 0.1 to 2.0 (equipment sink parallel to the Sun's rays, 65% of the time in sunlight), the curves are based on incident fluxes of:

Q_s = 0 Btu/h-ft^2
Q_a = 10.53 Btu/h-ft^2
Q_p = 15.39 Btu/h-ft^2

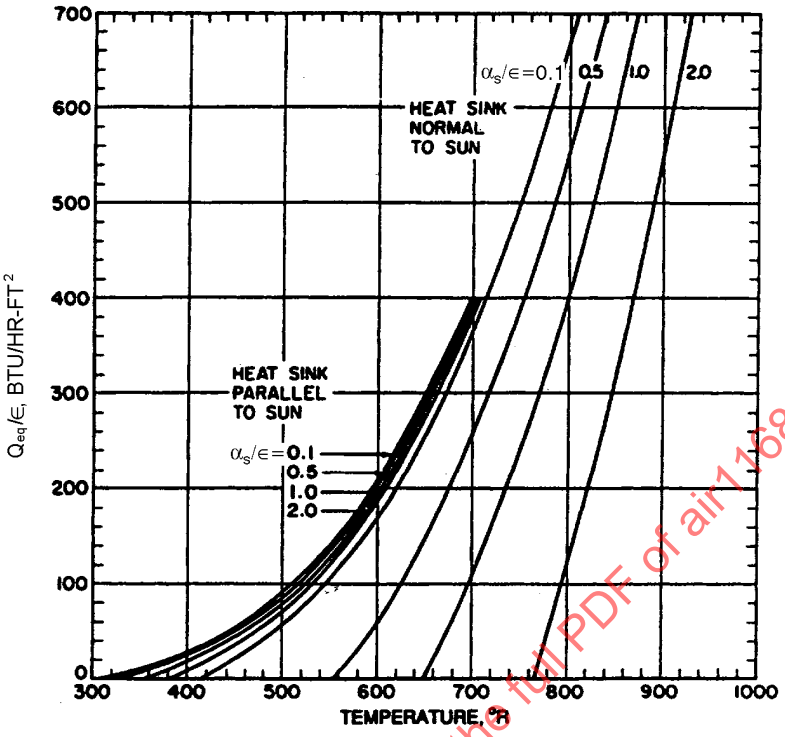

FIGURE 60 - Temperature of Equipment Heat Sink Versus Heat Sink Thermal Coating; α_s/ϵ for a Flat Plate; 500 mile Earth Orbit (Circular) in Plane of the Ecliptic

5.4.1.1 (Continued):

If the power dissipation per square foot of heat sink area is known, the thermal coating properties of α_s and ϵ can be selected so that temperature requirements are not exceeded, with the unit in or out of the Sun. The defining equation is

$$(Q_s + Q_a)\frac{\alpha_s}{\epsilon} + Q_p + \frac{Q_{eq}}{\epsilon} = \sigma T_{eq}^4 \qquad \text{(Eq.46)}$$

5.4.1.2 Equipment Facing a Skin (Reference 40): Other designs incorporating passive control systems utilize the equipment surfaces radiating to an outer skin of low α_s/ϵ (see Figure 61). In the general case the heat inputs to the skin are first calculated, averaged over an orbit for the skin both normal and parallel to the Sun's rays. It is assumed that the equipment box is heavy (approximately 20 lb) and transient effects around the orbit are negligible. A steady-state heat balance can then be made for the two conditions, based on the heat generated in the equipment and the heat inputs to the skin.

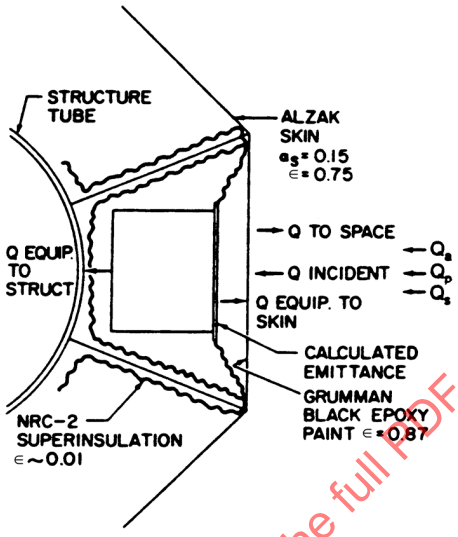

FIGURE 61 - OAO Equipment Design

From this heat balance an effective heat sink surface emittance can be calculated to maintain the equipment within its allowable temperature range. Assuming no heat transfer to the structure, the defining equation is

$$\sigma T_{eq}^4 = (Q_s + Q_a)\frac{\alpha_{s,sk}}{\epsilon_{sk}} + Q_p + Q_{eq}\left(\frac{A_H}{A_{sk}\,\epsilon_{sk}} + \frac{1}{F_{\epsilon,HB}F_{A,HB}}\right) \quad \text{(Eq.47)}$$

from which $F_{\epsilon,HB}$ is computed and the required heat sink emittance ϵ_H is calculated, assuming parallel flat plates,

$$\epsilon_H = \frac{1}{(1/F_{\epsilon,HB}) - (A_H/A_{sk})[(1/\epsilon_B) - 1]} \quad \text{(Eq.48)}$$

where:

$F_{\epsilon,HB}$ = Effective emittance between equipment and skin, dimensionless
$F_{A,HB}$ = Geometric form factor between equipment and skin, dimensionless

5.4.1.2 (Continued):

and other notations are defined in 1.2.

The calculated equipment emittance is achieved on the heat sink surface by applying a combination of paints or tapes, as required.

The limitations of this design require:

1. Stable and low α_s/ϵ skin surface.
2. Heat generated by equipment never less than 50% of the average of the peak power points resulting from long term fluctuations.

5.4.2 Superinsulation: Superinsulation is the general name given to insulation blankets that are built up of multiple separate sheets arranged to alternate low emittance surfaces with low conductance barriers. Each layer serves either as a radiation shield or as an insulator or it may combine the two functions. Superinsulation operates most effectively in vacuum and it is therefore particularly well suited for space flight applications.

Several varieties of superinsulation are commercially available. Some consist of a multitude of fiberglass sheets alternated with thin aluminum foils; others consists of Mylar sheets with aluminum layers that are vapor-deposited on one or both surfaces of the Mylar. Similar blankets of aluminized polymide film (H film) have been used on the Lunar Module (LM) for high temperature applications up to 800 °F.

An exhaustive comparative evaluation of the many superinsulations as to effectiveness per unit volume or per unit weight has yet to be made. At present, for cryogenic and room temperature applications, superinsulation consisting of 1/4 mil Mylar sheets, with an aluminum layer 0.001 mil thick vapor-deposited on one side of the Mylar, seems to have gained considerable favor. In application of this blanket, no spacers between sheets are used, and spacing is maintained by crinkling or wrinkling each sheet that makes up the blanket. Because of crinkling, the aluminized Mylar sheets touch at discrete points rather than over the entire surface. This reduces the amount of heat that can be conducted from sheet to sheet.

In Figure 62, the theoretical emittance of the superinsulation blankets is plotted as a function of the number of aluminized Mylar sheets in the blanket. This is based on the equation

$$\epsilon_{eff} = \frac{1}{(1/\epsilon_{A1}) + (1/\epsilon_{My}) - 1} \qquad \text{(Eq.49)}$$

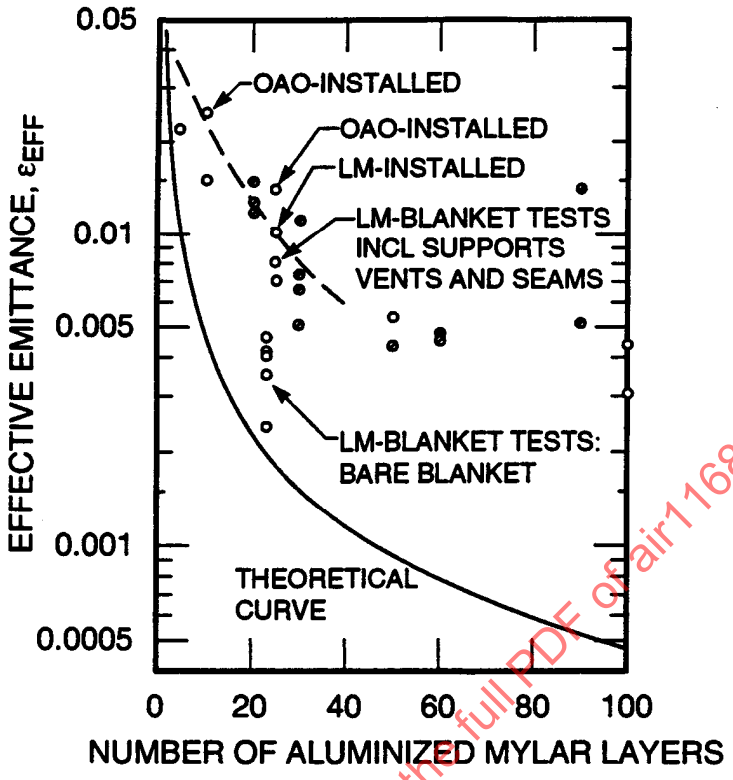

FIGURE 62 - Effective Emittance $\in_{eff}$ Versus Number of Aluminized Mylar Layers; Theoretical Curve for $\in_{My}$ = 0.4 and $\in_{Al}$ = 0.05; Circles Represent Experimental Data at Grumman Aircraft Corp. and Diagonals in Circles Represent Experimental Data Obtained in Private Communications from Other Companies

5.4.2 (Continued):

where:

$\in_{Al}$ = 0.05
$\in_{My}$ = 0.4

The theoretical equation is based on the assumptions of no significant contact between blanket sheets, of an effective vacuum within and around the blanket, and of no significant heat leakage through blanket edges.

5.4.2 (Continued):

In real installations of superinsulation blankets, aluminized Mylar sheets may touch each other to a greater or lesser extent, depending upon compression of the blanket. Some residual pressure may exist between layers, caused possibly by trapped air or material sublimation in vacuum, by edges of blankets at overlaps or around perforations, and all may conduct and radiate heat, thus decreasing the effectiveness of the blanket. All these factors, separately or in combination, may contribute to make the obtainable emittance in installed superinsulation much higher than the values calculated theoretically.

Experimental data for installed aluminized Mylar superinsulation blankets are shown in Figure 62. Most of the experimental effective emittances are several times higher than the theoretical values. Several points are noted to show the current (circa 1965) LM and OAO (Orbiting Astronomical Laboratory) state-of-the-art. Both designs are edge vented, and the as-installed conditions include support fittings, vent holes, seams, and hardware protrusions. The dashed curve in Figure 62 should be used as a first cut approximation of blanket performance as installed on spacecraft.

With the present (circa 1965) state of knowledge of the effectiveness of superinsulation blankets, it is best to use a judicious conservative approach, tailor-made for each application. The maximum effective emittance of a blanket is most likely to be close to the data obtained experimentally. The minimum effective emittance for the same blanket under certain favorable conditions, such as reduction of edge losses, reduction of pressure between sheets, and ballooning of the blanket (which reduces physical contact between sheets), is more likely to be close to the theoretical values.

In order to obtain effective emittances that are close to theoretical values for the superinsulation, the pressure between sheets should be maintained at less than 10^{-4} torr, blankets consisting of a given number of sheets should be made thick enough to assure separation of sheets so as to minimize solid conduction paths across blankets, and temperature gradients along the surfaces of the sheets should be minimized where possible.

The following set of rules should be followed in blanket installation:

1. The optimum spacing of aluminized Mylar sheets is usually 60 to 70 sheets per inch of blanket thickness. No significant reduction in heat leakage will be obtained by increasing the number of sheets over 80 per inch.

2. To maintain isothermal conditions for discrete sheets, the technique of interleaving should be used to connect adjacent blanket edges at discontinuities, joints, perforations, and overlaps. Interleaving consists essentially of staggering sheets at blanket edges and of placing each sheet of one blanket between two sheets of the overlapping blanket.

3. To maintain pressure between the sheets at less than 10^{-4} torr, the raw material (aluminized Mylar rolls) should be stored and used dry and free of dust or other contaminants. It is recommended that lint-free cotton gloves should be used in blanket assembly.

5.4.2 (Continued):

4. Venting paths must be provided to minimize evacuation time and assure vacuum conditions between layers. Edge venting relies on molecular travel between shields and appears to be effective for distances up to 20 in. In making seams, the blankets should overlap each other by at least 6 in to minimize edge heat leakage. An alternate approach is broadside venting consisting of 1/8 in holes randomly spaced in each layer and occupying about 1% of the surface area. Blankets can be attached to each other using a drug store type wrap.

The precautions outlined above should, if followed, greatly reduce the heat transfer through the aluminized Mylar superinsulation blankets. In general the design of such a blanket will have to be an engineering compromise, considering required thermal performance, available space, allowable weight, the need for quick venting, and necessity of optically sealed edges.

Finally, considering the present state of knowledge (circa 1965), it is recommended that superinsulation blankets used in particular applications and assembled in a particular manner should be tested for data of maximum reliability. For further superinsulation details, see References 55, 56, and 57.

5.4.3 Semipassive Control: For the case where the conditions cause the temperature to fall outside the required range, an active system may be employed.

Mechanical means such as pinwheels or louvers may be used to vary the α_s/ϵ of the heat sink. Other methods such as electrical thermostat heat controls or variable conductance heat pipes alter the internal heat flow to the heat sink surface and create a stabilizing effect on component temperatures.

An example of the pinwheel system used successfully on the Atlas Able-4 lunar satellite (Reference 28) is shown in Figure 63. The aluminum mask rotates in relation to the bimetal temperature, exposing a similarly designed aluminum and white cross on the payload fairing. Exposing the white cross cools the payload while covering it presents a low emittance surface to space, heating up the payload.

A louver type system was used in the Nimbus satellite design (Reference 36) and is shown in Figure 64. As the gas bubble is heated from the internal equipment, it expands, causing the shutters to open and increasing the emittance from equipment to space. A curve of the effective emittance and equipment surface temperature versus shutter angle is shown in Figure 65. A bimetallic actuated louver design is shown in Figure 66. The unit consist of two polished aluminum blades mounted on a single shaft having bearings at either end and coupled to a bimetallic spring in the center channel. The louver assembly has the emittance characteristics noted in Figure 65, and is shown installed on an OAO equipment heat sink in Figure 67 with the outer skins removed.

A slightly different active system was developed for the Telstar satellite (Reference 37). The design is shown in Figure 68.

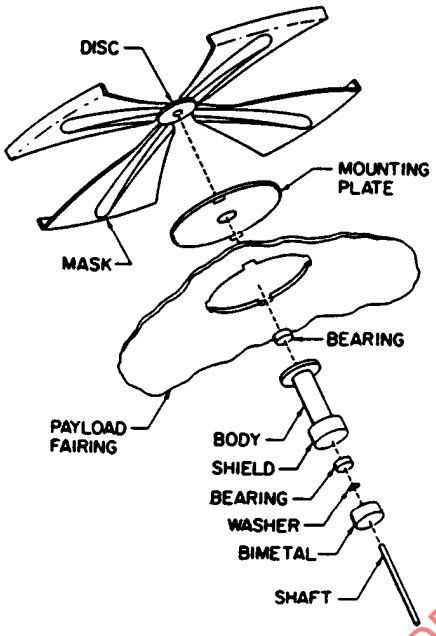

FIGURE 63 - Atlas-Able Temperature Control Unit (Exploded View) (Reference 28)

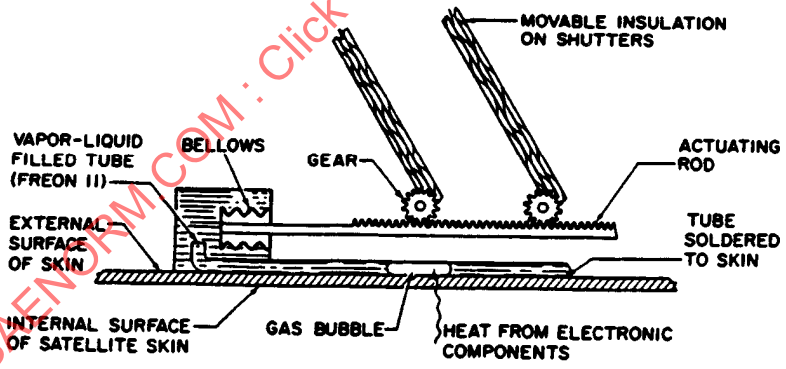

FIGURE 64 - Schematic of Nimbus Active Temperature Control Mechanism (Reference 36)

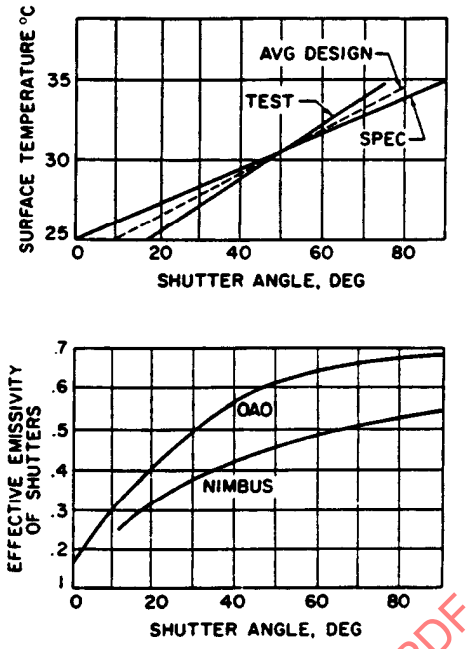

FIGURE 65 - Shutter Angle as a Function of Sensed Temperature for Nimbus and Effective Emittance for Nimbus and OAO Designs (References 20 and 36)

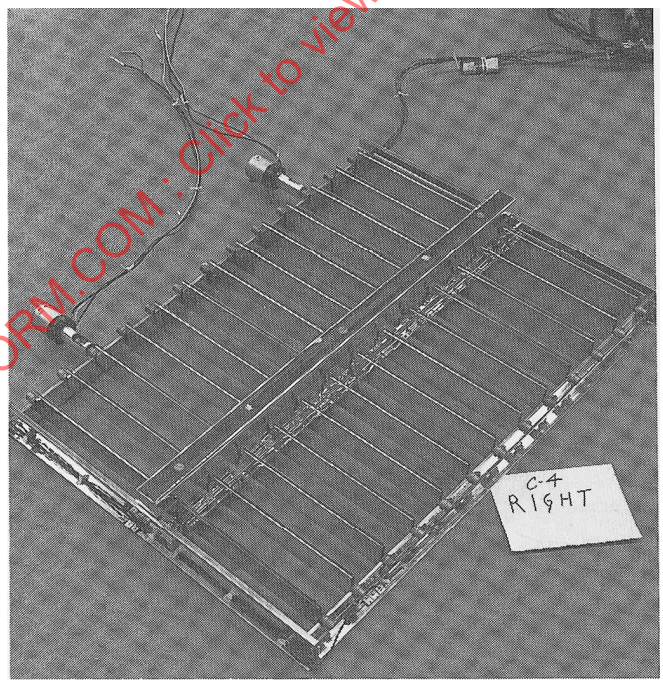

FIGURE 66 - OAO Bimetallic Actuated Thermal Control Louvers, Fairchild-Hiller (Reference 20)

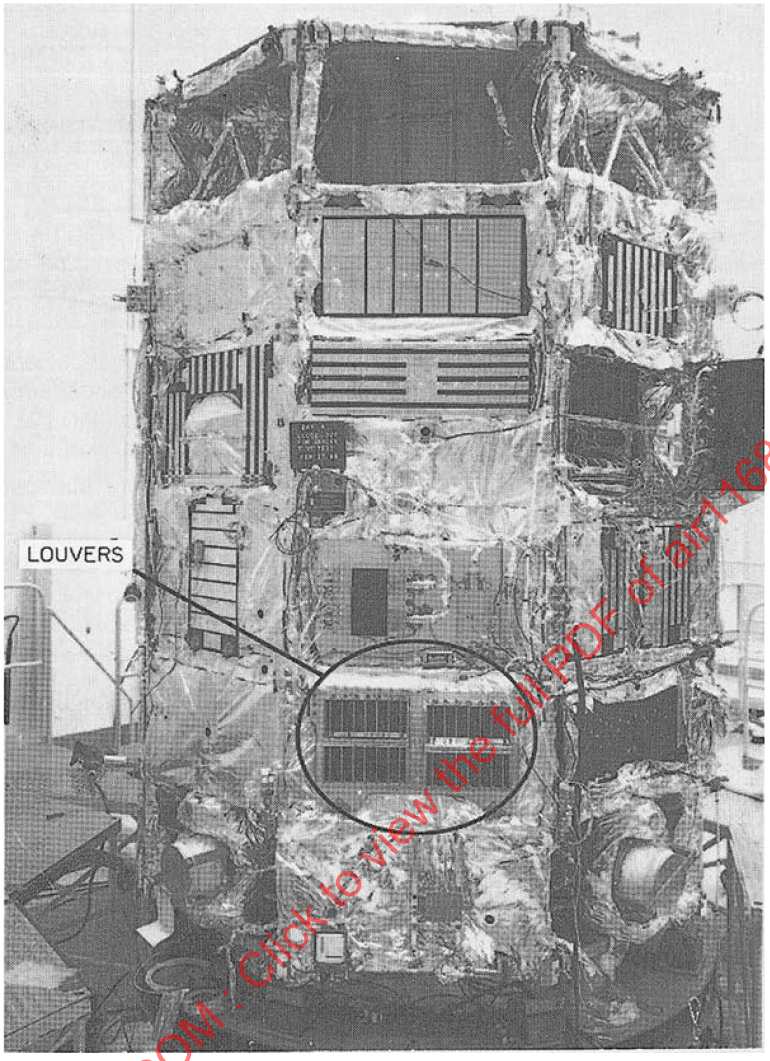

FIGURE 67 - Installation of Louver Mechanism on OAO (Reference 20)

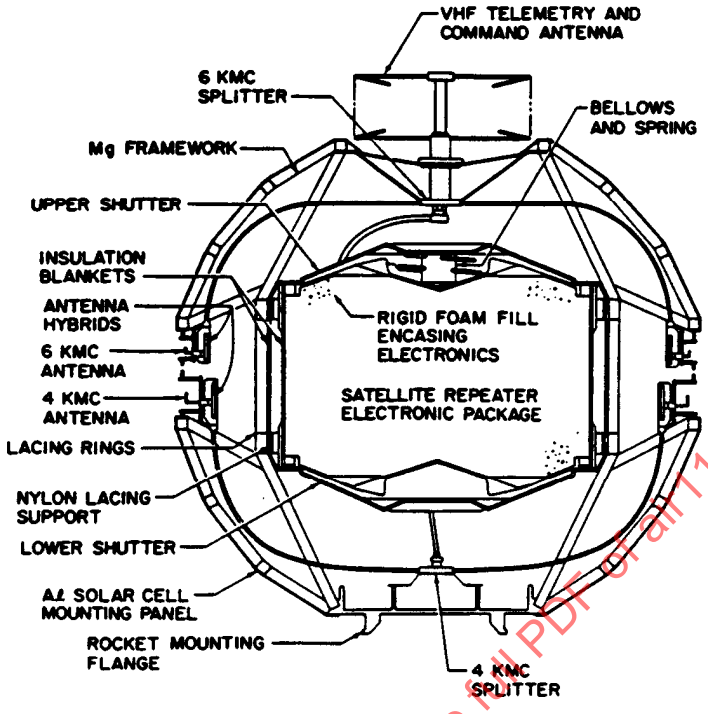

FIGURE 68 - Cross Section of Telstar Spacecraft (Reference 37)

5.4.3 (Continued):

The electronics are packaged in a container suspended and insulated from the satellite shell. Two umbrella-like covers on top and bottom are thermally activated by a spring and bellows filled with N-pentane. The covers open and close an annular gap, exposing the black interior electronics encapsulation to the colder satellite skin. The shutters are completely open at 75 °F and fully closed at 55 °F. Actual orbit telemetry showed the temperature response of the package with nearly closed shutters to be maintained within 3 °F.

5.4.4 Heat Pipe: The latest development (circa 1965) in semi-active control is the heat pipe. The device transfers heat by transporting a vapor phase of a fluid from a heat source (evaporator) to a heat sink (condenser). The condensate in the condenser section returns by capillary pressure along the wick to the evaporator where the continuous cycle is completed by boiling off the liquid again. Two highly desirable characteristics are inherent in its performance, extremely high effective thermal conductance and near isothermal operation. Used in connection with space vehicle thermal control, heat pipes are ideal for such tasks as isothermalization and temperature control of equipment with varying duty cycle in a varying environment. A schematic illustrating a typical heat pipe operation is shown in Figure 69. Wicking materials of the type shown in Figure 70 are currently in use and will be discussed in this paragraph.

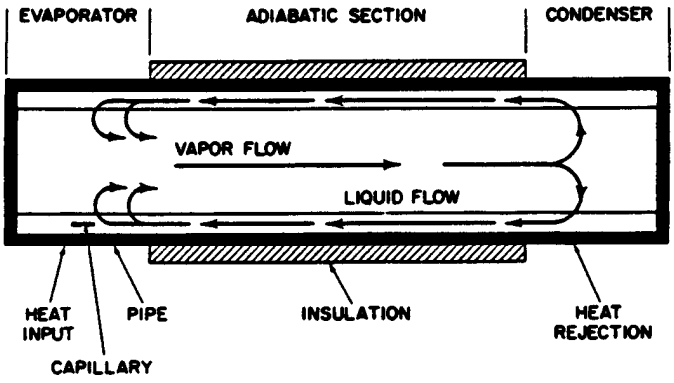

FIGURE 69 - Heat Pipe Schematic (Reference 20)

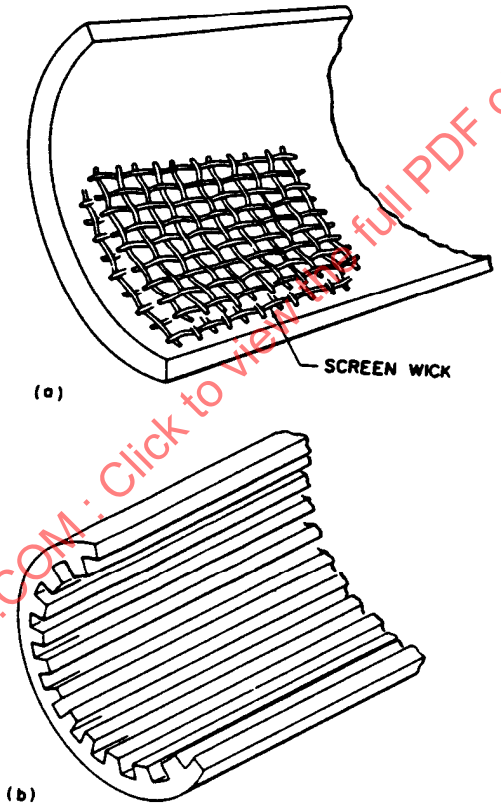

FIGURE 70 - Wick Designs (a) Plain Pipe With Screens, (b) Grooved Heat Pipe (Reference 20)

5.4.4 (Continued):

A general mathematical model of a heat pipe operation can be described by momentum and energy transport considerations.

1. Momentum transport balance. The capillary head should exceed the liquid and vapor pressure drop which is effected by the wicking geometry, wetting angle, fluid and heat flow.

$$\Delta P_{cap} \geq \Delta P_L + \Delta P_V \quad \text{(Eq.50)}$$

For an internally grooved pipe the capillary head is determined from:

$$\Delta P_{cap} = \frac{2\sigma}{w}\cos\theta \quad \text{(Eq.51)}$$

where:

σ = Surface tension, lb/ft
w = Groove width, ft
θ = Wetting angle, deg

The liquid pressure drop is:

$$\Delta P_L = \frac{f_L L_L (\rho_L g) V_L^{\,2}}{D_L (2g)} \quad \text{(Eq.52)}$$

and vapor pressure is:

$$\Delta P_V = \frac{f_L L_V (\rho_v g) V_v^{\,2}}{D_V (2g)} \quad \text{(Eq.53)}$$

where:

f = Friction factor, dimensionless
L = Flow length, ft
D = Hydraulic diameter in direction of flow, ft
V = Velocity along flow path, ft/s

5.4.4 (Continued):

2. Energy transport balance. Since the primary advantage of the heat pipe is its exceptionally high conductivity, the temperature drop across the evaporator and condenser sections should be small at maximum heat load. The energy transferred across the vapor-liquid evaporator interface is given in terms of a boiling coefficient h_{EV} referred to the temperature difference across the boiling film and the evaporator heat transfer area.

$$Q = Ah_{EV}\Delta T_{EV} \quad \text{(Eq.54)}$$

For a 1/2 in OD aluminum grooved pipe using Refrigerant 21 and having 30 internal fins, the following correlation was obtained (Reference 20) for the boiling coefficient.

$$N_{St} = 15.7N_{Re}^{-0.89}N_{Pr}^{-0.6} \quad \text{(Eq.55)}$$

or:

$$\frac{h}{(\rho g)C_p V} = 15.7\left(\frac{\rho g D_{EV} V}{\mu}\right)^{-0.89}\left(\frac{3600C_p\mu g}{k}\right)^{-0.6} \quad \text{(Eq.56)}$$

A different correlation was determined by Anand (Reference 58) for a 3/4 in OD stainless steel tube with a 100 mesh stainless steel screen using water as the fluid.

$$N_{St} = 0.0051N_{Re}^{-1.43}N_{Pr}^{-0.6}N_P^{-0.2} \quad \text{(Eq.57)}$$

where the pressure term

$$N_P = \frac{\sigma(\rho_L g)}{P^2 g} \quad \text{(Eq.58)}$$

Both correlations are shown in Figure 71.

The temperature drop can be found by equating the mass transfer equation of the fluid boiloff in the radial direction from the grooves with the evaporator heat transfer equation.

$$Q = AV_L(\rho_L g)\lambda = h_{EV}A\Delta T_{EV} \quad \text{(Eq.59)}$$

where:

λ = Heat of vaporization, Btu/lb

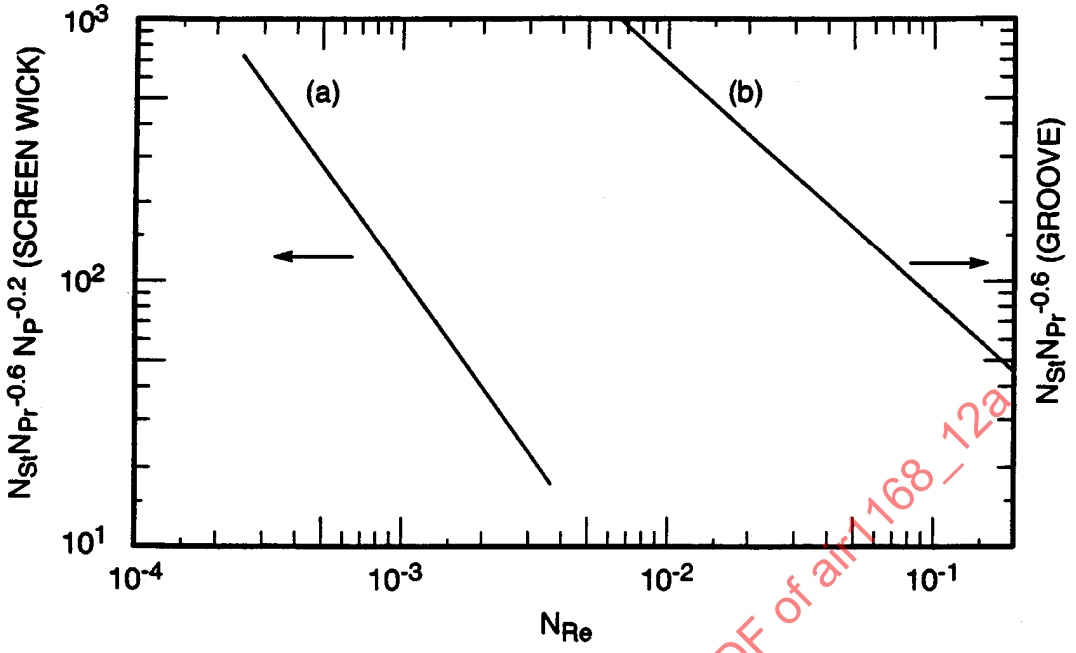

FIGURE 71 - Evaporator Film Coefficient Data (a) 3/4 in OD Stainless Steel Tube With 6 Layer Stainless Steel Screen Wick-Water, (b) 1/2 in Aluminum Grooved Tube, 30 Fins - Refrigerant 21 (References 20, 58)

5.4.4 (Continued):

Substituting h_{EV} for h in Equation 56 and solving for ΔT_{EV}

$$\Delta T_{EV} = \frac{1}{15.7}\frac{\lambda}{C_p}\left(\frac{(\rho g)DV}{\mu}\right)^{0.89}\left(\frac{3600 C_p \mu g}{k}\right)^{0.6} \quad \text{(Eq.60)}$$

Similarly the energy transferred across the vapor-liquid interface in the condenser section is given by

$$Q = Ah_c\Delta T_c \quad \text{(Eq.61)}$$

Test data for grooved pipes indicate that the condenser heat transfer coefficient is approximately 50% greater than the corresponding evaporator coefficient. For design purposes, due to the unavailability of test data, the condenser heat transfer coefficient can be assumed equal to the evaporator coefficient.

5.4.4 (Continued):

A figure of merit ($\sigma\lambda/\nu$) can be attributed to the fluid properties of surface tension, heat of vaporization and viscosity to optimize the capillary pressure. Through the manipulation of Equation 51 where $w = 2r_c \cos\theta$ and r_c is the meniscus radius, and equating this to the liquid pressure drop (Equation 52) where $f = 64/N_{Re}$ for laminar flow, then solving for the figure of merit as a function of heat flow (Equation 59) the following equation is obtained:

$$\frac{\sigma\lambda}{\nu} = \frac{32QL_L r_c}{AgD_L^2} \qquad \text{(Eq.62)}$$

Figures of merit for three fluids are shown in Table 20.

TABLE 20 - Fluid Properties

Property	Water	Ammonia	Refrigerant 21
Specific Heat, C_{PL}, Btu/lb-°F	1.0	1.2	0.25
Dynamic Viscosity, $g\mu_L$, lb/ft-h	2.4	0.5	0.9
Conductivity, k_L, Btu/h-ft-°F	0.34	0.30	0.06
Surface tension, σ, lb/ft	5×10^{-3}	1.4×10^{-3}	1.3×10^{-3}
Density, lb/ft^3			
$\rho_L g$	60	40	85
$\rho_v g$	0.001	0.4	0.4
Boiling Pressure, p, psia at 70 °F	0.4	130	23
Heat of Vapor, λ, Btu/lb	1000	500	100
Figure of Merit, $\sigma\lambda/\nu_L$ Btu-h/ft^3	125	56	12

ν = Kinematic viscosity, ft^2/h

In the initial design of a heat pipe, Equations 50, 55, and 62 are used to guide the designer in choosing an effective groove geometry, and fluid that will meet the applications of the heat pipe. Several boundary conditions such as temperature drop, operating temperature range, pipe material and compatibility with the fluid may alter the optimum design solution, and engineering judgment must prevail to satisfy the primary heat pipe objective. With the scant amount of data currently available (circa 1965) all heat pipe designs should be performance tested. Some thermal performance data on a 1/2 in OD aluminum internally finned heat pipe with 30 fins for both Refrigerant 21 and water is shown in Figure 72 along with a 3/4 in OD stainless steel pipe with six layers of 100 mesh stainless screen and water as the working fluid.

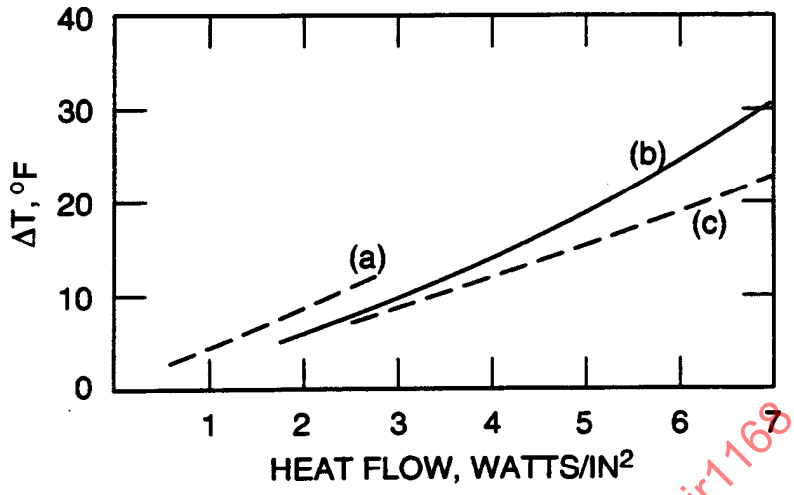

FIGURE 72 - Heat Pipe Thermal Performance Test Data
Temperature Drop Between Evaporator and Condenser Tube Walls as a Function of Evaporator Heat Input (a) Same as Figure 71a, (b) Same as Figure 71b, (c) Same as Figure 71a but with Water (References 20, 58)

5.4.4 (Continued):

One of the major problems associated with heat pipes is the noncompatibility of materials and the eventual evolution of noncondensible gases forming a thermal barrier at the condenser section. Trapped gases in the pipe can be avoided by pulling a vacuum on the pipe while heating it to drive off residual gas. Material compatibility tests can be accelerated by operating the pipes vertically, heater section down and maintaining higher than required temperature levels to increase the chemical reaction times. The upper end of the pipe is to be temperature instrumented so that any noncondensible gas evolved will show a marked temperature drop from the normal vapor temperature. A plot of trapped gas length as a function of time can be used to extrapolate long term effects.

Typical applications of heat pipes in spacecraft are described in Reference 59 where a noncondensible vapor chamber is used to alter the conductivity of the heat pipe thereby maintaining semi-passive control on electronics and spacecraft structure. A second application shown in Figure 73 uses the inherent high conductivity of the pipe to isothermalize the OAO inner 48 in diameter telescope housing. The heat pipe is a 1/2 in OD aluminum internally grooved pipe using Refrigerant 21 as the working fluid, for operation at -100 to +100 °F. The pipe is bonded to eight aluminum saddles which are then bonded to the spacecraft structure. Each OAO utilizes three heat pipes to lower temperature gradients to less than 4 °F and provide a near isothermal enclosure for the telescope.

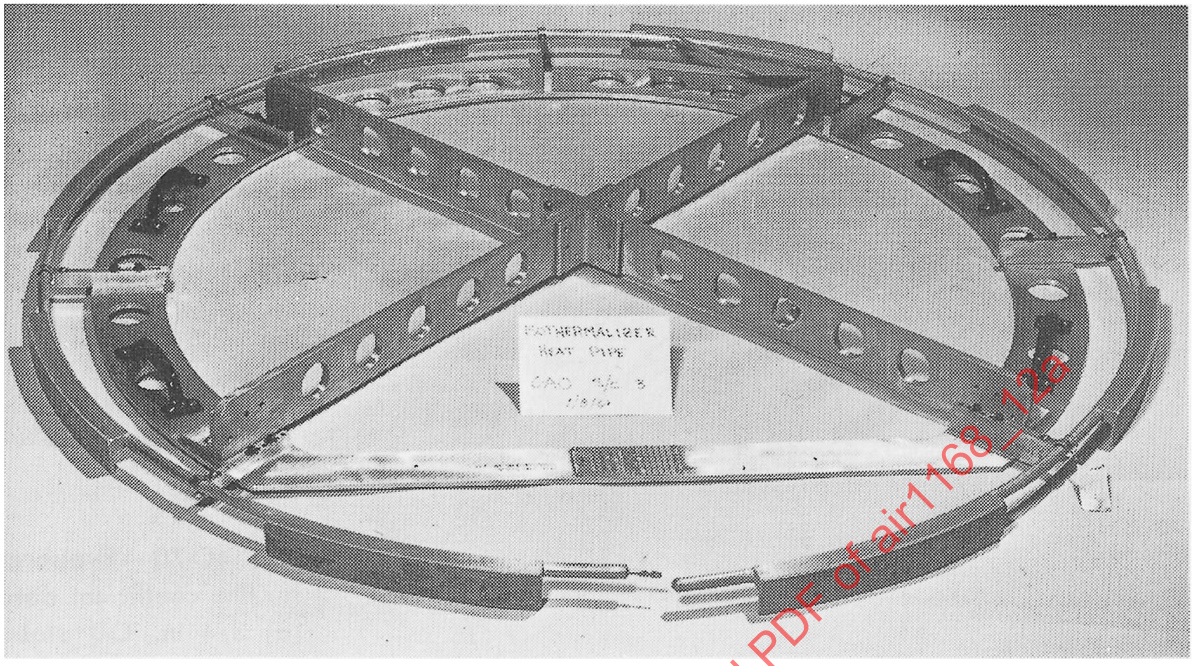

FIGURE 73 - OAO Isothermalizer Heat Pipe in Handling Fixture (Reference 20)

6. TESTING:

The first flight of a spacecraft must be an unqualified success, since there is little chance of repairing or retrieving it once it is launched. Because of this type of one-shot scheduling, spacecraft must be completely tested, from the full simulation of launch vibrations to the simulation of thermal vacuum conditions in the space environment. A step-by-step program of testing becomes a major factor in the design of a spacecraft, and begins with material tests, advances to component, full system tests, and concludes with a complete test of the flight vehicle.

Material and component testing includes physical property measurements such as absorptance, emittance, and conductance, form factor determination, and performance and life tests of electronic components under vacuum and temperature extremes.

Component and system test temperature levels for mechanical systems and electronics are presently (circa 1965) nonstandardized. The OAO requirements for high reliability were to qualify most electronics at heat sink temperature levels of -30 °F and 160 °F. Acceptance tests were run at 0 °F and 130 °F, while actual design and flight levels were well within these values.

The LM project qualified and acceptance tested most electronics at 0 °F and 130 °F. Temperature levels of the electronics during flight spacecraft qualification tests rarely reached component acceptance test levels, although maximum external fluxes with maximum equipment heat generation were imposed during testing.

6. (Continued):

For both the OAO and LM, external equipment subject to the space environment were generally specified at acceptance temperature levels consistent with the "worst case" thermal balance analysis of the unit. An additional margin of 30 °F was added or subtracted from maximum and minimum acceptance temperature levels, respectively, to obtain qualification test temperatures that would ensure an added degree of reliability.

The following paragraphs describe test facilities and methods of testing spacecraft. Since the field of spacecraft testing is all-encompassing, only the major test facilities and procedures will be mentioned.

6.1 Space Simulators:

The culmination of all testing occurs when a complete spacecraft is subjected to a thermal vacuum test. The results of this test determine its performance when exposed to the vacuum and temperature extremes of the anticipated space environment.

Since the analyses of spacecraft are complex, the simulation of space must produce accurate heat fluxes to all surfaces of the vehicle so that heat balance and temperature predictions can be verified. The NASA and GE thermal vacuum facilities (References 38 and 39) are shown in Figures 74 and 75 and corresponding characteristics are shown in Table 21. These two systems illustrate the current (circa 1965) design philosophy of space simulators.

Each system is capable of producing a pressure of 10^{-9} torr (empty) in its vacuum chamber, which contains a blackened liquid N_2 cold wall to simulate the absorptance of black space. The main design difference between the systems is in the simulation of the solar load. The problems associated with the design of the NASA-GSFC chamber are discussed in Reference 39. Excessive heat loads from the 2.5 kW lamps caused severe distortion of the lenses and mirrors in the collimation system and produced failures of the vacuum seals around lamp fixtures. The problems have been solved at the expense of increased cost and time and a degradation of performance.

Similar performance degradation has occurred in the GE facility, owing to warping of the off-axis parabolic mirrors. Each of these simulators also has problems with spectral match of the Johnson curve (Figure 8) and beam uniformity so that local test conditions may be representative only to within ±10%. Neither of these chambers is fitted with true albedo or Earth simulators. An example of a nonspectral Earth simulator is shown in Figure 76 proposed for the Nimbus satellite.

The space simulator (Reference 32) shown in Figure 77 duplicates the transient thermal loading of a satellite spinning about the Earth and tends to duplicate Earth, albedo, and solar irradiation. Its drawback is that it is small in size and can be used only for component or model testing.

TABLE 21 - NASA-Goddard and General Electric Facilities

Simulation Items	NASA-Goddard	General Electric
Chamber Size	35D x 60H (ft)	32D x 54H (ft)
Test Section	27D x 35H (ft)	27D x 21H (ft)
Cryowall Temp.	≈ 144 °R	≈ 144 °R
Cryowall Emissivity	≈ 0.9	≈ 0.95
Vacuum Capability	10^{-9} mm Hg	10^{-9} mm Hg
Cryo Pumping	Gaseous He	Gaseous He
SOLAR SIMULATOR		
Primary Mirror Size	20D (ft)	22D (ft)
Source	Hg-Xe	Xe
Lamp Power and Number	2.5 kW, 127	5.0 kW, 148
Beam Size		
Rated	20D (ft)	20D (ft)
Actual	17D (ft)	17D (ft)
Intensity		
Range	170-510 Btu/h-ft^2	410-480 Btu/h-ft^2
Uniformity	±5%	±5% (70% area)
Decollimation	±2 deg (±4 deg)[1]	±3 deg (±2 deg)[1]
Spectrum	Typical[2]	Typical[3]

[1] Pertains to original specifications.
[2] Lamp spectrum; does not include chamber optics. See Figure 80.
[3] See Figure 79.

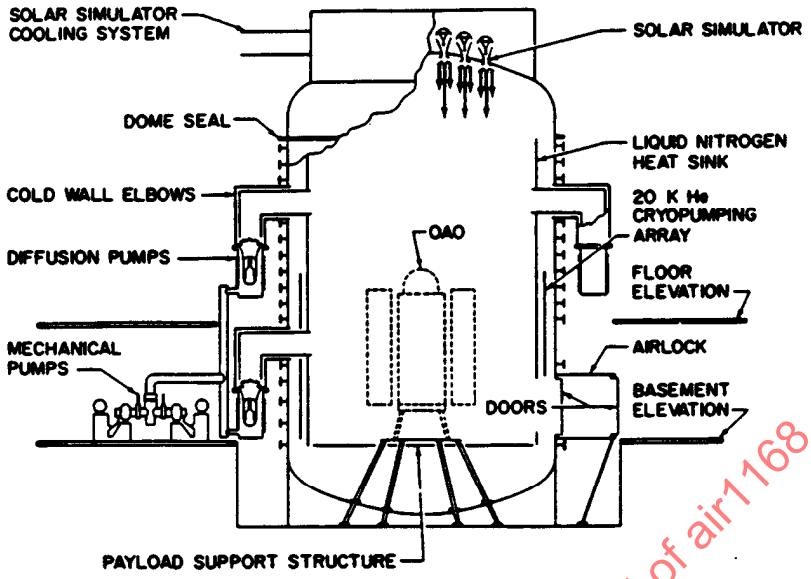

FIGURE 74 - NASA Goddard Space Environmental Simulator (Reference 39)

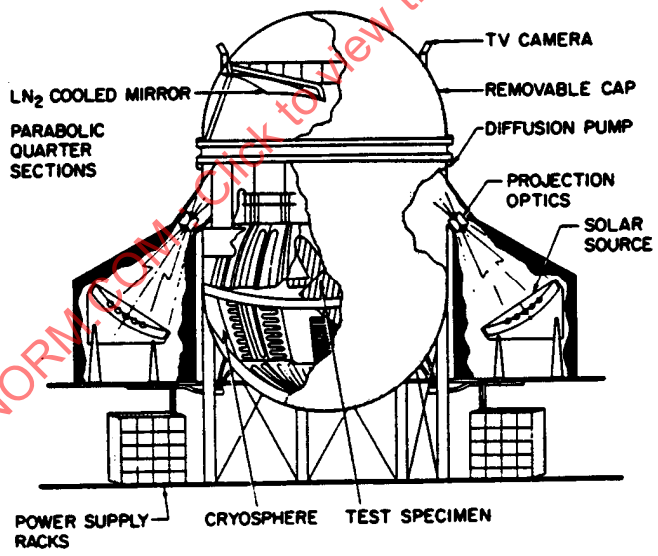

FIGURE 75 - General Electric Space Environmental Simulator (Reference 38)

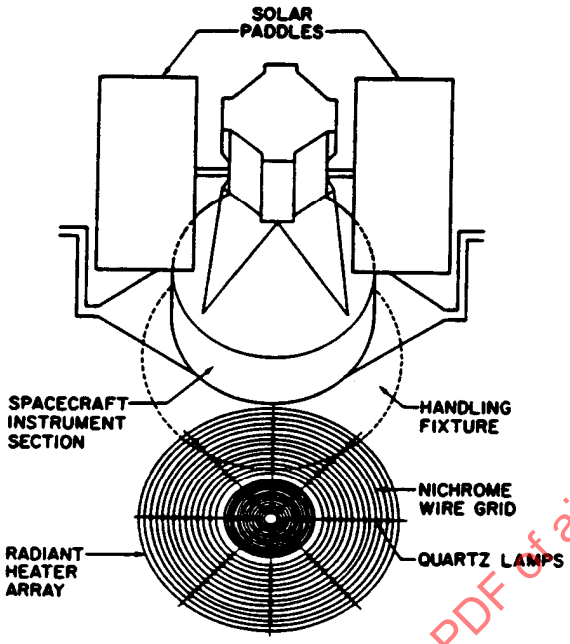

FIGURE 76 - Schematic of Heat Flux Simulator for Earth Oriented Satellite (Reference 38)

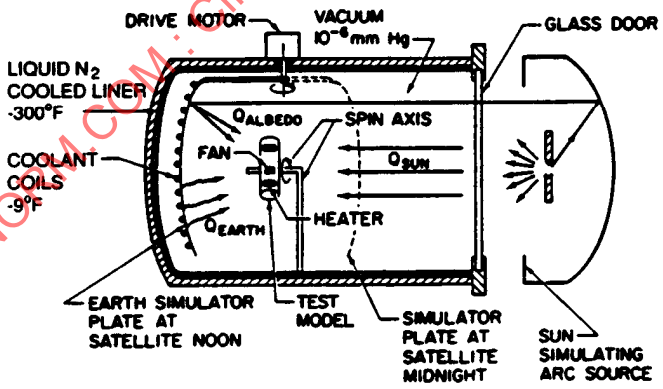

FIGURE 77 - Langley's Space Thermal Environmental Facility with Components for Thermal Balance Experiments of Thermally Scaled Space Station Models (Reference 32)

6.1.1 Simulation with Heated Skins: An alternate method of simulation is to use a liquid N_2 cooled vacuum chamber, but to impose directly on the satellite skins the calculated heat fluxes of the space environment, using nichrome heater strips. This method is discussed in References 40 and 56 and is used in testing the OAO and the LM. The total heat inputs from Earth, albedo, and solar radiation must be calculated for each skin in its desired orientation.

The calculations should be based on accurate measurements of the α_s and ϵ of the skin. Heaters are attached to the interior skin surface by laying down a layer of double backed H film tape upon which strips of 1 mil nichrome ribbon are attached in series covering at least 90% of the skin surface. Over this, a second layer of H film or Mylar tape is applied to electrically insulate the nichrome. A cover paint or tape may then be applied to simulate the actual flight skin internal emittance. This method allows heat to be radiated from the exterior surface to the cold walls, as it would be in space. Appropriate heat fluxes are imposed through a battery of Variacs controlling the power supplied to each skin heater on the model.

Simulation is more complete in this method, since it includes albedo and Earth radiation and can be easily adjusted to simulate qualification levels or orbital transient fluxes if desired. However, it relies on the accuracy of calculations and is only approximate for surfaces that see each other. Small protuberances and their effects on the thermal balance cannot be determined analytically with accuracy.

6.1.2 Solar Simulation: To assure solar absorption of the correct amount of energy during environmental simulation tests, a space vehicle model should be irradiated by a source possessing a spectral intensity distribution similar to that of the Sun. The Johnson curve (Figure 8), which shows the spectral solar irradiance at the Earth outside the atmosphere, should be used as a reference for simulation of the solar energy spectrum.

When selecting a source for solar energy simulation, there are several considerations besides spectral matching. Source life, intensity, ease of maintenance, reliability, and accessibility are all factors that should be investigated before the final selection is made. Three presently available (circa 1965) sources are considered acceptable solar simulators: the carbon arc, xenon short arc lamp, and the mercury-xenon short arc lamp. The spectral energy distributions of these sources (Reference 38), referenced to the solar spectrum are shown in Figures 78, 79, and 80.

The carbon arc approximates the solar spectrum more closely than the high-pressure short arc lamps, but is generally excluded from large-scale simulators because it requires constant monitoring, has transient intensity variations due to unevenness of the arc burning process, and produces a non-uniform beam due to shadowing by the carbon rods.

From Figures 79 and 80 it is evident that neither of the two short arc lamps provides satisfactory simulation of the solar spectrum if it is used without a filter. Figures 81 through 84, however, show the results of filtering the short arc lamps (Reference 42). Notice that by filtering approximately 50% of the energy output of two lamps, their spectral intensity distribution may be made to approximate that of the Sun.

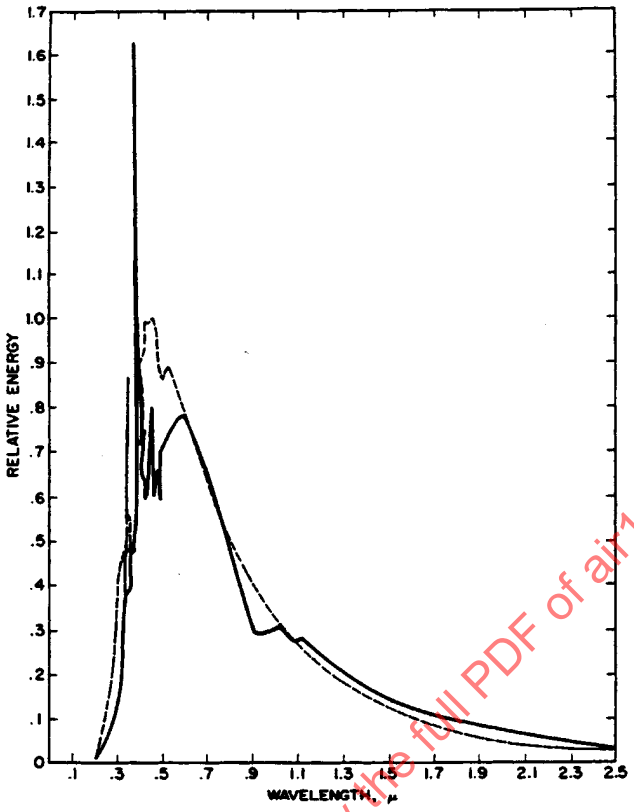

FIGURE 78 - Carbon Arc Spectrum; Solid Line is 13.6 mm High Carbon Bare Arc at 160 amp as Measured by Natl. Carbon Co.; Dotted Line is the Johnson Spectrum (Reference 38)

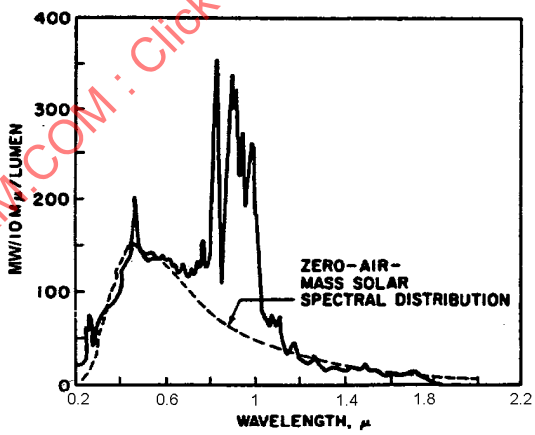

FIGURE 79 - Xenon Short Arc Spectrum; Solid Line is Initial Spectral Energy Distribution of Typical Lamp Operating at 5000 W, 275,000 lumens Output; Data Taken Perpendicular to Lamp Axis, With Electrode and Bulb Radiation Excluded; Varying Bandpass of Spectroradiometer Optical System Has Been Compensated by Corresponding Variation in Detector System Sensitivity (Adapted from NRL Memo Report 1005, December 1959) (Reference 38)

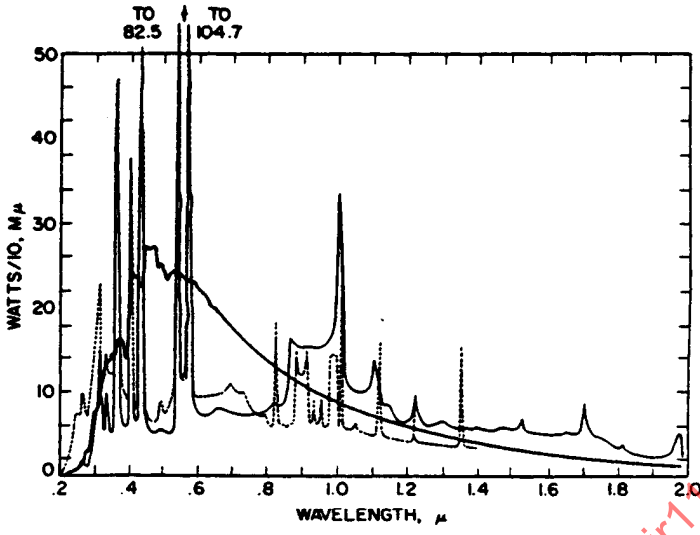

FIGURE 80 - Hg-Xe Arc Spectrum; Light Solid Line, Data from Westinghouse 2500 W Lamp SAHX-2500B (Total Output 1729 W in Range 0.2 to 5 μ); Dotted Line, Data From Hanovia Lamp; Heavy Solid Line, Data from Solar Spectrum Irradiance Outside Earth's Atmosphere (Reference 38)

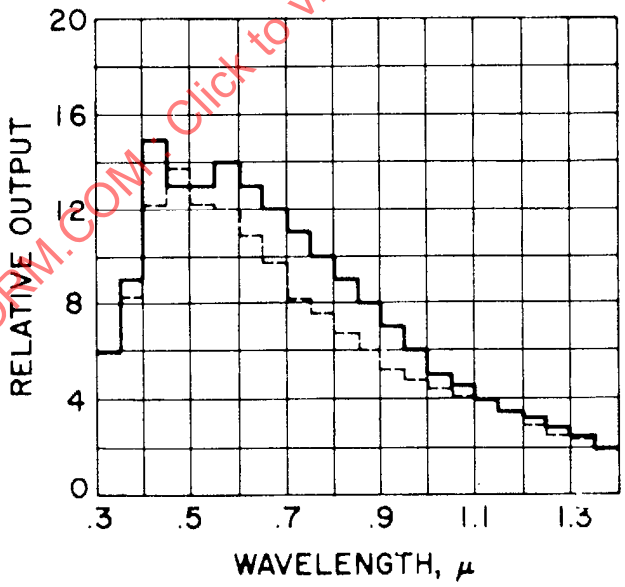

FIGURE 81 - Solid Line-Spectral Distribution for Super High-Intensity Carbon Arc (0.3 to 1.4 μ, 0.05 μ Integrations); Dotted Line = Zero-Air-Mass-Sun; Filter Factor = 79% (Reference 42)

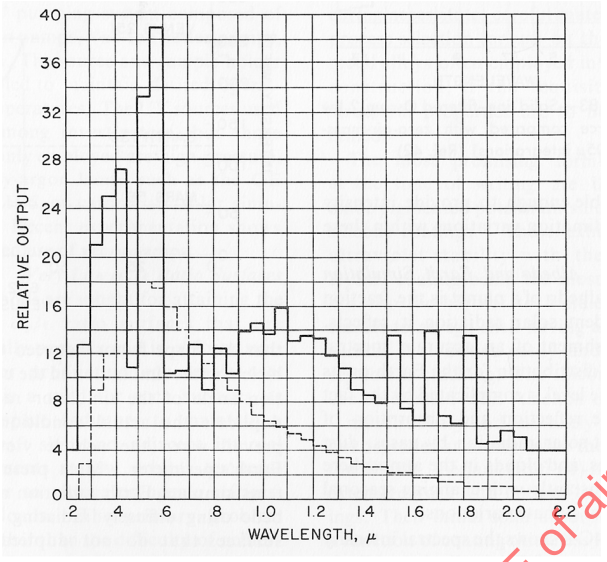

FIGURE 82 - Solid Line-Spectral Distribution of Hanovia Xe-Hg Lamp (0.2 to 2.2 μ), 0.05 μ Integrations; Dotted Line = Zero-Air-Mass-Sun; Filter Factor = 51% (Reference 42)

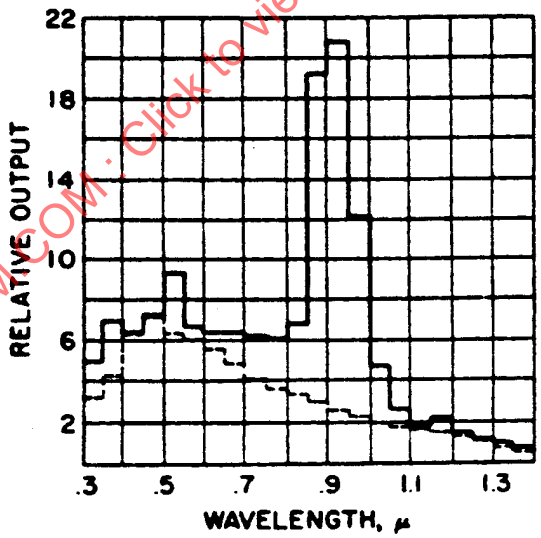

FIGURE 83 - Solid Line-Spectral Distribution for Osram 2 kW Xenon Lamp (0.3 to 1.4 μ, 0.05 μ Integrations); Dotted Line = Zero-Air-Mass-Sun; Filter Factor = 48.5% (Reference 42)

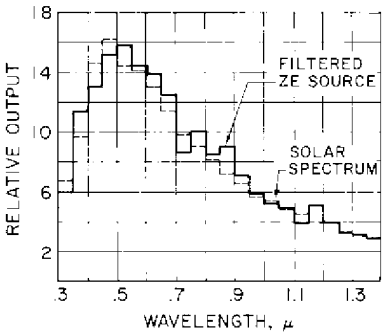

FIGURE 84 - Solid Line-Filtered Osram 2 kW Xe Source;
Dotted Line = Zero-Air-Mass-Sun (0.05 μ Integrations) (Reference 42)

6.1.2 (Continued):

Although a high energy penalty must be paid to obtain good solar spectrum simulation, short arc lamps are available in high-output modules that make the use of filters practicable. Because large quantities of energy must be removed from the output of these lamps and much of the energy they emit is in the ultraviolet region of the spectrum, the filters used must be cooled and checked periodically for degradation.

This means that the filters should be readily accessible and replaceable. Unfiltered, the Xenon lamp is presently the best source available for ultraviolet degradation studies if cooled specimens are used to remove the temperature effects produced by the excessive infrared energy of its spectrum.

Short arc lamps have an average rated lifetime of 1000 h, which makes them suitable for long-term testing. Reference 41 describes various types of lamps; a tabulation of their properties is given in Table 22.

Figure 85 shows the solar intensity and collimation angle (Reference 42) for the Earth, Mars, and Venus. To prevent obsolescence, a space simulator should be flexible enough to provide intensity and collimation variations within these limits.

6.1.3 Albedo and Earth Simulation: The albedo of a planet is the fraction of incident solar radiation it reflects. Establishment of an accurate spectral albedo distribution for the Earth or its absolute level is complicated by the fact that the reflection and absorption of incident solar radiation by gases, dust particles, and clouds in the atmosphere vary constantly with changing seasonal and local climate variations.

Figure 9 showed the spectral intensity distribution of Earth albedo. Albedo radiation may be simulated with a secondary filtered source such as a xenon or mercury-xenon lamp. Earth planetary radiation simulation requires an infrared or heated body that produces a heat flux corresponding to 75 Btu/h-ft^2 (Table 1) on the test vehicle.

TABLE 22 - Characteristics of a Xenon (Xe) and Two Mercury-Xenon (Hg-Xe) Compact Arc Lamps for D-C Operation

Characteristic	491 °C	Hanovia Lamp Styles 929B	Hanovia Lamp Styles 932B
Gas-Vapor	Xe	Hg-Xe	Hg-Xe
Watts, Nominal	2200	2500	5000
Operating Voltage, DC	20-30	45-55	54-66
Current, DC amp,			
Nominal			
Starting	100	100 max	130 max
Operating	100	50	100
Warm-up Time for			
Full Output, min	...	8	8
Operating Vapor Pressure			
(approx atm)	16	18	15
Arc Length, Operating, mm	4.0	4.0	5.0
Brightness, max, c/mm^2	3300	2050	2250
Brightness, avg, c/mm^2	440	540	780
For arc area	2.5 x 4	2.5 x 4	3 x 5
Initial Lumens	75,000	120,000	230,000
Overall Length, max in	12-1/2	12-1/2	13-1/2
Bulb Dia, mm	57	64	86
Bulb Length, mm	61	68	96
Bulb Wall Thickness, in	3.5	3.5	4.5
Rated Avg Life, h, at 12 h/start	1000	1000	Experimental

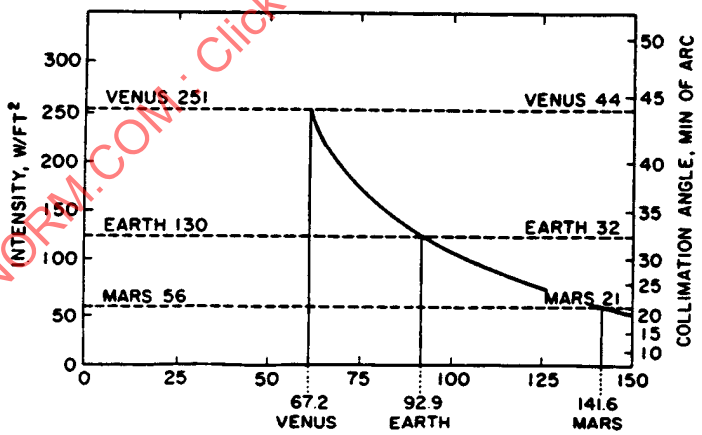

FIGURE 85 - Intensity and Collimation of Solar Simulation; Planetary Orbital Distances in Millions of Miles (Reference 42)

6.1.3 (Continued):

Although production of either flux appears simple, optimum albedo and planetary radiation simulation requires that the shape factor between the vehicle and the simulator and the collimation angle of the simulator radiation duplicate the actual conditions that prevail when the vehicle views the Earth's perimeter. Most present systems (circa 1965) simulate Earth radiation and albedo using diffusely radiating heated surfaces that do not duplicate the proper collimation angle, and therefore provide improper shadowing of the test vehicle.

7. MATERIAL DEGRADATION:

The surface thermal properties of materials may be degraded in space by ultraviolet radiation, or particulate, electron or micrometeorite bombardment.

The design criteria for thermal control surfaces include the following:

1. The coating must not change its initial value of α_s/ϵ by more than a given amount in a specified period of time, dependent upon the mission and its objectives and upon vehicle design.

2. Induced changes in optical properties should occur in as short a period of time as possible.

3. The coating materials must not be chemically or mechanically unstable (even though optically stable) or suffer loss in adhesion to the substrate through the effects of various environments.

4. Decomposition products must be compatible with the coating or substrate, and should not affect adjacent surfaces (for example, by outgassing or smoking).

To determine that candidate materials conform to these requirements, a large amount of information must be collected, most of which is obtained through testing by exposure of materials to ultraviolet, nuclear radiation, and micrometeorite bombardment.

7.1 Ultraviolet Degradation:

7.1.1 Mechanism of Damage: The ultraviolet (UV) radiation spectrum extends from 1800 (far-UV) to 3800 Å (near-UV and lower threshold of ocular vision). The Sun, radiating energy approximately as a 6000 K blackbody, produces an intensity of 440 Btu/h-ft^2 outside the Earth's atmosphere and at the Earth's distance from the Sun; 9% of this is in the UV region, as defined above.

The intensity of UV radiation in space is sufficient to induce appreciable changes in the composite chemical and physical structure of many thermal control materials. Experimental evidence has established the facts that ultraviolet damage must be a primary design consideration and that it is an extremely effective and operative agent in producing optical damage.